

การย่อยสลายไอโซโทปรูธอนด้วยแสงบนไททานเนียมไดออกไซด์และซิงค์ออกไซด์

นางสาวนภพร ชาญเจริญลาภ

วิทยานิพนธ์นี้เป็นส่วนหนึ่งของการศึกษาตามหลักสูตรปริญญาวิทยาศาสตรมหาบัณฑิต

สาขาวิชาวิศวกรรมเคมี ภาควิชาวิศวกรรมเคมี

คณะวิศวกรรมศาสตร์ จุฬาลงกรณ์มหาวิทยาลัย

ปีการศึกษา 2556

ลิขสิทธิ์ของจุฬาลงกรณ์มหาวิทยาลัย

บทคัดย่อและแฟ้มข้อมูลฉบับเต็มของวิทยานิพนธ์ตั้งแต่ปีการศึกษา 2554 ที่ให้บริการในคลังปัญญาจุฬาฯ (CUIR)

เป็นแฟ้มข้อมูลของนิสิตเจ้าของวิทยานิพนธ์ที่ส่งผ่านทางบัณฑิตวิทยาลัย

The abstract and full text of theses from the academic year 2011 in Chulalongkorn University Intellectual Repository (CUIR) are the thesis authors' files submitted through the Graduate School.

PHOTODEGRADATION OF ISOPROTURON ON  
TITANIUM DIOXIDE AND ZINC OXIDE

Miss Napaporn Chanchaoenlap

A Thesis Submitted in Partial Fulfillment of the Requirements  
for the Degree of Master of Engineering Program in Chemical Engineering

Department of Chemical Engineering

Faculty of Engineering

Chulalongkorn University

Academic Year 2013

Copyright of Chulalongkorn University

Thesis Title                                   PHOTODEGRADATION OF ISOPROTURON ON TITANIUM  
  DIOXIDE AND ZINC OXIDE  
By   Miss Napaporn Chanchaorenlap  
Field of study                                 Chemical Engineering  
Thesis Advisor                                 Assistant Professor Varong Pavarajarn, Ph.D.

---

Accepted by the Faculty of Engineering, Chulalongkorn University in Partial  
Fulfillment of the Requirements for the Master's Degree

.....Dean of the Faculty of Engineering  
(Professor Bundhit Eua-Arporn, Ph.D.)

THESIS COMMITTEE

.....Chairman  
(Professor Suttichai Assabumrungrat, Ph.D.)

.....Thesis Advisor  
(Assistant Professor Varong Pavarajarn, Ph.D.)

..... Examiner  
(Assistant Professor Apinan Soottitantawat, D.Eng.)

.....External Examiner  
(Pamornrat Chantam, D.Eng)

นภพร ชาญเจริญลาภ: การย่อยสลายไอโซโพรทูรอนด้วยแสงบนไททาเนียมไดออกไซด์ และซิงค์ออกไซด์ (PHOTODEGRADATION OF ISOPROTURON ON TITANIUM DIOXIDE AND ZINC OXIDE) อ.ที่ปรึกษาวิทยานิพนธ์หลัก: ผศ.ดร. วรงค์ ปวราจารย์, 134 หน้า.

การย่อยสลายสารกำจัดวัชพืชไอโซโพรทูรอนซึ่งจัดเป็นสารกำจัดวัชพืชในกลุ่มพีนิลยูเรียที่มักพบปนเปื้อนในแหล่งน้ำด้วยแสงได้ถูกศึกษาโดยใช้ทั้งไทเทเนียมไดออกไซด์และซิงค์ออกไซด์ที่มีในท้องตลาดและซิงค์ออกไซด์ที่สังเคราะห์ด้วยวิธีโซลเจลเป็นตัวเร่งปฏิกิริยา ในกระบวนการย่อยสลายทำการศึกษากการย่อยสลายไอโซโพรทูรอนที่ความเข้มข้น 10 ppm ภายใต้แสงจากหลอดไฟ UV-A 6 หลอดในเครื่องปฏิกรณ์แบบกะ โดยเก็บสารละลายตัวอย่างขึ้นมาเป็นระยะๆ เพื่อวัดความเข้มข้นของสารละลายไอโซโพรทูรอนที่เปลี่ยนแปลงด้วยเครื่องโครมาโทกราฟีชนิดของเหลว ทั้งยังศึกษาการลดลงของปริมาณคาร์บอนอินทรีย์รวมซึ่งเป็นผลของการย่อยสลายไอโซโพรทูรอน นอกจากนี้การระบุสารตัวกลางที่เกิดขึ้นในระบบถูกวิเคราะห์ด้วยเครื่องโครมาโทกราฟีชนิดของเหลวและแมสสเปกโตรมิเตอร์ การศึกษาไอโซเทอร์มของการดูดซับเพื่ออธิบายการดูดซับของสารไอโซโพรทูรอนบนพื้นผิวของตัวเร่งปฏิกิริยา พบว่าพฤติกรรมการดูดซับของสารไอโซโพรทูรอนบนไทเทเนียมไดออกไซด์และซิงค์ออกไซด์แตกต่างกัน เมื่อเปรียบเทียบกับไทเทเนียมไดออกไซด์และซิงค์ออกไซด์ที่มีในท้องตลาด ประสิทธิภาพในการย่อยสลายของซิงค์ออกไซด์ที่มีในท้องตลาดมีค่ามากกว่าไทเทเนียมไดออกไซด์ที่มีในท้องตลาด แม้ว่าซิงค์ออกไซด์ที่มีในท้องตลาดมีพื้นที่ผิวที่ต่ำกว่ามาก ในขณะที่ความแตกต่างของประสิทธิภาพการย่อยสลายของซิงค์ออกไซด์ที่มีในท้องตลาดและที่สังเคราะห์ขึ้นมีความแตกต่างอาจเป็นผลมาจากการดูดซับของไอโซโพรทูรอนบนตัวเร่งปฏิกิริยาที่ต่างกันเนื่องมาจากการจัดเรียงตัวของ  $Zn^{2+}$  กับ  $O^{2-}$  ที่พื้นผิวของตัวเร่งปฏิกิริยาทั้งสองต่างกัน นอกจากนี้สารตัวกลางที่เกิดขึ้นจากปฏิกิริยาเมื่อใช้ตัวเร่งปฏิกิริยาที่แตกต่างกันและมีค่า pH ต่างๆของสารละลายพบว่าให้สารตัวกลางที่แตกต่างกัน

ภาควิชา.....วิศวกรรมเคมี.....ลายมือชื่อนิสิต.....  
 สาขาวิชา.....วิศวกรรมเคมี.....ลายมือชื่อ อ.ที่ปรึกษาวิทยานิพนธ์หลัก.....  
 ปีการศึกษา.....2556.....

## 5470236021: MAJOR CHEMICAL ENGINEERING

KEYWORDS: ISOPROTURON/ PHOTOCATALYTIC DEGRADATION/ TITANIUM  
DIOXIDE/ZINC OXIDE /INTERMEDIATE

NAPAPORN CHARCHAROENLAP: PHOTODEGRADATION OF ISOPROTURON  
ON TITANIUM DIOXIDE AND ZINC OXIDE. ADVISOR: ASST. PROF. VARONG  
PAVARAJARN, Ph.D., 134 pp.

Photocatalytic degradation of isoproturon (N,N-dimethyl-N-[4-(1- methylethyl) phenyl] urea), which is one of phenylurea herbicides often found contaminating ground and surface waters, was investigated by using commercial titanium dioxide, commercial zinc oxide and synthesized zinc oxide as photocatalysts. The synthesized zinc oxide was synthesized by sol-gel method. In the process, 10-ppm of isoproturon in aqueous solution was conducted in a batch photo-reactor with 6 UV-A lamps. The solution was periodically sampled to monitor the concentration of isoproturon by using high performance liquid chromatography (HPLC). The decrease of total organic carbon (TOC) as a result of mineralization of isoproturon was also observed. In addition, identification degradation intermediates was detected through liquid chromatography with mass spectroscopy (LC-MS/MS). Studies of adsorption isotherms were used to describe the adsorption of isoproturon on surface of the photocatalysts. It was found that adsorption behavior of isoproturon on titanium dioxide and zinc oxide are different. Comparing between commercial titanium dioxide and commercial zinc oxide, the degradation performance on the commercial zinc oxide is much higher than that on the commercial titanium dioxide, although commercial zinc oxide has much lower surface area while the difference of photocatalytic efficiency of commercial and synthesized zinc oxide are different may come from the different of isoproturon adsorption on catalyst which may result from the rearrangement of  $Zn^{+}$  and  $O^{-}$  on surface are different. Moreover, intermediates formed by the reaction on different photocatalysts and various pH of solution are also different.

Department Chemical Engineering Student's Signature:.....

Field of study Chemical Engineering Advisor's Signature:.....

Academic Year: 2013

## ACKNOWLEDGEMENTS

The author would like to express her gratitude to her advisor, Assistant Professor Dr.Varong Pavarajarn, for his extensive guidance, patience, support, and encouragement throughout the research.

I would also grateful to thank to Professor Dr. Sutthichai Assabumrungrat as the chairman, Assistant Professor Dr. Apinan Sootitantawat , Dr.Pamornrat Chantam, and Associate Professor Puangrat Kajitvichyanukul, members of the thesis committee for their kind cooperation, comment, and discussions.

I would like to thank the Scientific and Technological Research Equipment Centre for analysis of LC-MS/MS.

I would also like to thank all my friends and all members of the Center of Excellent in Particle Technology who always provide the encouragement and cooperate along the research study.

This work was also partially by Centennial Fund of Chulalongkorn University for the partial financial support to this work.

Finally, I would like to dedicate this thesis to my parents and my families, who have always been the source of her support and encouragement.

# CONTENTS

	<b>Page</b>
ABSTRACT (THAI).....	iv
ABSTRACT (ENGLISH).....	v
ACKNOWLEDGEMENTS.....	vi
CONTENTS.....	vii
LIST OF TABLES.....	x
LIST OF FIGURES.....	xii
CHAPTER	
I INTRODUCTION.....	1
II THEORY AND LITERATURE REVIEWS.....	3
2.1 Photocatalysts .....	3
2.1.1 Physical and Chemical Properties of Titanium Dioxide.....	3
2.1.2 Physical and Chemical Properties of Zinc Oxide .....	5
2.1.3 Photocatalyst Synthesis .....	7
2.2 Isoproturon .....	9
2.3 Photocatalytic Degradation .....	10
2.4 Photocatalytic Degradation of Isoproturon .....	21
2.4.1 Kinetics of Photocatalytic Degradation of Isoproturon .....	22
2.4.2 Adsorption of Isoproturon on Photocatalyst .....	23
2.4.3 Isoproturon Degradation Products .....	24
III EXPERIMENTAL .....	30
3.1 Chemicals .....	30
3.2 Synthesis of Zinc Oxide Nanoparticles .....	31

3.3 Characterizations of the Photocatalysts .....	31
3.4 Adsorption Studies .....	32
3.5 Photodegradation Apparatus .....	33
3.5.1 Photodegradation Apparatus .....	33
3.5.2 Photodegradation Experiment .....	33
3.5.3 Analyses .....	34
IV RESULTS AND DISCUSSION .....	35
4.1 Properties of Photocatalysts .....	35
4.2 Adsorption Studies .....	42
4.3 Photodegradation of Isoproturon .....	48
4.3.1 Comparative Study on Photocatalytic Degradation of Isoproturon on Commercial Titanium Dioxide and Commercial Zinc Oxide .....	49
4.3.2 Comparative Study on Photocatalytic Degradation of Isoproturon on Commercial Zinc Oxide and Synthesized Zinc Oxide .....	53
4.4 Intermediate Products of the Photodegradation of Isoproturon .....	56
4.4.1 Effect of Type of Photocatalysts .....	57
4.5 Effect of pH of Isoproturon Solution .....	66
4.5.1 Effect of pH of Isoproturon Solution on Commercial Titanium Dioxide .....	67
4.5.2 Effect of pH of Isoproturon Solution on Commercial Zinc Oxide .....	76
4.5.3 Effect of pH of Isoproturon Solution on Synthesized Zinc Oxide .....	84



	<b>Page</b>
V CONCLUSIONS AND RECOMMENDATIONS .....	95
4.1 Summary of results .....	95
4.2 Conclusions .....	95
4.3 Recommendations .....	96
REFERENCES .....	97
APPENDICES .....	102
APPENDIX A ISOPROTURON CALIBRATION CURVE. ....	103
APPENDIX B POIN OF ZERO CHARGE DETERMINATION.....	104
APPENDIX C LC-MS/MS MASS SPECTRUM. ....	106
APPENDIX D LIST OF PLUBLICATION .....	133
VITA .....	134

## LIST OF TABLES

Table	Page
2.1	Physical and structural properties of anatase and rutile..... 4
2.2	Thermochemical data for formation of titanium dioxide compound ..... 5
2.3	Properties of wurtzite zinc oxide ..... 6
2.4	Physicochemical properties of isoproturon ..... 10
2.5	Possible intermediates generated from photodegradation of diuron on zinc oxide and titanium dioxide ..... 14
2.6	Possible intermediates generated from photodegradation of linuron on commercial titanium dioxide, synthesized titanium dioxide, commercial zinc oxide and synthesized titanium dioxide ..... 17
2.7	Possible structures of all intermediate products in photodegradation of isoproturon over TiO <sub>2</sub> /Al-MCM-41 catalyst ..... 25
2.8	Proposed structures for the by-products arising from photocatalytic degradation of isoproturon ..... 26
2.9	Possible structures of main intermediate products from photocatalytic degradation of isoproturon ..... 29
3.1	List of chemical agents used in the research ..... 30
4.1	Crystallite size and surface area of photocatalysts ..... 37
4.2	Constants of Langmuir and Freundlich isotherm model for adsorption of isoproturon on commercial TiO <sub>2</sub> , commercial ZnO and synthesized ZnO ..... 47
4.3	The apparent rate constant ( $k_{ap}$ ), reaction rate constants ( $k_r$ ), and the adsorption constant ( $K$ ) for the photocatalytic degradation of isoproturon using commercial titanium dioxide and commercial zinc oxide as catalyst ..... 51
4.4	Band energy position of titanium dioxide and zinc oxide in aqueous solution ..... 53
4.5	The apparent rate constant ( $k_{ap}$ ), reaction rate constants ( $k_r$ ), and the adsorption constant ( $K$ ) for the photocatalytic degradation of isoproturon using commercial zinc oxide and synthesized zinc oxide as catalyst ..... 55

<b>Table</b>	<b>Page</b>
4.6 Main fragments obtain from MS/MS spectra in positive mode and proposed structures of intermediates generated from photodegradation of isoproturon on commercial titanium dioxide, commercial zinc oxide and synthesized zinc oxide .....	61
4.7 The apparent rate constant ( $k_{ap}$ ), reaction rate constants ( $k_r$ ), and the adsorption constant ( $K$ ) for the photocatalytic degradation of isoproturon using commercial titanium dioxide as catalyst at pH 3, pH 5 and pH 10 .....	68
4.8 Main fragments obtain from MS/MS spectra in positive mode and proposed structures of intermediates generated from photodegradation of isoproturon on different pH of commercial titanium dioxide .....	72
4.9 The apparent rate constant ( $k_{ap}$ ), reaction rate constants ( $k_r$ ), and the adsorption constant ( $K$ ) for the photocatalytic degradation of isoproturon using commercial zinc oxide as catalyst at pH 3, pH 5 and pH 10 .....	77
4.10 Main fragments obtain from MS/MS spectra in positive mode and proposed structures of intermediates generated from photodegradation of isoproturon on different pH of commercial zinc oxide .....	81
4.11 The apparent rate constant ( $k_{ap}$ ), reaction rate constants ( $k_r$ ), and the adsorption constant ( $K$ ) for the photocatalytic degradation of isoproturon using synthesized zinc oxide as catalyst at pH 3, pH 5 and pH 10 .....	85
4.12 Main fragments obtain from MS/MS spectra in positive mode and proposed structures of intermediates generated from photodegradation of isoproturon on different pH of synthesized zinc oxide .....	88

## LIST OF FIGURES

Figure		Page
2.1	Crystal structure of TiO <sub>2</sub> ; (a) Anatase, (b) Rutile, (c) Brookite.....	4
2.2	Stick and ball representation of zinc oxide crystal structures: (a) cubic rocksalt, (b) cubic zinc blende, and (c) hexagonal wurtzite. The shaded gray and black spheres denote Zn and O atoms, respectively .....	6
2.3	Schematic representation of the photochemical activation of a semiconductor and formation of the hydroxyl radical. VB: valence band; CB: conduction band; A: electronic acceptor compound; D: electronic donating compound .....	11
2.4	Benzene oxidation pathways on lanthanum -doped TiO <sub>2</sub> thin film .....	21
3.1	Diagram of the equipment setup for the photocatalytic degradation .....	33
4.1	XRD patterns of the commercial titanium dioxide powder. ....	36
4.2	XRD patterns of the commercial zinc oxide and synthesized zinc oxide powder .....	36
4.3	Adsorption/desorption isotherm of commercial titanium dioxide .....	38
4.4	Adsorption/desorption isotherm of commercial zinc oxide .....	38
4.5	Adsorption/desorption isotherm of synthesized zinc oxide .....	39
4.6	Absorbance spectra for commercial titanium dioxide .....	40
4.7	Absorbance spectra for commercial zinc oxide .....	40
4.8	Absorbance spectra for synthesized zinc oxide .....	41
4.9	TGA curves of the synthesized zinc oxide powder after calcined at 500°C for 2 h .....	41
4.10	Adsorption of isoproturon on the surface of commercial titanium dioxide when the initial concentration was 1, 5, 10, 15 and 20 ppm .....	42
4.11	Adsorption of isoproturon on the surface of commercial zinc oxide when the initial concentration was 1, 5, 10, 15 and 20 ppm .....	43
4.12	Adsorption of isoproturon on the surface of synthesized zinc oxide when the initial concentration was 1, 5, 10, 15 and 20 ppm .....	43

<b>Figure</b>	<b>Page</b>
4.13 Adsorption isotherm of isoproturon onto the surface of commercial titanium dioxide, commercial zinc oxide and synthesized zinc oxide at room temperature .....	44
4.14 Langmuir isotherm (a-c) and Freundlich isotherm (d-f) for adsorption of isoproturon on: (■) commercial titanium dioxide, (●) commercial zinc oxide and (▲) synthesized zinc oxide. ....	46
4.15 Concentration of isoproturon with respect to the initial isoproturon concentration ( $C/C_0$ ) during the photocatalytic degradation on: (△) photolysis, (○) commercial titanium dioxide and (□) commercial zinc oxide .....	49
4.16 First-order linear transforms plot of the photocatalytic degradation on: (○) commercial titanium dioxide, (□) commercial zinc oxide .....	50
4.17 Total organic carbon (TOC) with respect to the initial TOC of isoproturon solution ( $TOC/TOC_0$ ) during the photocatalytic degradation on: (○) commercial titanium dioxide and (□) commercial zinc oxide .....	52
4.18 Concentration of isoproturon with respect to the initial isoproturon concentration ( $C/C_0$ ) during the photocatalytic degradation on: (△) photolysis, (□) commercial zinc oxide and (◇) synthesized zinc oxide .....	54
4.19 First-order linear transforms plot of the photocatalytic degradation on: (□) commercial zinc oxide, (◇) synthesized zinc oxide .....	55
4.20 Total Organic Carbon (TOC) with respect to the Initial TOC of Isoproturon Solution ( $TOC/TOC_0$ ) during the Photocatalytic Degradation on: (□) commercial zinc oxide and (◇) synthesized zinc oxide .....	56
4.21 Chemical structure of Isoproturon .....	57
4.22 (a) HPLC peak height of intermediates generated during photocatalytic degradation of isoproturon on commercial titanium dioxide and (b) enlargement of (a). ....	58
4.23 (a) HPLC peak height of intermediates generated during photocatalytic degradation of isoproturon on commercial zinc oxide and (b) enlargement of (a) .....	59

<b>Figure</b>	<b>Page</b>
4.24 (a) HPLC peak height of intermediates generated during photocatalytic degradation of isotroturon on synthesized zinc oxide and (b) enlargement of (a) .....	60
4.25 Hydroxylation Reaction .....	66
4.26 Decarboxylation Reaction .....	66
4.27 Effect of pH of the solution on photodegradation of isotroturon using commercial titanium dioxide as catalyst: ( $\Delta$ ) pH 3, ( $\circ$ ) pH 5 and ( $\square$ ) pH 10 .....	67
4.28 HPLC peak height of intermediates generated during photocatalytic degradation of isotroturon on commercial titanium dioxide at different retention time in pH of solution is ( $\Delta$ ) pH 3, ( $\circ$ ) pH 5 and ( $\square$ ) pH10 .....	69
4.29 Effect of pH of the solution on photodegradation of isotroturon using commercial zinc oxide as catalyst: ( $\Delta$ ) pH 3, ( $\circ$ ) pH 5 and ( $\square$ ) pH 10 .....	76
4.30 HPLC peak height of intermediates generated during photocatalytic degradation of isotroturon on commercial zinc oxide at different retention time in pH of solution is ( $\Delta$ ) pH 3, ( $\circ$ ) pH 5 and ( $\square$ ) pH10 .....	78
4.31 Effect of pH of the solution on photodegradation of isotroturon using synthesized zinc oxide as catalyst: ( $\Delta$ ) pH 3, ( $\circ$ ) pH 5 and ( $\square$ ) pH 10 .....	85
4.32 HPLC peak height of intermediates generated during photocatalytic degradation of isotroturon on synthesized 1 zinc oxide at different retention time in pH of solution is ( $\Delta$ ) pH 3, ( $\circ$ ) pH 5 and ( $\square$ ) pH10 .....	86
4.33 Proposed mechanism of photodegradation of isotroturon. ....	94
A.1 The calibration curve of isotroturon .....	103
B.1 Determination of the point of zero charge of commercial titanium dioxide .....	104

<b>Figure</b>	<b>Page</b>
B.2	Determination of the point of zero charge of commercial zinc oxide ..... 104
B.3	Determination of the point of zero charge of synthesized zinc oxide ..... 105
C.1	Chromatogram of isoproturon solution ..... 106
C.2	Chromatogram of isoproturon solution during photodegradation process using commercial titanium dioxide as catalyst at natural of solution (0-360 min during reaction process) are shown in (a). MS/MS spectrums at various retention times are display in (b)-(j) ..... 107
C.3	Chromatogram of isoproturon solution during photodegradation process using commercial titanium dioxide as catalyst at pH 3 of solution (0-360 min during reaction process) are shown in (a). MS/MS spectrums at various retention times are display in (b)-(j) ..... 109
C.4	Chromatogram of isoproturon solution during photodegradation process using commercial titanium dioxide as catalyst at pH 5 of solution (0-360 min during reaction process) are shown in (a). MS/MS spectrums at various retention times are display in (b)-(j) ..... 110
C.5	Chromatogram of isoproturon solution during photodegradation process using commercial titanium dioxide as catalyst at pH 10 of solution (0-360 min during reaction process) are shown in (a). MS/MS spectrums at various retention times are display in (b)-(j) ..... 113
C.6	Chromatogram of isoproturon solution during photodegradation process using commercial zinc oxide as catalyst at natural of solution (0-360 min during reaction process) are shown in (a). MS/MS spectrums at various retention times are display in (b)-(j) ..... 115
C.7	Chromatogram of isoproturon solution during photodegradation process using commercial zinc oxide as catalyst at pH 3 of solution (0-360 min during reaction process) are shown in (a). MS/MS spectrums at various retention times are display in (b)-(j) ..... 117

<b>Figure</b>	<b>Page</b>
C.8 Chromatogram of isoproturon solution during photodegradation process using commercial zinc oxide as catalyst at pH 5 of solution (0-360 min during reaction process) are shown in (a). MS/MS spectrums at various retention times are display in (b)-(j) .....	119
C9 Chromatogram of isoproturon solution during photodegradation process using commercial zinc oxide as catalyst at pH 10 of solution (0-360 min during reaction process) are shown in (a). MS/MS spectrums at various retention times are display in (b)-(j) .....	122
C.10 Chromatogram of isoproturon solution during photodegradation process using synthesized zinc oxide as catalyst at natural of solution (0-360 min during reaction process) are shown in (a). MS/MS spectrums at various retention times are display in (b)-(j) .....	124
C.11 Chromatogram of isoproturon solution during photodegradation process using synthesized zinc oxide as catalyst at pH 3 of solution (0-360 min during reaction process) are shown in (a). MS/MS spectrums at various retention times are display in (b)-(j) .....	126
C.12 Chromatogram of isoproturon solution during photodegradation process using synthesized zinc oxide as catalyst at pH 5 of solution (0-360 min during reaction process) are shown in (a). MS/MS spectrums at various retention times are display in (b)-(j) .....	129
C.13 Chromatogram of isoproturon solution during photodegradation process using synthesized zinc oxide as catalyst at pH 10 of solution (0-360 min during reaction process) are shown in (a). MS/MS spectrums at various retention times are display in (b)-(j) .....	131



# CHAPTER I

## INTRODUCTION

Thailand is an agricultural country. Approximately 40.9% of the total area is used for agricultural production. For the agricultural section, one of the important input factors is pesticides, especially herbicides, insecticides and fungicides. According to the data of the Office of Agriculture Regulation, Department of Agriculture, the herbicides import of Thailand in January – March 2011 was approximately 25 million kilograms, which is the highest category for imported pesticides. The widely use of herbicides is one of the main present environmental problems, particularly for phenylurea herbicides which are widely applied for weed control on agriculture soils. Isoproturon (N,N-dimethyl-N-[4-(1-methylethyl) phenyl] urea) is one of the phenylurea herbicides. It is mainly used for the control of annual grasses and many broad leaved weeds in the cereals and wheat crops [1]. Its application in modern agriculture practices results in toxic contamination of ground and surface waters, due to its solubility in water, low chemical and biochemical degradation rates [2, 3].

In this regard, several techniques have been developed for elimination these pollutants from water. Conventional biological treatment processes are based on the requirement of a long residence time to degrade the pollutants because microorganisms are affected by the toxicity of the herbicides. On the other hand, the traditional physico-chemical treatments (such as adsorption on activated carbon, nano-filtration and ozonation) are efficient but they have inherent limitations in applicability, effectiveness and cost [4-6]. Photocatalytic degradation process is an alternative method for treatment of contaminants in water. The photocatalytic degradation of isoproturon has been reported on oxide semiconductor photocatalysts. Among various oxide semiconductors, titanium dioxide (titania,  $\text{TiO}_2$ ) is one of the most suitable catalysts for environmental applications due to its high photocatalytic activity, non-toxic, low cost, and good chemical stability [2, 3, 7-9]. Another important oxide semiconductor photocatalyst is zinc oxide (ZnO) that has been considered as an alternative to titanium dioxide because its photocatalysis mechanism has been proven to be similar to that of titanium dioxide [10-12]. Although, both of titanium dioxide and zinc oxide have similar band gap [12], many researches show the different efficiency in photodegradation of titanium dioxide and zinc oxide [11, 13, 14]. In addition, the different synthesis technique results in the different properties of the product and consequently affects the interaction between the catalyst surface and the compound to be

degraded [15], so the synthesized zinc oxide are studied to compare with commercial zinc oxide.

One of the popular techniques for synthesis photocatalyst is sol-gel method owing to its low cost, reliability, reproducibility, simplicity and relative mild conditions of synthesis [9, 16].

The photocatalytic degradation of isoproturon in aqueous solution has been previously reported in many literatures and several researches have studied the disappearance of the pollutants in the degradation of pollutants. However, the detailed investigations of intermediate compounds that occur during the decomposition process are not frequently reported, although intermediate compounds can be even more toxic or greater persistent than the parent herbicides.

In this work, the comparative study on photodegradation of isoproturon on titanium dioxide and zinc oxide are investigated including comparative study on zinc oxide and synthesized zinc oxide. Moreover, the formation of intermediates during the photocatalytic degradation will be identified.

The present thesis is arranged as follows:

Chapter I is the introduction of this work.

Chapter II describes the basic theory about photocatalysts such as chemical properties of titanium dioxide and zinc oxide photocatalyst synthesis and about isoproturon such as chemical and properties of isoproturon. For the photocatalytic degradation process, photocatalytic degradation of isoproturon, kinetics of photodegradation of isoproturon and adsorption of isoproturon including literature review of previous works relating to this research are also presented in this chapter.

Chapter III shows chemicals, the experimental equipments and the procedures for the preparation of photocatalyst by the sol-gel process, the photocatalytic degradation and identifies the intermediates products.

Chapter IV presents the experimental results and discussion of the research.

In the last chapter, the overall conclusions of this research are given.

## CHAPTER II

### THEORY AND LITERATURE REVIEWS

Theory and literature reviews relating to properties of photocatalyst, isoproturon photocatalytic degradation and photocatalytic degradation of isoproturon are described as followed.

#### 2.1 Photocatalyst

In the photodegradation process, photocatalyst is used as the catalyst that produces free radicals by absorption of light. In recent year, it has been demonstrated that many types of semiconductors are successful as photocatalyst to remove of organic pollutants from water. In this research, titanium dioxide and zinc oxide, which are inexpensive, non-toxic and highly active, are used.

##### *2.1.1 Physical and Chemical Properties of Titanium Dioxide*

Titanium dioxide, also known as titanium (IV) oxide or titania, is the naturally occurring oxide of titanium. Titanium dioxide has great potential for many industrial applications such as filter material, anti-reflection film, sensor, dye-sensitise solar cell and photocatalyst. Titanium dioxide occurs in three different crystalline polymorphic forms: rutile (tetragonal), anatase (tetragonal), and brookite (orthorhombic) [17, 18].

In all three forms, titanium ( $\text{Ti}^{4+}$ ) atoms are co-ordinated to six oxygen ( $\text{O}^{2-}$ ) atoms, forming  $\text{TiO}_6$  octahedra. All three forms differ only in the arrangement of these octahedra. The anatase structure is made up of corner (vertice) sharing octahedral resulting in a tetragonal structure. In rutile, the octahedra share edges to give a tetragonal structure and in brookite both edges and corners are shared to give an orthorhombic structure. All of structures are shown in Figure 2.1.

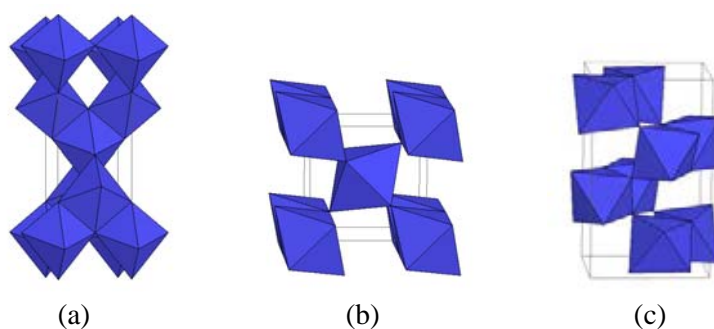


**Figure 2.1** Crystal structure of  $\text{TiO}_2$ ; (a) Anatase, (b) Rutile, (c) Brookite.

Rutile is the most stable form of titanium dioxide, while anatase and brookite are metastable, transforming to rutile under calcination, typically at 600-700 °C [17, 19]. Moreover, anatase and rutile are the most researched polymorphs but anatase form is preferred to be used in photocatalytic degradation. Their properties and basic thermochemical data of titanium dioxide are summarized in Table 2.1 – 2.2 [17-20].

**Table 2.1** Physical and structural properties of anatase and rutile [17-20].

Property	Anatase	Rutile
Molecular Weight (g/mol)	79.88	79.88
Phase transformation temperature (°C)	600	N/A
Melting point (°C)	N/A	1825
Boiling Point (°C)	N/A	2500 ~ 3000
Specific gravity	3.9	4.0
Light absorption (nm)	< 390	< 415
Mohr's Hardness	5.5	6.5 – 7.0
Refractive index	2.55	2.75
Dielectric constant	31	114
Crystal structure	Tetragonal	Tetragonal
Lattice constants (Å)	$a = 3.78$ $c = 9.52$	$a = 4.59$ $c = 2.96$
Density (g/cm <sup>3</sup> )	3.79	4.13
Ti–O bond length (Å)	1.94 (4) 1.97 (2)	1.95 (4) 1.98 (2)

**Table 2.2** Thermochemical data for formation of titanium dioxide compound [20].

Compound	State	Heat of formation		Free energy of formation		Entropy	
		$\Delta H_f^\circ$ , kJ/mol		$\Delta G_f^\circ$ , kJ/mol		S, J/mol.K	
		At 298 K	At 1300 K	At 298 K	At 1300 K	At 298 K	At 1300 K
TiO <sub>2</sub>							
-Anatase	Crystal	-933.0	-930.0	-877.6	-697.4	49.9	150.6
-Rutile	Crystal	-944.7	-942.4	-889.5	-707.9	50.3	149.0

The use of titanium dioxide as a photocatalyst has been of great interest due to its high activity, non-toxicity, efficiency, and low cost [2-4, 8, 17, 21]. Titanium dioxide has a band gap of 3.2 eV for anatase, 3.0 eV for rutile, and ~3.2 eV for brookite. Charge carriers, i.e. electrons and holes, are produced when titania is excited. Consequently, highly reactive radicals are generated and oxidation-reduction reaction of species adsorbed on the surface of titanium dioxide can occur.

### 2.1.2 Physical and Chemical Properties of Zinc Oxide

Zinc oxide is an inorganic compound with the formula ZnO. It usually appears as a white powder normally known as zinc white and commonly occurs in nature as the mineral zincite. Most zinc oxide is prepared in industrial scale by vaporizing zinc metal and oxidizing the generated zinc vapor with preheated air. Zinc oxide is important due to its wide range of applications such as gas sensor, chemical sensor, bio-sensor, cosmetics, optical and electrical devices, solar cell, and photocatalyst. Zinc oxide crystallizes in three forms: hexagonal wurtzite, cubic zinc blende, and the rarely observed cubic rocksalt, as schematically shown in Figure 2.2.

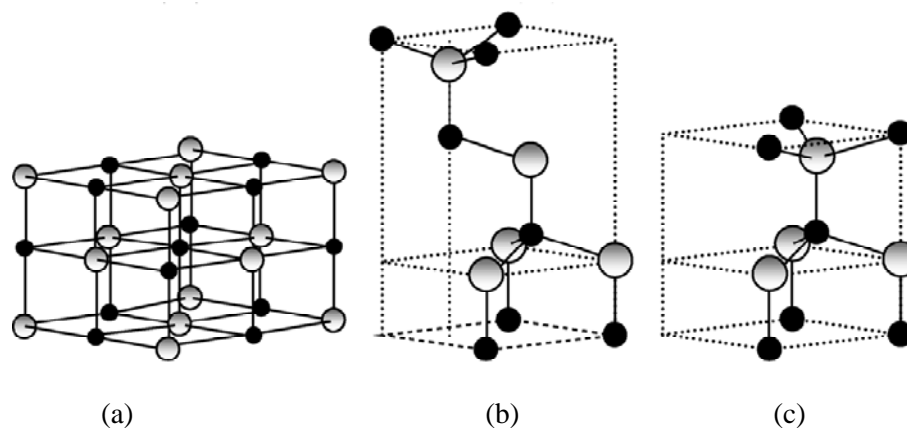


**Figure 2.2** Stick and ball representation of zinc oxide crystal structures: (a) cubic rocksalt, (b) cubic zinc blende, and (c) hexagonal wurtzite. The shaded gray and black spheres denote Zn and O atoms, respectively.

The hexagonal wurtzite structure is the most stable crystal structure of zinc oxide at ambient conditions. The cubic zinc blende structure can be formed only by the growth of ZnO on cubic substrate while the cubic rocksalt structure may be obtained at relatively high pressure.

Zinc oxide is an n-type semiconductor with a wide band gap of 3.20 eV and large excitation binding energy of 60 meV, which makes it very high potential for room temperature light emission. This also gives zinc oxide strong resistance to high temperature electronic degradation during operation. Therefore, it is attractive for many opto-electronic applications in the range of blue and violet light as well as UV devices for wide range of technological applications. Zinc oxide also exhibits dual semiconducting and piezoelectric properties. The other properties are given in Table 2.3 [22].

**Table 2.3** Properties of wurtzite zinc oxide [22].

Molecular formula	ZnO
Molecular weight	81.38 g/mole
Lattice parameters at 300 K	
$a$	0.32495 nm
$c$	0.52069 nm
$c/a$	1.602 (ideal hexagonal structure is 1.633)
Density	5.606 g/cm <sup>3</sup>

**Table 2.3** (continued)

Melting point	1970 – 1975 °C (decomposes)
Thermal conductivity	130 W/m.K
Linear expansion coefficient (/°C)	<i>a</i> : $6.5 \times 10^{-6}$ <i>c</i> : $3.0 \times 10^{-6}$
Static dielectric constant	8.656
Energy gap	3.2 eV, direct
Excitation binding energy	60 meV
Appearance	White solid
Synonyms	Zinc white; Zinc flowers; Calamine; C.I. pigment white 4
Solubility	Insoluble in water and alcohols. Soluble in acids and bases.
Physicochemical stability	Stable under normal conditions of handling and storage.

### 2.1.3 Photocatalyst Synthesis

There are several methods for synthesizing photocatalyst, such as thermal decomposition method, precipitation method, flame spray pyrolysis method and sol–gel method. The choice of the synthesis technique results in the different properties of the product and consequently affects the interaction between the catalyst surface and the compound to be degraded. Chen et al. investigated the crystalline size of synthesized ZnO nanoparticles and found that it was different when various synthesis routes were used, e.g., direct precipitation, sol-gel method and hydrothermal method [15].

Sol-gel method is one of the popular techniques to produce catalyst powder because of its low cost, reliability, reproducibility, simplicity and relatively mild condition of synthesis [9, 16]. This technique finds applications in the development of new materials for catalysis, chemical sensors, membranes, fibers, optical gain media, photochromic applications, and solid state electrochemical devices, and in a diverse range of scientific and engineering fields, such as ceramic industry, nuclear industry and electronic industry [23].

The sol–gel process, as the name implies, involves the evolution of inorganic networks through the formation of a colloidal suspension (sol) and gelation of the sol to form

a network in a continuous liquid phase (gel). A sol is a dispersion of the solid particles, with diameter of 1–1000 nm, in a liquid where only the Brownian motions kept particles in suspension while a gel is a state where both liquid and solid are dispersed in each other, which presents a solid network filled with liquid components. The precursors for synthesizing these colloids consist of a metal or metalloid element surrounded by various reactive ligands. Metal alkoxides are most popular because they react readily with water [24]. The alkoxides are hydrolyzed giving the oxide as a colloidal product. The sol is then either treated or simply left to form gel. To obtain a final product, the gel is heated. This heating serves several purposes; it removes the solvent, decomposes anions such as alkoxides or carbonates to give oxides, allows rearrangement of the structure of the solid and allows crystallization.

Main reactions that occur during the sol–gel involve hydrolysis of the metal alkoxide and followed by condensation.

Hydrolysis:



Condensation:



Whereas, M is metal and OR is alkoxy group.

The parameters affecting reaction rate of the sol-gel process include pH, molar ratio of reactants, aging time and temperature. Alias et al. reported the effect pH (8-11) on ZnO nanoparticle properties synthesized by sol–gel centrifugation. The results show that the particle size ranged from 36 to 49 nm Particle size analysis reveals that the largest particle size occurs at pH 8, and the smallest particle size occurs at pH 11 [25]. Hayat et al. investigated the effect of various calcination temperatures on ZnO nanoparticles synthesized via sol–gel method including its application in heterogeneous photocatalytic removal of phenol from water. They explained that, as the calcination temperature was increased, crystallites tended to agglomerate with simultaneous loss of activity of the catalyst. Nano ZnO calcined at 500°C was found to be more active for photocatalytic oxidation of phenol as compared to all other photocatalysts employed (Nano ZnO calcined at 400°C, 550°C, 600°C and 700°C) [26]. Li et al. reported the effect of aging time of ZnO sol on the structural and optical properties of ZnO thin films prepared by sol–gel method. They found that ZnO thin



film prepared by the as-synthesized ZnO sol had relatively poor crystalline quality, low optical transmittance in the visible range and relatively weak ultraviolet emission performance. With the prolonging of sol aging time, the structural and optical properties of ZnO thin films were improved gradually. The ideal aging time was suggested to be 24 h. The film prepared by 24 h aged sol had good quality. Moreover, 24 h was not too long and it would not affect the film preparation efficiency [27].

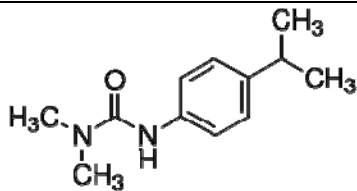
Since the sol-gel process is easy to produce nanoparticles and properties of the catalysts (such as surface area, pore size and perfection of crystals) can be easily customized by adjusting the synthesis parameters (e.g. solution pH, calcination temperature, concentration of reactants and aging time), the sol-gel method was selected for the synthesis ZnO in this research, according to the method proposed by Tian et al. [9].

## **2.2 Isoproturon**

Nowadays, herbicides are widely in agricultures. Phenylurea herbicides are a chemical family of herbicides that have been extensively used for weed control. One of the widely used phenylurea herbicide is isoproturon.

Isoproturon (N,N-dimethyl-N-[4-(1-methylethyl) phenyl] urea) is a herbicide that inhibits photosynthetic electron transfer. It is mainly used for the control of annual grasses and many broad leaved weeds in the cereals and wheat [1]. Its application results in highly toxic contamination of ground and surface waters, because of its highly relative solubility in water, low chemical and biological degradation rates [2, 3]. Moreover, its half-life in water is 30 days. Thus it becomes a potential risk for environment. Its properties are shown in Table 2.4.

**Table 2.4** Physicochemical properties of isoproturon

Structure formula	
Molecular weight	206.29 g/mol
Molecular formula	C <sub>12</sub> H <sub>18</sub> N <sub>2</sub> O
Melting point	155 – 156°C
Vapor pressure	0.003 mPa at 20°C
Appearance	White crystalline solid
Solubility	72 ppm in water at 20°C
Toxicity	Low toxic, acute oral to mouse is over 10000 mg/kg
Half-life	30 days in water, 6.5 to 30 days in soil

For the treatment of the pollutants, there are several techniques to remove them from water such as biological, physical and chemical treatments but all of these techniques have limitations in applicability, effectiveness, and costs [2-5]. An alternative method is photocatalytic degradation which is an effective process for degradation of pesticide in water [2-5, 7, 8].

### 2.3 Photocatalytic Degradation

The photocatalytic process is a promising technology for the oxidation/degradation of organic contaminants in environmental control. It has been widely used as an alternative physical-chemical process for the elimination of toxic and hazardous organic substances in liquid (e.g. wastewater and contaminated groundwater) and gaseous streams (e.g. VOC emission). The end products of this treatment process are usually harmless compounds such as carbon dioxide, water and inorganic ions such as chloride and nitrate. The advantage of this process is that it achieves complete mineralization of organic contaminants, whether they are simple or complex molecules. Moreover, the utilization of sunlight can be applied to reduce

the energy cost for the process. In this process, a semiconductor activated by ultraviolet (UV) radiation is used as a catalyst to destroy organic contaminants [28-30].

For the heterogeneous photocatalytic process, which is used in pollutant degradation, it involves the adsorption of pollutants on the surface sites, and the chemical reaction to convert pollutant into carbon dioxide and water [30]. Semiconductors are usually used as the catalyst in this process. Among several semiconductors, titanium dioxide and zinc oxide have attracted great interest as promising photocatalysts in areas of environmental and energy, due to their high photocatalytic activity, resistance to photocorrosion, photo-stability, low cost and non-toxicity [31].

Photocatalytic reactions take place when the semiconductor particle absorbs photon with energy equal to or more than the band gap, the electron is excited from the valence band (VB) to the conduction band (CB), producing electron-hole ( $e^-/h^+$ ), able to initiate the oxidation and reduction processes (Figure.2.3) [32].

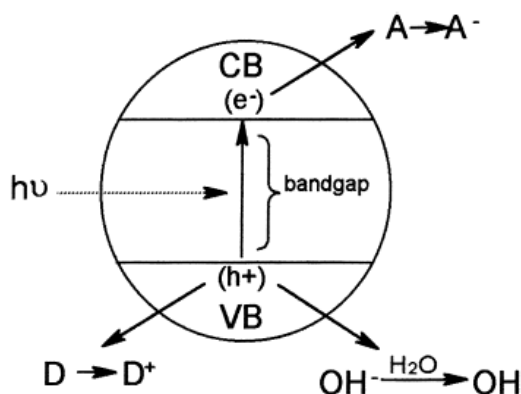
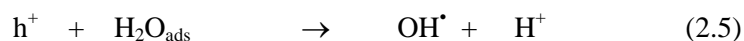
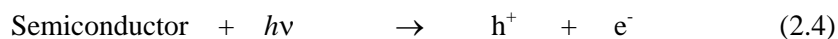


**Figure 2.3** Schematic representation of the photochemical activation of a semiconductor and formation of the hydroxyl radical. VB: valence band; CB: conduction band; A: electronic acceptor compound; D: electronic donating compound [32].

The generation of electron-hole pairs is represented in Eq. (2.4). In aqueous solution, the hole oxidizes hydroxyl group ( $\text{OH}^-$ ) to generate the strong oxidizing hydroxyl radical ( $\text{OH}^\bullet$ ), which can promote the oxidation of organic compounds. In addition, the process is usually carried out in aerobic conditions so that the electron reduces oxygen to generate the superoxide radical ( $\text{O}_2^-$ ) as following Eq. (2.5) - (2.7).





Support of the OH<sup>•</sup> radical as the main reactive oxidant derives from the observation that intermediates detected during the photocatalytic degradation of halogenated aromatic compounds are typically hydroxyl structures as those found when similar aromatics react with a known source of OH<sup>•</sup> radicals.

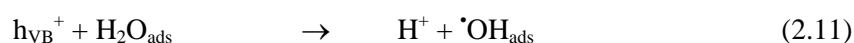
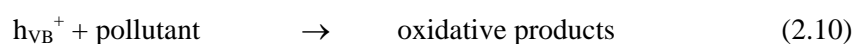
Most studies about the degradation of pollutants focuses on the disappearance of the pollutants. For example, Daneshvar et al studied the influence of various parameters on photocatalytic decomposition of an azo dye, Acid Red 14, in the presence of TiO<sub>2</sub>. The result showed that UV/TiO<sub>2</sub> process could be efficiently used to degrade the Acid Red 14. Photodegradation efficiency of dye was obviously affected by the initial dye concentration, pH and the amount of TiO<sub>2</sub> [33]. Oyama et al. investigated the photodegradation of a commercial detergent in aqueous TiO<sub>2</sub> dispersions under sunlight irradiation. They found that a commercial detergent whose major components are an anionic surfactant and a fluorescent whitening agent can be photodegraded in aqueous TiO<sub>2</sub> dispersions under irradiation with concentrated sunlight in the presence of air. TiO<sub>2</sub> loading and flow rate influence the degradation process [34]. Pourata et al. reported the photocatalytic removal of the bentazon from contaminated water in the presence of nanosized TiO<sub>2</sub> powders under UV light illumination. The results indicated that photocatalytic removal efficiency of Bentazon is affected by the crystalline phases and size of TiO<sub>2</sub>, amount of TiO<sub>2</sub>, irradiation time and initial concentration of bentazon [35].

In case of ZnO used as photocatalyst, many reports have been published. For example, Behnajady et al. investigated the effects of process parameters such as, catalyst loading, initial dye concentration, light intensity, and pH on the photodegradation of C.I. AcidYellow23. They found that the photodegradation percentage is increased with increasing catalyst loading, pH, light intensity and decreasing initial concentration [36]. Daneshvar et al studied the removal of C.I. acid orange7 from aqueous solution under UV irradiation in the presence of ZnO nanopowder. The results showed that the complete removal of color, after selecting desired operational parameters (amount of catalyst, initial concentration and initial pH) could be achieved in a relatively short time, i.e., about 60 min [37]. Mijin et al studied photocatalytic degradation of the herbicide metamitron in water using ZnO and light. The obtained results indicated that the photodegradation of metamitron is affected by the concentration of ZnO, the initial metamitron concentration and pH values [38].

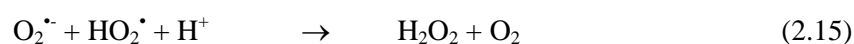
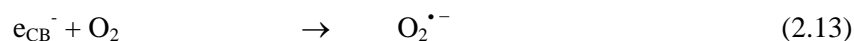
The mechanism of photocatalytic degradation of organic matter on titanium dioxide/zinc oxide is mostly expressed, by the following reactions, Eq. (2.8 – 2.16) [33-38].



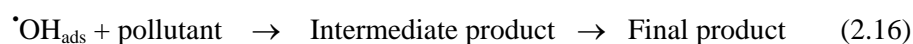
The highly oxidative potential of the hole ( $h_{\text{VB}}^+$ ) in the catalyst permits the direct oxidation of herbicide into the reactive intermediates (Eq. (2.10)) or can also induce the formation of hydroxyl radical ( $\cdot\text{OH}$ ) either by the decomposition of water (Eq. (2.11)) or by the reaction of the hole with  $\text{OH}^-$  (Eq. (2.12))



Electrons in the conduction band ( $e_{\text{CB}}^-$ ) on the catalyst surface can reduce molecular oxygen to superoxide anion (Eq. (2.13)). This radical, in the presence of organic scavengers, may form organic peroxides (Eq. (2.14)) or hydrogen peroxide (Eq. (2.15)).



Hydroxyl radicals ( $\cdot\text{OH}$ ) have been indicated as the primary cause of organic matter mineralization (Eq. (2.16)).



However, the detailed investigations of intermediate compounds that occur during the decomposition process are not frequently reported. Pradittakan, et al. studied the comparison of the intermediates formed from the degradation of pesticide, i.e., diuron using different photocatalysts, i.e. titanium dioxide and zinc oxide and revealed common intermediates as well as different intermediates. The results confirmed that the degradation of diuron generates lots of intermediates [39]. The structures of all intermediates detected were proposed in Table 2.5[39].

**Table 2.5** Possible intermediates generated from photodegradation of diuron on zinc oxide and titanium dioxide [39].

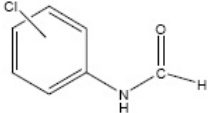
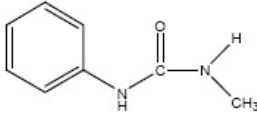
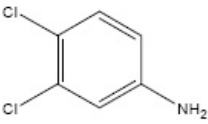
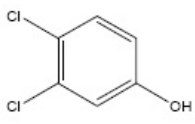
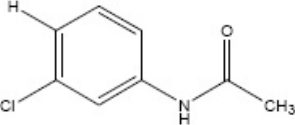
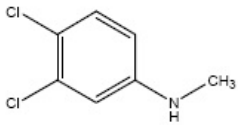
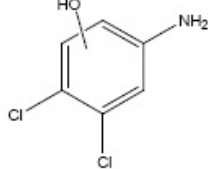
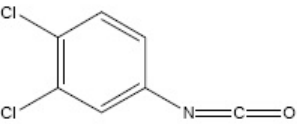
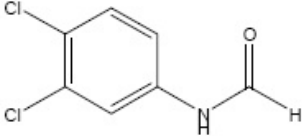
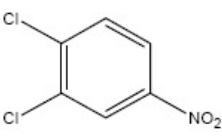
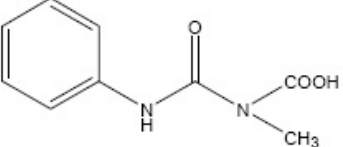
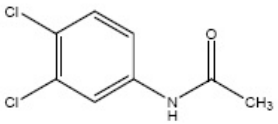
Structure	ZnO	TiO <sub>2</sub>	Structure	ZnO	TiO <sub>2</sub>
	✓	✓		✓	✓
	✓	✓		✓	✓
	✓				✓
		✓			✓
		✓		✓	
		✓		✓	✓

Table 2.5 (continued)

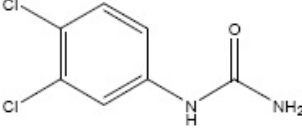
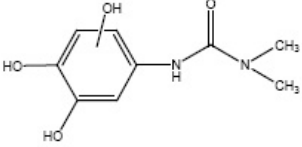
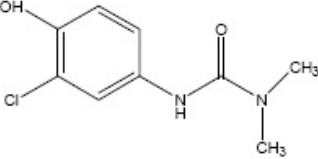
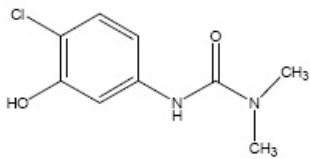
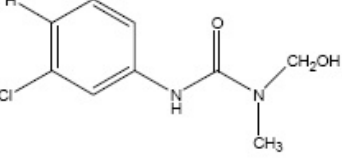
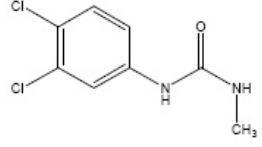
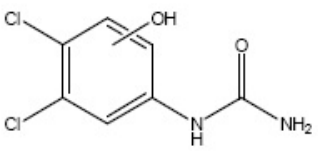
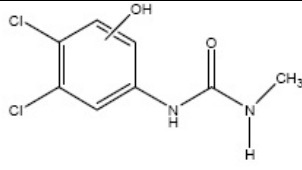
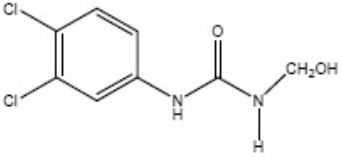
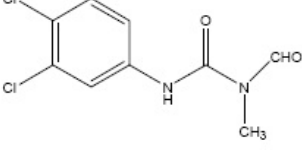
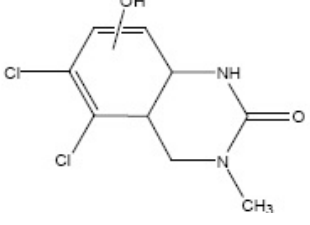
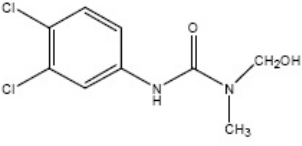
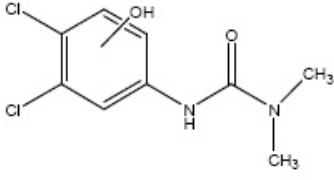
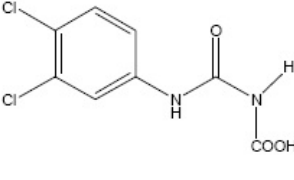
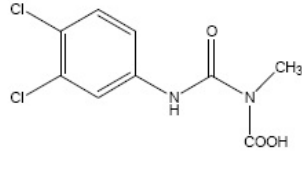
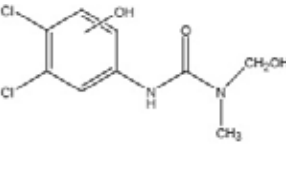
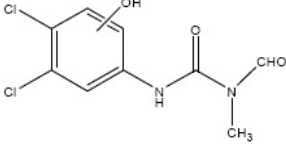
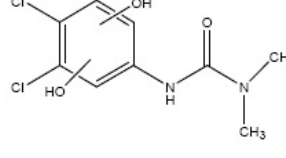
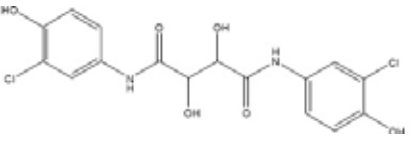
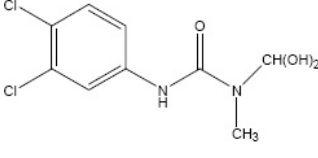
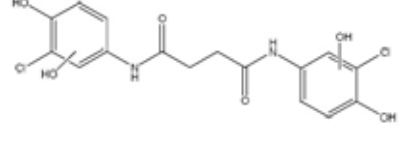
Structure	ZnO	TiO <sub>2</sub>	Structure	ZnO	TiO <sub>2</sub>
	✓	✓			✓
		✓		✓	✓
	✓	✓		✓	✓
	✓	✓		✓	
	✓			✓	✓
	✓	✓		✓	✓

Table 2.5 (continued)

Structure	ZnO	TiO <sub>2</sub>	Structure	ZnO	TiO <sub>2</sub>
	✓	✓		✓	✓
	✓			✓	
	✓			✓	
	✓			✓	
	✓				

Sittichoktum and Pavarajarn investigated the comparison of the intermediates formed by using different photocatalysts, i.e. TiO<sub>2</sub> and ZnO, in photodegradation of linuron [40]. The structures of all intermediates detected were proposed in Table 2.6 [40].



**Table 2.6** Possible intermediates generated from photodegradation of linuron on commercial titanium dioxide, synthesized titanium dioxide, commercial zinc oxide and synthesized titanium dioxide [40].

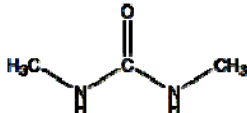
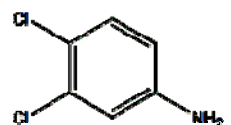
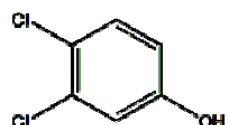
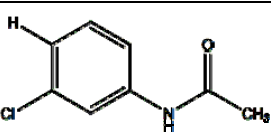
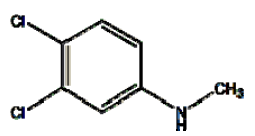
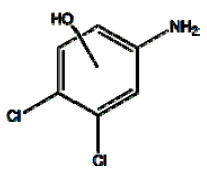
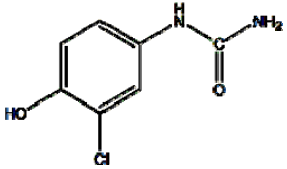
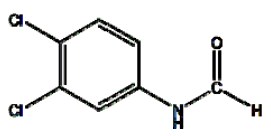
Proposed structure	commercial TiO <sub>2</sub>	synthesized TiO <sub>2</sub>	commercial ZnO	synthesized ZnO
				✓
	✓	✓	✓	✓
	✓	✓		
		✓		✓
	✓			✓
	✓		✓	
			✓	✓
	✓			

Table 2.6 (continued)

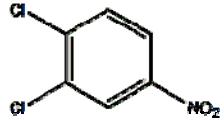
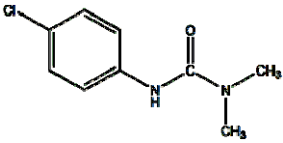
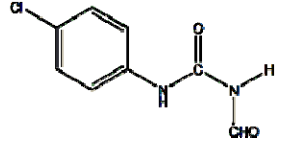
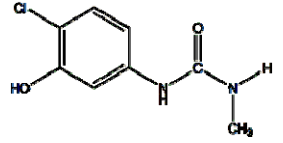
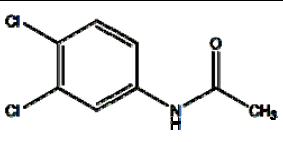
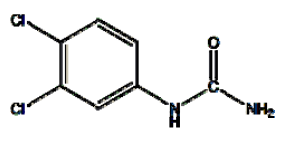
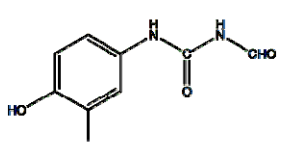
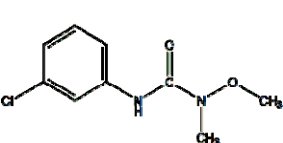
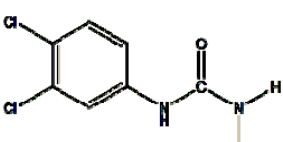
Proposed structure	commercial TiO <sub>2</sub>	synthesized TiO <sub>2</sub>	commercial ZnO	synthesized ZnO
			✓	
	✓		✓	
	✓		✓	
		✓	✓	
	✓	✓	✓	✓
	✓	✓	✓	✓
		✓	✓	✓
		✓	✓	✓
	✓	✓	✓	✓

Table 2.6 (continued)

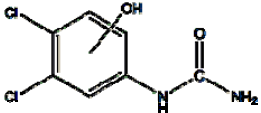
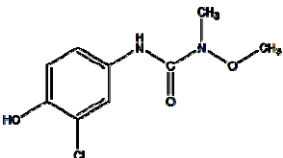
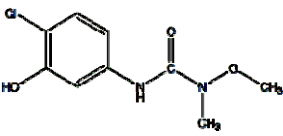
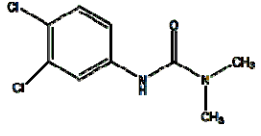
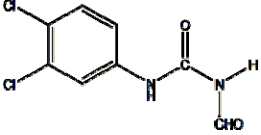
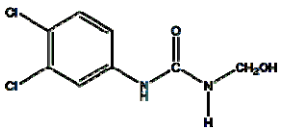
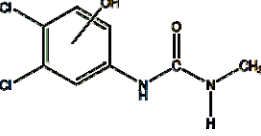
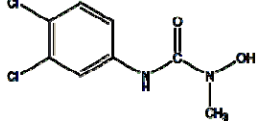
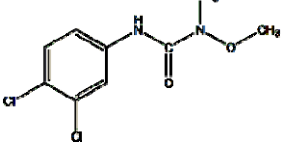
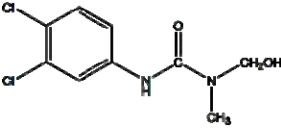
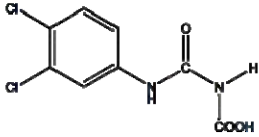
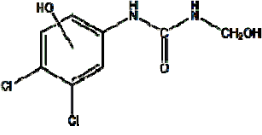
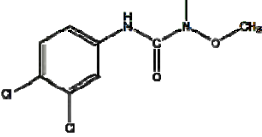
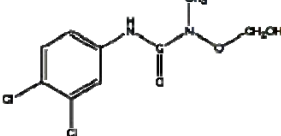
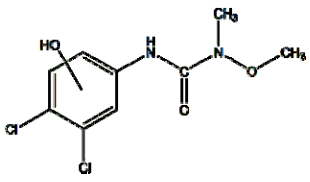
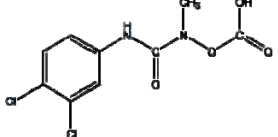
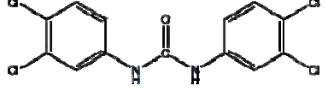
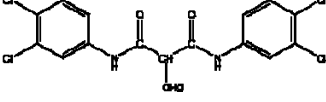
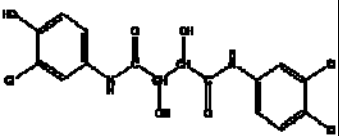
Proposed structure	commercial TiO <sub>2</sub>	synthesized TiO <sub>2</sub>	commercial ZnO	synthesized ZnO
	✓			
	✓	✓	✓	✓
	✓	✓	✓	✓
	✓	✓	✓	
	✓	✓	✓	
	✓	✓	✓	✓
	✓	✓	✓	✓
	✓	✓	✓	✓
	✓	✓	✓	✓

Table 2.6 (continued)

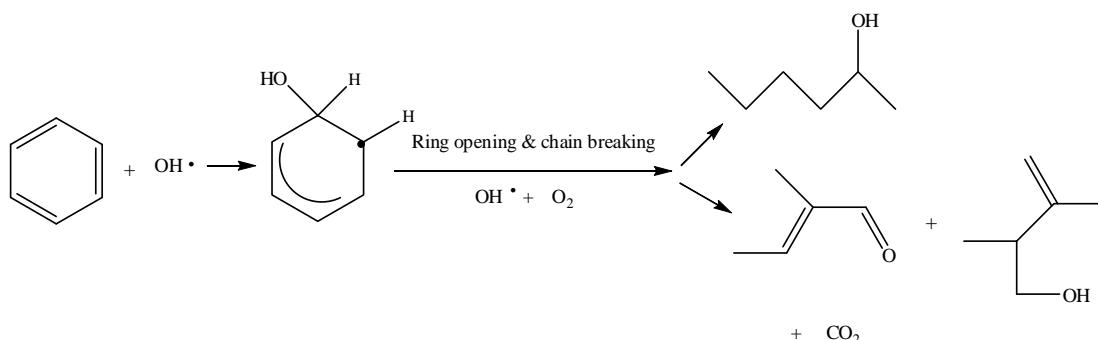
Proposed structure	commercial TiO <sub>2</sub>	synthesized TiO <sub>2</sub>	commercial ZnO	synthesized ZnO
	✓	✓	✓	✓
	✓	✓	✓	✓
	✓	✓	✓	✓
	✓	✓	✓	✓
	✓	✓	✓	✓
	✓	✓	✓	✓
	✓			✓
	✓	✓	✓	✓
		✓		

**Table 2.6** (continued)

Proposed structure	commercial TiO <sub>2</sub>	synthesized TiO <sub>2</sub>	commercial ZnO	synthesized ZnO
		✓		

From the results of the difference in intermediate products from the degradation of diuron and linuron, they indicated that the difference in properties of the catalyst and the different conditions of the reaction generate the different intermediate products.

Moreover, Zhang, et al studies the photodecomposition of benzene over lanthanum-doped TiO<sub>2</sub> film, the predominant mechanism is the attack of hydroxyl radical (OH•) on the benzene ring as shown in Figure 2.4[41].

**Figure 2.4** Benzene oxidation pathways on lanthanum -doped TiO<sub>2</sub> thin film [41].

## 2.4 Photocatalytic Degradation of Isoproturon

Isoproturon (N,N-dimethyl-N-[4-(1-methylethyl) phenyl] urea) is one of the widely used phenylurea herbicide. There are many different methods to remove these pollutants. One of the attractive methods for the treatment of contaminated in water is advanced oxidation processes (AOPs). These methods are generally based on the generation of OH radicals which interact with organic pollutants leading to progressive degradation and subsequently complete mineralization [2].

### 2.4.1 Kinetics of Photocatalytic Degradation of Isoproturon

According to several papers on photocatalytic processes that have been reported in the recent years, the degradation rate depends on parameters influencing the oxidation such as pH value, initial concentration, catalyst loading [2-4, 7]. They have also found that the kinetic model suitable for representing photocatalytic reaction is the Langmuir – Hinshelwood model [4]. In this model, it is assumed that the reaction occurs on the surface and the rate of reaction ( $r$ ) is proportional to the fraction of surface covered by the substrate ( $\theta$ ) [42]:

$$r = -\frac{dC}{dt} = k_r\theta = k_r \frac{KC}{1 + KC} \quad (2.17)$$

This equation can be integrated, becoming:

$$\ln\left(\frac{C_0}{C}\right) + K(C_0 - C) = k_r Kt \quad (2.18)$$

where  $C_0$  is the initial concentration of the organic substrate,  $C$  is the concentration of the substance being degraded,  $K$  is the constant of adsorption equilibrium,  $k_r$  is true rate constant and  $t$  is the irradiation time.

When the solution is highly diluted, the term  $KC$  becomes  $\ll 1$ , the denominator of Eq. (2.17) is neglected and the reaction is essentially an apparent first order reaction [42].

$$r = -\frac{dC}{dt} = k_r KC = k_{ap}C \quad (2.19)$$

Thus, Eq. (2.18) can be simplified to a first order reaction when  $C_0$  is very small, in which case one has:

$$\ln \frac{C_0}{C} = k_{ap}t \quad (2.20)$$

where  $C_0$  is the initial concentration of the organic substrate,  $C$  is the concentration of the substance being degraded and  $k_{ap}$  is the apparent rate constant of the pseudo first order reaction. By plotting  $\ln(C_0/C)$  versus  $t$ , the apparent rate constant ( $k_{ap}$ ) can be determined from the slope of the curve obtained.

Sharma et al. studied photocatalytic degradation of isoproturon, using  $\text{TiO}_2/\text{Al-MCM-41}$  composite as catalalyst. The  $\text{TiO}_2$  supported Al-MCM-41 catalysts were prepared by solid-state dispersion (SSD) method. The results showed that the influence of initial concentration of isoproturon on the photocatalytic degradation rate is described by pseudofirst-order kinetics [3].

#### 2.4.2 Adsorption of Isoproturon on Photocatalyst

The study of the adsorption of the herbicides onto photocatalyst was undertaken in order to investigate the relationship between the observed reactivity of each herbicide with the degree of adsorption onto the catalyst [43]. The two models most commonly employed to describe adsorption processes in aqueous solutions are the models proposed by Langmuir and Freundlich isotherm models [29, 44, 45].

The Langmuir isotherm which has been successfully applied to many other sorption processes can be used to explain the sorption of isoproturon into photocatalyst. A basic assumption of the Langmuir theory is that the sorption takes place at specific sites within the adsorbent and it has been used successfully for many adsorption processes of monolayer adsorption. The saturation monolayer can be represented by the expression Eq. (2.21) [44].

$$q_e = \frac{bq_{\max}C_e}{1 + bq_{\max}C_e} \quad (2.21)$$

The linearized form of the Langmuir isotherm model is:

$$\frac{1}{q_e} = \frac{1}{q_{\max}} + \frac{1}{bq_{\max}} \frac{1}{C_e} \quad (2.22)$$

where  $q_e$  is amount of adsorbate on adsorbent at equilibrium (mg/g),  $q_{\max}$  is maximum adsorption capacity (mg/g),  $C_e$  is equilibrium concentration (mg/l), and  $b$  is Langmuir's equilibrium constant related to energy of the sorption system (l/mg).

Thus, by plotting  $1/q_e$  versus  $1/C_e$  one can determine the maximum adsorption capacity  $q_{\max}$  and Langmuir's equilibrium constant ( $b$ ) through the slope and linear coefficient of the straight line [29, 44].

The essential characteristic of the Langmuir isotherm can be expressed in terms of a dimensionless equilibrium factor ( $r$ ) which was calculated by following Eq. (2.23) [44, 45]:

$$r = \frac{1}{1 + bC_0} \quad (2.23)$$

This parameter indicates that isotherm will be shaped according to the following adsorption characteristics:  $r > 1$  indicates the isotherm shape that unfavorable adsorption

condition. The values  $0 < r < 1$  indicates favorable adsorption conditions. In the special cases where  $r=1$  and  $r=0$  the adsorption is linear and irreversible, respectively [44, 45].

The Freundlich isotherm is used for a heterogeneous surface energy system in which energy varies as a function of the surface coverage. The Freundlich isotherm can be represented by Eq. (2.24) [44, 46].

$$q_e = K_f + C_e^{1/n} \quad (2.24)$$

The linearized form of the Freundlich isotherm model is:

$$\ln q_e = \ln K_f + \frac{1}{n} \ln C_e \quad (2.25)$$

where  $q_e$  is amount of adsorbate on adsorbent at equilibrium (mg/g),  $C_e$  is equilibrium concentration (mg/l),  $1/n$  is adsorption intensity and  $K_f$  is Freundlich constant related to adsorption capacity (mg/g(mg/l)<sup>-1/n</sup>).

The value of  $k$  and  $n$  can be estimated from the intercept and slope of the linear plot of experimental data of  $\ln q_e$  versus  $\ln C_e$ .

Freundlich's parameter relates to the mean energy of adsorption. A very weak adsorbent/adsorbate interaction occurs at values of  $n$  lower than 1, while values higher than 1 suggest a strong adsorbent/adsorbate interaction. At value of  $n$  equal to 1 it is assumed that all sites are energetically similar [29].

Gora et al. studied photocatalytic oxidation of herbicides, i.e., isoproturon, simazine and propazine over irradiated TiO<sub>2</sub> suspension in single-component and in multicomponent systems. The results showed the adsorption behavior following the Langmuir adsorption model. Isoproturon was found to have a slightly higher adsorption capacity than simazine and propazine, which had similar values in accordance to the similarity in their molecular structure. Moreover comparison of the Langmuir's equilibrium constant of the herbicides observed under dark adsorption and under photocatalytic oxidation showed that these are very similar suggesting that the degradation of isoproturon, simazine and propazine mixtures follows a surface or near-surface reaction according to a competitive L-H mechanism [43].

### 2.4.3. Isoproturon Degradation Products

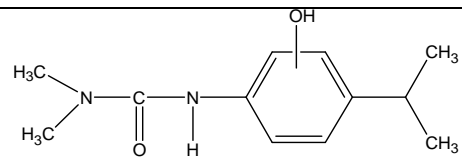
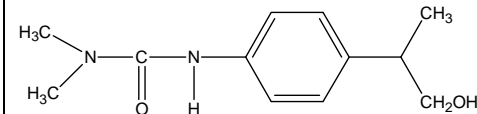
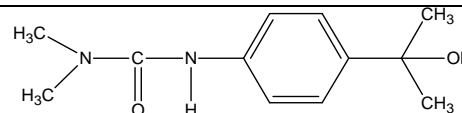
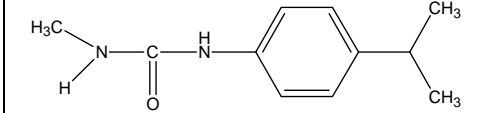
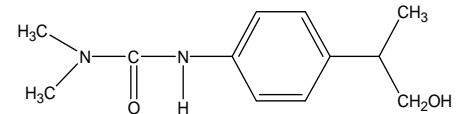
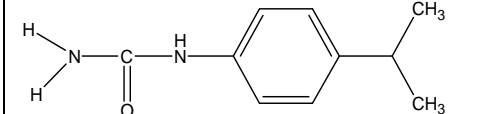
In the study of intermediate compounds resulting from the degradation of herbicides, many researchers have proposed degradation pathway of various herbicides. The



differences in the intermediate compounds and degradation pathway have been reported to depend on the degradation process. It is known that the degradation starts with an attack of OH radicals in photocatalytic reactions.

Sharma et al. studied photocatalytic degradation of isoproturon, using  $\text{TiO}_2/\text{Al-MCM-41}$  composite as catalyst. The  $\text{TiO}_2$  supported Al-MCM-41 catalysts were prepared by solid-state dispersion (SSD) method. The degradation reaction in this process involves mainly hydroxylation, dealkylation, dehydrogenation and decarboxylation. The molecular structure of isoproturon allows OH radical to attack at different sites such as the CH of isopropyl group,  $\text{CH}_3$  of dimethyl urea, and an aromatic ring that corresponds to isoproturon mono-hydroxylated products. All of these compounds are the primary degradation intermediates of isoproturon. Later, the attack of hydrogen forms the methyl group followed by addition of oxygen and decarboxylation leading to dealkylated products and following by hydroxylation. After irradiation for long time, the intermediate compounds disappear because the cleavage of aromatic ring with OH radical resulting aliphatic compounds like aldehydes, ketones and acids that leads to mineralization [3]. The possible structures of all intermediate products in photodegradation of isoproturon over  $\text{TiO}_2/\text{Al-MCM-41}$  catalyst were represented in Table 2.7 [3].

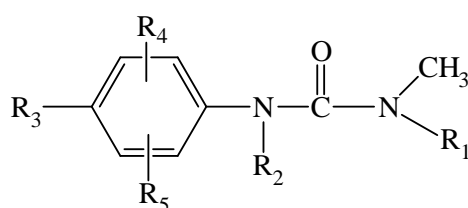
**Table 2.7** Possible structures of all intermediate products in photodegradation of isoproturon over  $\text{TiO}_2/\text{Al-MCM-41}$  catalyst [3].

Comp.	Structure	Comp.	Structure
1		4	
2		5	
3		6	

**Table 2.7** (continued)

Comp.	Structure	Comp.	Structure
7		9	
8		10	

Amorisco et al. identified the structure of degradation by-products of isoproturon generated during the photocatalytic process of the immobile TiO<sub>2</sub> on polyvinylidene fluoride substrate. Structural information of by-products, formed at different degradation times, was identified through MS/MS spectra, and in many cases several isomers were found. As expected, most by-products were resulted from single or multiple hydroxylation (by photo-generated OH radicals) of the isoproturon molecule at different positions [5]. The structures for the by-products arising from photocatalytic degradation of isoproturon were proposed in Table 2.8 [5].

**Table 2.8** Proposed structures for the by-products arising from photocatalytic degradation of isoproturon [5].

Compound	R <sub>1</sub>	R <sub>2</sub>	R <sub>3</sub>	R <sub>4</sub>	R <sub>5</sub>
1	CH <sub>3</sub>	H	OH	-	-
2	H	H		-	-

Table 2.8 (continued)

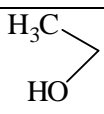
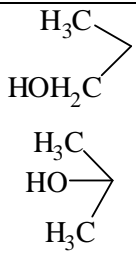
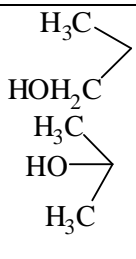
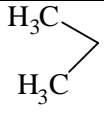
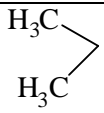
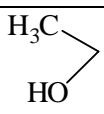
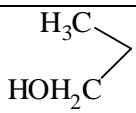
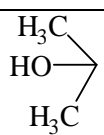
Compound	R <sub>1</sub>	R <sub>2</sub>	R <sub>3</sub>	R <sub>4</sub>	R <sub>5</sub>
3	CH <sub>3</sub>	H			
4	H	H		-	-
5	CH <sub>3</sub>	H		-	-
6	CH <sub>3</sub>	H		OH	-
7	CH <sub>3</sub>	OH		-	-
8	CH <sub>3</sub>	H OH		OH H	- -
9	CH <sub>3</sub>	H		-	-
10	CH <sub>3</sub>	H		OH	-

Table 2.8 (continued)

Compound	R <sub>1</sub>	R <sub>2</sub>	R <sub>3</sub>	R <sub>4</sub>	R <sub>5</sub>
11	CH <sub>3</sub>	H	$  \begin{array}{c}  \text{HOH}_2\text{C} \\  \diagdown \\  \text{HOH}_2\text{C} \\  \diagup \\  \text{H}_3\text{C} \\  \text{HO} \rightarrow \\  \text{HOH}_2\text{C}  \end{array}  $	-	-
12	CH <sub>3</sub>	H	$  \begin{array}{c}  \text{H}_3\text{C} \\  \diagdown \\  \text{H}_3\text{C}  \end{array}  $	OH	OH
13	CH <sub>2</sub> OH	H	$  \begin{array}{c}  \text{H}_3\text{C} \\  \diagdown \\  \text{HOH}_2\text{C} \\  \diagup \\  \text{H}_3\text{C} \\  \diagdown \\  \text{H}_3\text{C}  \end{array}  $	OH	-
14	CH <sub>3</sub>	H	$  \begin{array}{c}  \text{H}_3\text{C} \\  \diagdown \\  \text{HOH}_2\text{C} \\  \diagup \\  \text{H}_3\text{C} \\  \text{HO} \rightarrow \\  \text{H}_3\text{C}  \end{array}  $	OH	OH
15	CH <sub>3</sub>	OH	$  \begin{array}{c}  \text{H}_3\text{C} \\  \diagdown \\  \text{HOH}_2\text{C} \\  \diagup \\  \text{H}_3\text{C} \\  \text{HO} \rightarrow \\  \text{H}_3\text{C}  \end{array}  $	OH	-

Mangalampalli et al. investigated immobilization of titanium dioxide over zeolite NH<sub>4</sub>Y support for the treatment of isoproturon pesticide under solar light in aqueous suspensions. The influence of parameters such as amount of the catalyst, concentration of substrate and pH are studied. In addition, a plausible mechanism is proposed for photocatalytic degradation based on degradation products. The photocatalytic degradation of

isoproturon showed the formation of several intermediate products [2]. Three main products are showed in Table 2.9 [2].

**Table 2.9** Possible structures of main intermediate products from photocatalytic degradation of isoproturon [2].

Component	Structure
1	
2	
3	

The intermediates are formed by the attack of OH radicals on the aromatic ring and abstraction of hydrogen atoms of the methyl group followed by addition of oxygen and decarboxylation leading to formation of dealkylated products. The photoreactivity is also related to the donor or withdrawing effect induced by the different substituents of the aromatic ring. The first hydroxylation occurs either on the aromatic ring or on the alkyl groups leading to different monohydroxylated products. It further forms di- and polyhydroxylated compounds. Then, successive oxidations lead to ketones, organic acids formation and ultimately to complete mineralization.

However, the study of different condition of degradation and different properties of the photocatalyst resulting in the different intermediate products are rarely reported. So, it is objectives of this work, to study the photodegradation of isoproturon on titanium dioxide and zinc oxide in an aqueous solution, to identify intermediate compounds during photodegradation and to investigate kinetic model for this process.

## CHAPTER III

### EXPERIMENTAL

This chapter describes the experimental procedures for catalyst preparation and photodegradation of isoproturon. It is divided into seven parts: chemicals used, Synthesis of zinc oxide nanoparticles, characterizations of the catalyst, adsorption studied, photodegradation apparatus, photocatalytic experiment and analysis.

#### 3.1 Chemicals

List of the chemicals employed in this work are illustrated in Table 3.1.

**Table 3.1** List of chemical agents used in the research.

Chemical agents	Manufacturer / Grade	Using for
1. Titanium dioxide	Sigma-Aldrich, 99.9%	Adsorption studies Photocatalytic degradation
2. Zinc oxide	Thai-Lysaght, 99.8%	Adsorption studies Photocatalytic degradation
1. Zinc acetate (CH <sub>3</sub> COO) <sub>2</sub> Zn.2H <sub>2</sub> O	Ajax Finechem, 99.5%	Synthesis of ZnO
2. Diethanolamine (HOCH <sub>2</sub> CH <sub>2</sub> ) <sub>2</sub> NH	Ajax Finechem, 98.5%	Synthesis of ZnO
5. Ethanol C <sub>2</sub> H <sub>6</sub> O	VWR Internation, 99.9%	Synthesis of ZnO
6. DI-Water H <sub>2</sub> O		Synthesis of ZnO, Mobile phase for HPLC analysis
7. Hydrochloric acid HCl	J. T. Baker, 37.7%	Synthesis of ZnO, Adjust pH
8. Sodium hydroxide NaOH	Ajax Finechem, 97%	Adjust pH
9. Isoproturon [3-(4-isopropylphenyl)-1,1-dimethyl-urea]	Sigma-Aldrich Laborchemikalien GmbH, 99.9%	Substrate of degradation
10. Acetonitrile CH <sub>3</sub> CN	RCI Labscan, 99.9%	Mobile phase for HPLC analysis

### 3.2 Synthesis of Zinc Oxide Nanoparticles

Zinc oxide nanoparticles was prepared according to the method proposed by Tian et al. [9] as well. Zinc acetate was used as a precursor to prepare ZnO sol. At first, 3.29 g of zinc acetate was dissolved in 20 ml ethanol and stirred at 50°C for 5 min to get the precursor solution. In the mean time, 0.26 ml of distilled water, 1.58 ml of diethanolamine, 0.18 ml of hydrochloric acid and 5 ml of ethanol were mixed together. Then, the solution was dropped into the precursor solution under strong stirring. After stirring for 2 hours, a transparent ZnO sol was obtained. The ZnO sol was gelled at room temperature and dried in an oven at 80°C for 24 hours. Then, the obtained product was calcined in a furnace at 500 °C for 2 hours with heating rate of 10°C/min.

### 3.3 Characterizations of the Photocatalysts

The photocatalysts were characterized by various techniques, as following:

Phase composition of the photocatalysts was determined though X-ray diffraction (XRD) method by Bruker AXS D8 Advance using Cu K $\alpha$  radiation of wavelength 1.5406 Å at 40 kv. The measurements were carried out in the 2 $\theta$  range of 20-80 degree with 0.04 degree scan step. The half-height width of the diffraction peak of XRD pattern was analyzed by Debye-Scherrer equation to calculate the crystallite size of synthesized photocatalysts. The Debye-Scherrer equation is given by

$$D = \frac{k\lambda}{\beta \cos \theta} \quad (3.1)$$

where  $D$  is crystal size,  $k$  is a constant equal to 0.9,  $\lambda$  is wavelength of X-ray,  $\beta$  is full width at half maximum and  $\theta$  is diffraction angle.

The specific surface area, pore volume and pore size distribution of the synthesized photocatalysts were determined by nitrogen adsorption-desorption analysis. The specific surface area were calculated using the Brunauer-Emmett-Teller model (BET) and the pore size distributions were obtained from desorption branches of the isotherms using the Barret, Joyner, Halenda method (BJH), by Belsorp mini II BEL, Japan at the Center of Excellence on Particle Technology, Chulalongkorn University. The operating conditions are as follows:

Sample weight	~ 0.1- 0.2 g
Degas temperature	200°C
Vacuum pressure	< 10 mmHg

The band gap of all photocatalysts was measurement by UV-VIS spectrophotometer analysis on UV-Vis-NIR (Cary 5000, Agilent Technologies, Australia), wavelength between 220 and 800 nm and step size 1 nm at National Nanotechnology Center (NANOTEC).The spectra recorded at wave number 400-800  $\text{cm}^{-1}$ . The Tauc plot is a method that is widely used for the determination of band gap, the relational expression proposed by Tauc, Davis, and Mott as follows:

$$(h\nu\alpha)^{1/n} = A(h\nu - E_g) \quad (3.2)$$

The acquired diffuse reflectance spectrum is converted to Kubelka-Munk function. Thus, in the actual experiment, the relational expression becomes:

$$[f(R_\infty)h\nu]^2 = A(h\nu - E_g) \quad (3.3)$$

where  $h$  is Planck's constant ( $6.63 \times 10^{-34}$ ),  $\nu$  is frequency of vibration,  $\alpha$  is absorption coefficient,  $E_g$  is band gap enegy,  $A$  is proportional constant and  $n$  is the value of the exponent equal to 1/2.

Finally, the thermal behavior of the synthesized photocatalysts was analyzed by using thermo-gravimetric analysis (TGA) on a Mettler-Toledo TGA/DSC1 STARe System at Center of Excellence in Particle and Technology Engineering laboratory, Chulalongkorn University. The samples were analyzed using heating rate of 10°C/min in 40 ml/min flow of oxygen from temperature of 25 to 1000°C.

### 3.4 Adsorption Studies

All adsorption equilibrium experiments of isoproturon onto the surface of titanium dioxide and zinc oxide were carried out in batches under stirring in the dark condition at the room temperature. Studies were conducted with suspensions prepared by mixing the photocatalyst with 200 ml of isoproturon solution which initial concentration solution was varies from 1, 5, 10, 15 to 20 ppm, respectively, and the content of the photocatalyst was kept



at 1 mg/1 ml of the isoproturon solution. The concentration of isoproturon was measured by high performance liquid chromatography (HPLC). The HPLC system included reverse phase C18 (Luna 5 $\mu$  C18 (2), 250x4.6 mm, Phenomenex, USA) with a mobile phase of 70% (v/v) acetonitrile and 30% (v/v) DI water; a flow rate of 1.5 ml/min and a UV detector at 254 nm.

### 3.5 Photodegradation Apparatus

#### 3.5.1 Photodegradation Apparatus

The schematic diagram of the photodegradation apparatus used in this work is shown in Figure 3.1. The equipments of the apparatus and their functions are described as the follows.

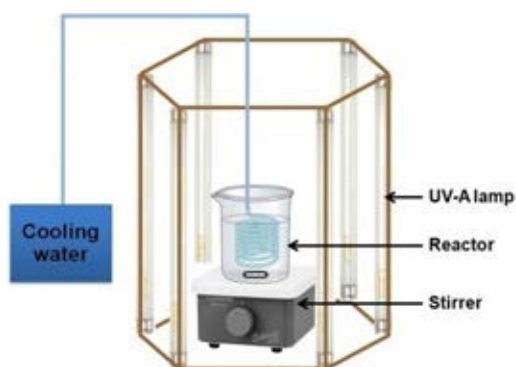


**Figure 3.1** Diagram of the equipment setup for the photocatalytic degradation.

The system is consisting of:

- Cooling coil is used as a temperature controller during the experiment at  $30 \pm 2$  °C.
- 6 UV-A lamps (Phillips TLD 15W/05) is used as a light source of the photocatalytic reaction.
- A magnetic stirrer is used to generate turbulent conditions in mixture to keep the mixture is in homogeneous during the experiment.

#### 3.5.2 Photodegradation Experiment

The photocatalytic activities of the synthesized photocatalysts were determined from the photodegradation of isoproturon solution under UV irradiation. The

photodegradation was conducted in a 600 ml pyrex reactor in which 550 ml of isoproturon solution and photocatalysts were added. In general, isoproturon is contaminated in water approximately 0.0001 ppm. so the initial concentration is 10 ppm. The content of the photocatalyst was kept at 1 mg of the catalyst per 10 ml of the solution. Prior to the start of the reaction, the mixture was kept in dark for 30 min under continuously stirring to allow the complete adsorption of isoproturon on to the surface of catalysts. After that, the solution was irradiated with six UV-A lamps and continuously stirred by a magnetic stirrer to keep the catalyst uniformly dispersed within the solution.

### *3.5.3 Analyses*

The isoproturon solution was periodically collected during irradiation to monitor the concentration of isoproturon by using HPLC. The HPLC peak heights were used instead HPLC peak area due to some peak is overlap each other. The sample collected at regular intervals during the irradiation was filtered through micro syringe filters (0.45  $\mu\text{m}$ ). While the total organic carbon (TOC) analyzer (Shimadzu, TOC-VCPH) measures the depletion in total organic carbon for monitoring mineralization of isoproturon. Furthermore, an attempt will be made to identify the intermediate products formed in the photocatalytic degradation of isoproturon in aqueous suspension of photocatalysts through LC-MS analysis (Bruker Daltonics). The mass spectrometer was equipped with phenyl column (Vertisep UPS column, 2.1x100mm) and an ESI ion source operating in positive ion mode in the range 70-1,000 m/z. The mobile phase was 60% (v/v) acetonitrile mixed with 40% (v/v) deionized water and total flow rate was 0.2 ml/min.

## **CHAPTER IV**

### **RESULTS AND DISCUSSION**

The photocatalytic reaction on photocatalysts can be applied to remove many organic compounds from wastewater. In this research, the photocatalytic degradation of isoproturon on commercial titanium dioxide, commercial zinc oxide and synthesized zinc oxide were investigated. Properties of photocatalysts were characterized by various techniques. Moreover, the formation of intermediates during the photocatalytic degradation will be identified.

#### **4.1 Properties of Photocatalysts**

In this research, commercial titanium dioxide and zinc oxide were purchased from Sigma Aldrich and Thai-Lysaght company limited, respectively, while synthesized zinc oxide was synthesized by sol gel method and subsequently calcined at 500°C for 2 hours. Physical properties of photocatalysts were characterized by many techniques such as X-ray Diffraction analysis (XRD), nitrogen adsorption-desorption analysis, UV-VIS spectroscopy and thermogravimetric analysis (TGA).

Commercial titanium dioxide, commercial zinc oxide and synthesized zinc oxide powder were analyzed by XRD. The result confirms that the diffraction peaks of commercial titanium dioxide could be inferred to anatase and rutile phase, as shown in Figure 4.1. For commercial zinc oxide and synthesized zinc oxide, the XRD patterns indicated both of commercial and synthesized zinc oxide are wurtzite phase, as shown in Figure 4.2.

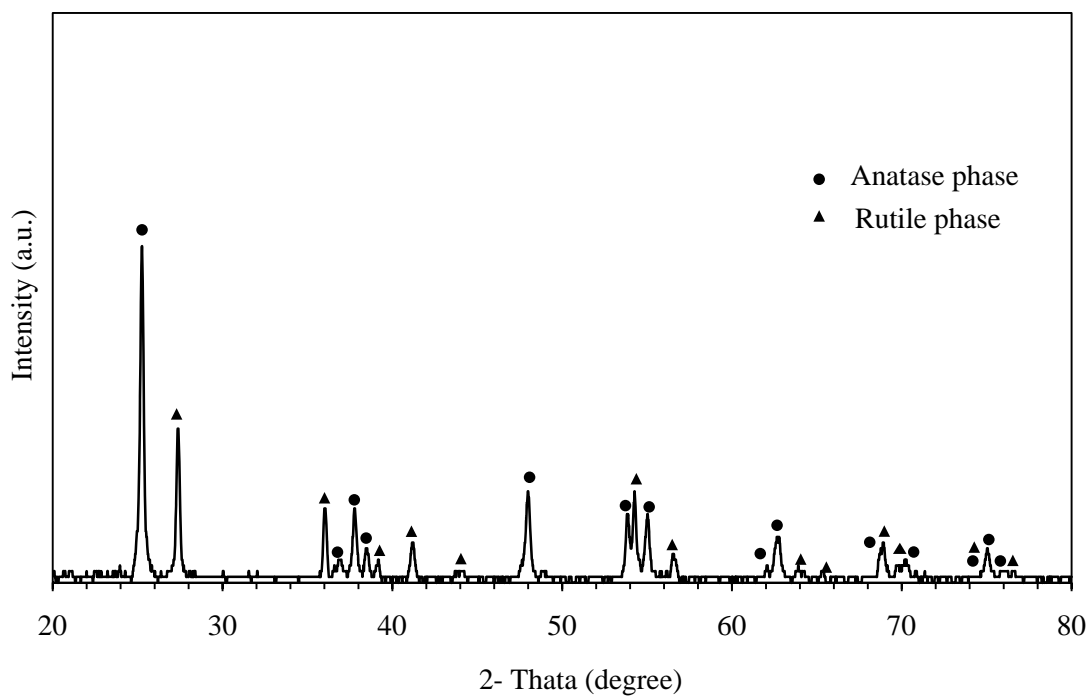


**Figure 4.1** XRD patterns of the commercial titanium dioxide powder.

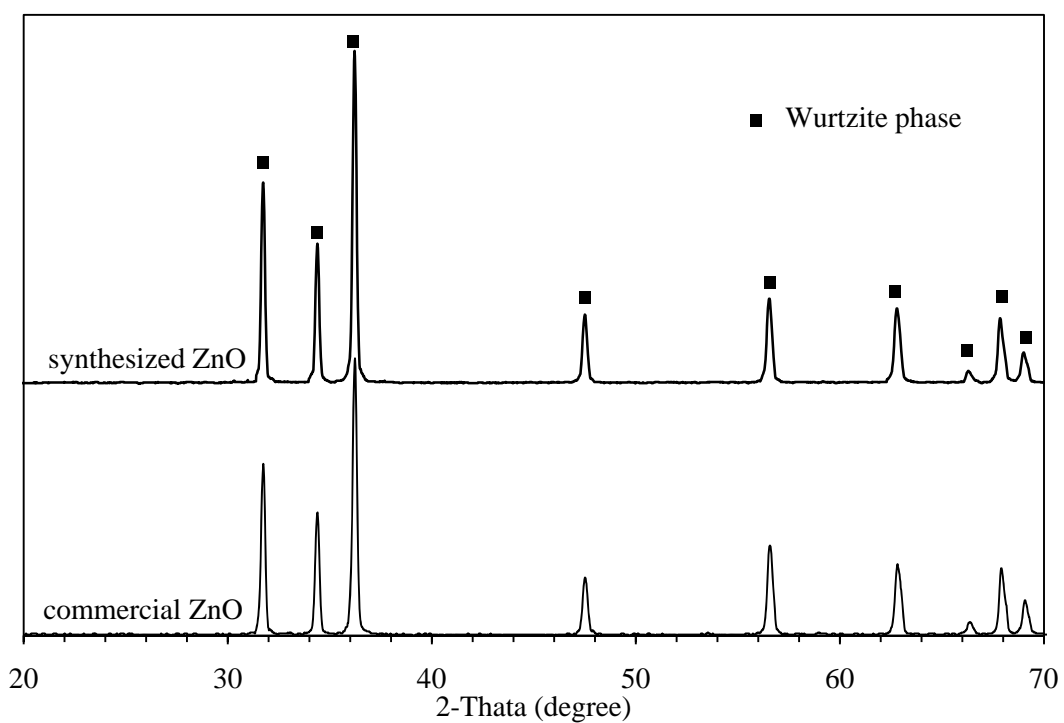


**Figure 4.2** XRD patterns of the commercial zinc oxide and synthesized zinc oxide powder.

The crystallite size of all catalysts was determined from the half-height width of the diffraction peak of XRD pattern, using the Debye-Scherrer equation:

$$D = \frac{k\lambda}{\beta \cos \theta} \quad (4.1)$$

where  $D$  is crystal size,  $k$  is a constant equal to 0.9,  $\lambda$  is wavelength of X-ray (1.5406 Å),  $\beta$  is full width at half maximum and  $\theta$  is diffraction angle. The calculated results are shown in Table 4.1.

**Table 4.1** Crystallite size and surface area of photocatalysts.

Catalyst	Crystallite size, (nm)	Specific surface area, $S_{\text{BET}}$ , ( $\text{m}^2/\text{g}$ )	Average pore diameter (nm)	Band gap energy (eV)
Commercial $\text{TiO}_2$	Anatase : 32.36 Rutile : 80.48	25.51	5.8	3.4
Commercial ZnO	44.26	4.62	5.4	3.3
Synthesized ZnO	46.30	3.33	6.8	3.2

The specific surface area for all catalysts measured by nitrogen adsorption-desorption are also shown in Table 4.1. Figure 4.3- 4.5 show nitrogen adsorption-desorption isotherms of commercial titanium dioxide, commercial zinc oxide and synthesized zinc oxide, respectively. The results show that the adsorption-desorption isotherm of the commercial titanium dioxide is type-II, which indicates non-porosity, moreover those of both commercial zinc oxide and synthesized zinc oxide are type-II, which indicates non-porosity.

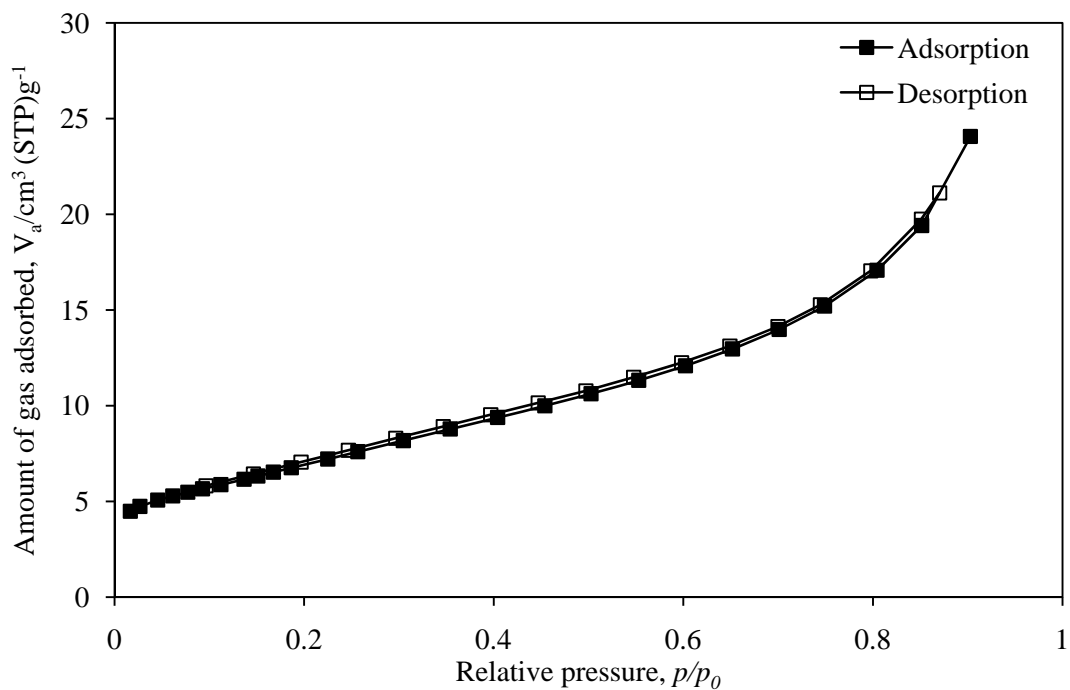


**Figure 4.3** Adsorption/desorption isotherm of commercial titanium dioxide.

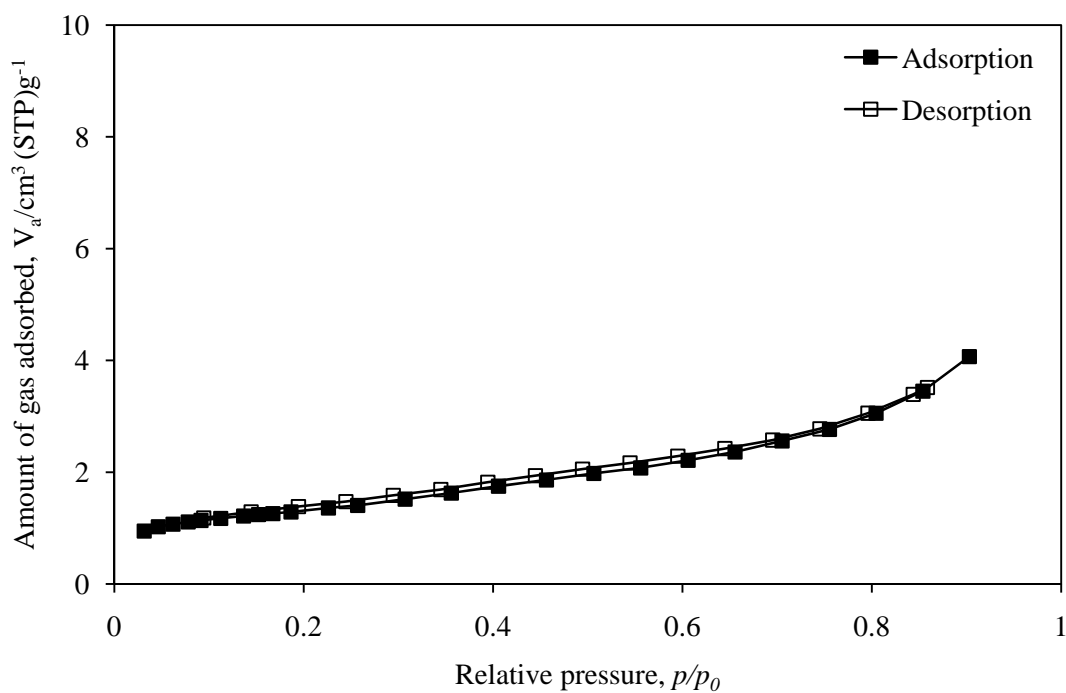


**Figure 4.4** Adsorption/desorption isotherm of commercial zinc oxide.

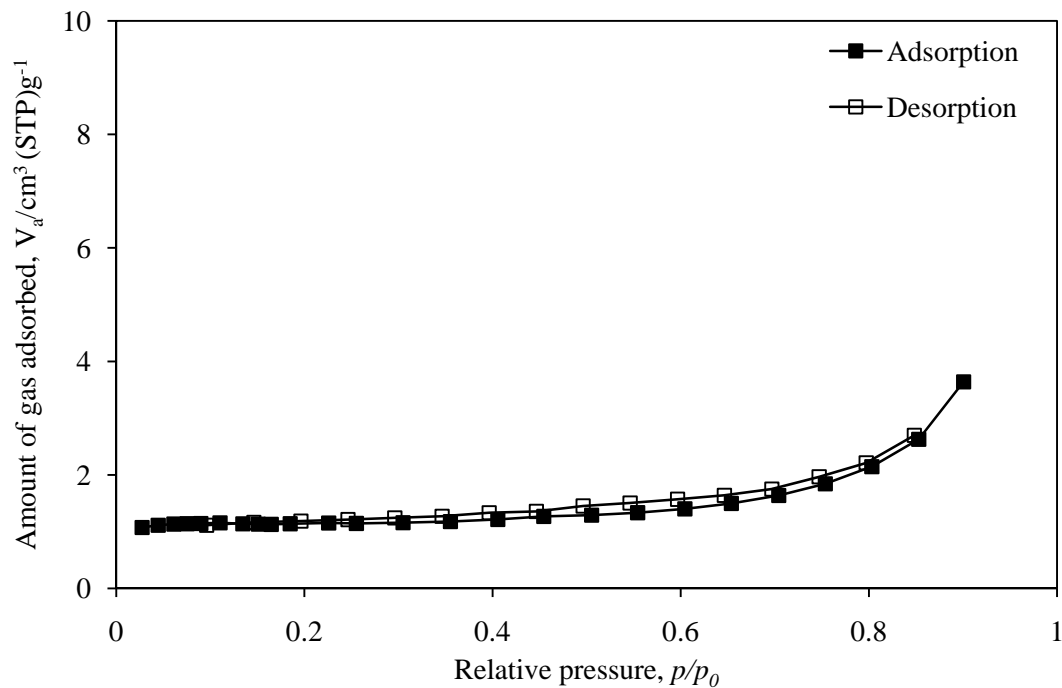


**Figure 4.5** Adsorption/desorption isotherm of synthesized zinc oxide.

The band gap of all photocatalysts was determined from their UV absorption spectrum. When a semiconductor absorbs photons of energy larger than the gap of the semiconductor, an electron is transferred from the valence band to the conduction band where there occurs an abrupt increase in the absorbency of the material to the wavelength corresponding to the band gap energy. The Tauc plot is a method that is widely used for the determination of band gap, the relational expression proposed by Tauc, Davis, and Mott as follows:

$$(h\nu\alpha)^{1/n} = A(h\nu - E_g) \quad (4.2)$$

where  $h$  is Planck's constant ( $6.63 \times 10^{-34}$ ),  $\nu$  is frequency of vibration,  $\alpha$  is absorption coefficient,  $E_g$  is band gap energy,  $A$  is proportional constant and  $n$  is the value of the exponent equal to 1/2.

The acquired diffuse reflectance spectrum is converted to Kubelka-Munk function. Thus, in the actual experiment, the relational expression becomes:

$$[f(R_\infty)h\nu]^2 = A(h\nu - E_g) \quad (4.3)$$

The band gap energy of photocatalysts was determined from the intersection of the tangent line and the x-axis, as shown in Figure 4.6-4.8. The result values are presented in Table 4.1

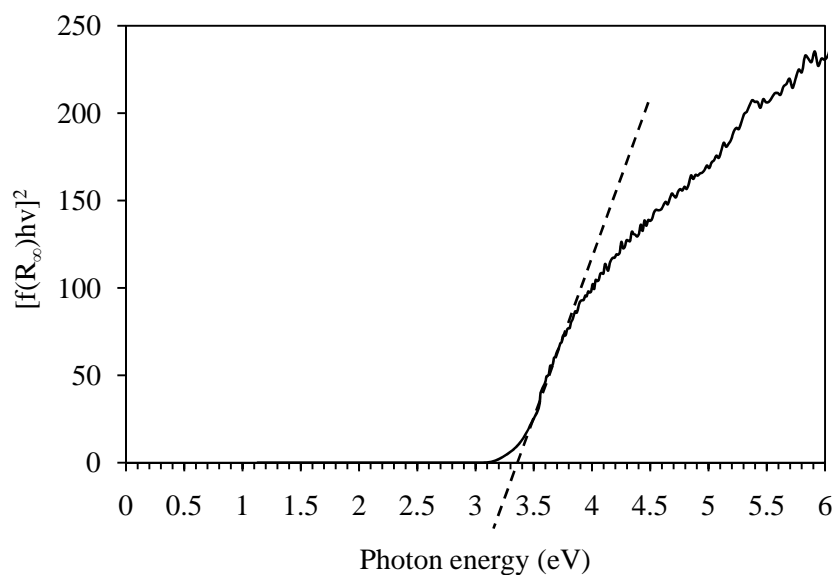


**Figure 4.6** Absorbance spectra of commercial titanium dioxide

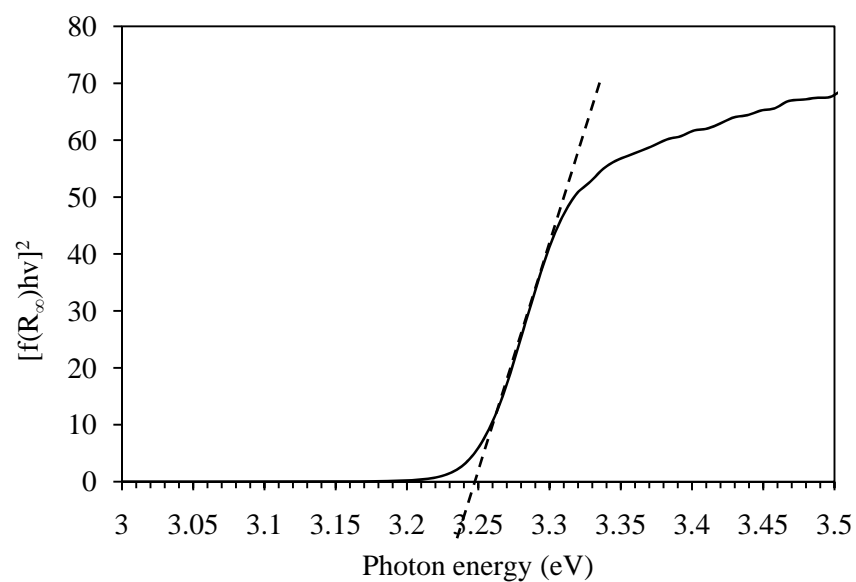


**Figure 4.7** Absorbance spectra of commercial zinc oxide



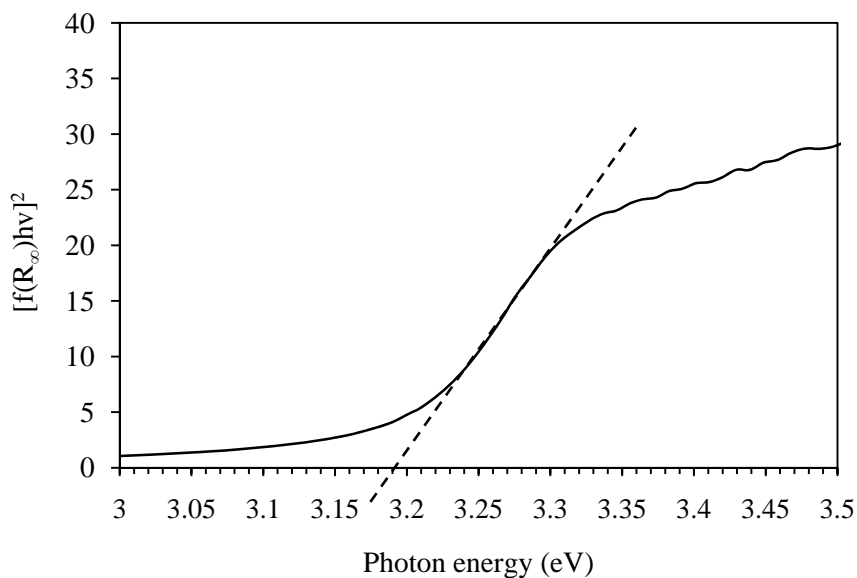


**Figure 4.8** Absorbance spectra of synthesized zinc oxide.

The thermogravimetric result for the synthesized zinc oxide powder, after calcined at 500°C for 2 hours, heated from 25-1000°C in 40 ml/min flow of oxygen is shown in Figure 4.9. The TGA result indicates that there is no weight loss which confirms that the synthesized zinc oxide had no residual organics compound within the powder. Therefore, it can be assumed that calcination temperature of 500°C is enough for complete combustion of organic residue in the catalyst.

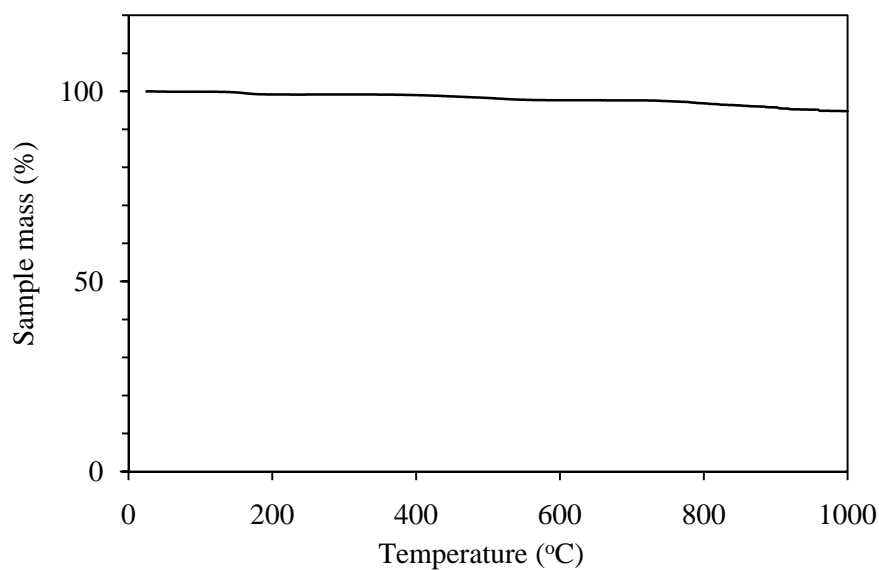


**Figure 4.9** TGA curves of the synthesized zinc oxide powder after calcined at 500°C for 2 h.

## 4.2 Adsorption Studies

In this section, isotroturon was adsorbed onto the surface of the photocatalysts. The adsorption experiments were carried out in batches under stirring in the dark condition at the natural pH and at the room temperature. Studies were conducted with suspensions prepared by mixing the photocatalyst with 200 ml of isotroturon solution in which initial concentration solution was varied from 1, 5, 10, 15, to 20 ppm, respectively, and the content of the photocatalyst was kept at 1 mg/1 ml of the isotroturon solution. The concentration of isotroturon was measured by high performance liquid chromatography (HPLC). From the adsorption studies, the degrading reaction is not occurred in these studies. Figure 4.10 -4.12 show the adsorption of isotroturon on commercial titanium dioxide, commercial zinc oxide and synthesized zinc oxide respectively. The results exhibit that the quantity of isotroturon adsorbed increases with increasing the concentration of isotroturon since increased isotroturon concentration may lead higher chance of molecules of isotroturon interact with the catalyst [47].

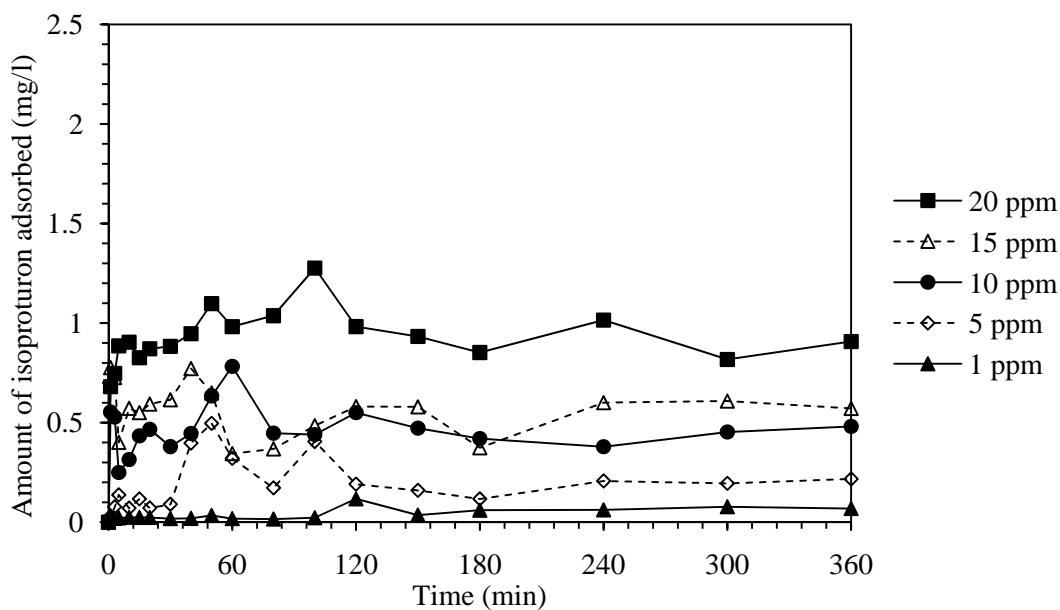


**Figure 4.10** Adsorption of isotroturon on the surface of commercial titanium dioxide when the initial concentration was 1, 5, 10, 15 and 20 ppm.

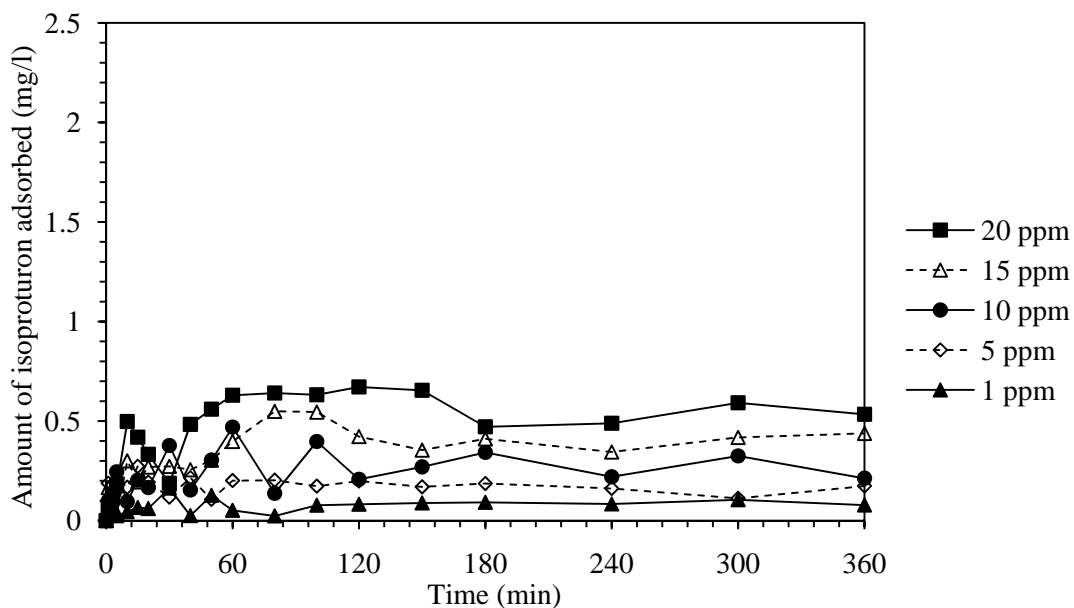


**Figure 4.11** Adsorption of isotroturon on the surface of commercial zinc oxide when the initial concentration was 1, 5, 10, 15 and 20 ppm.

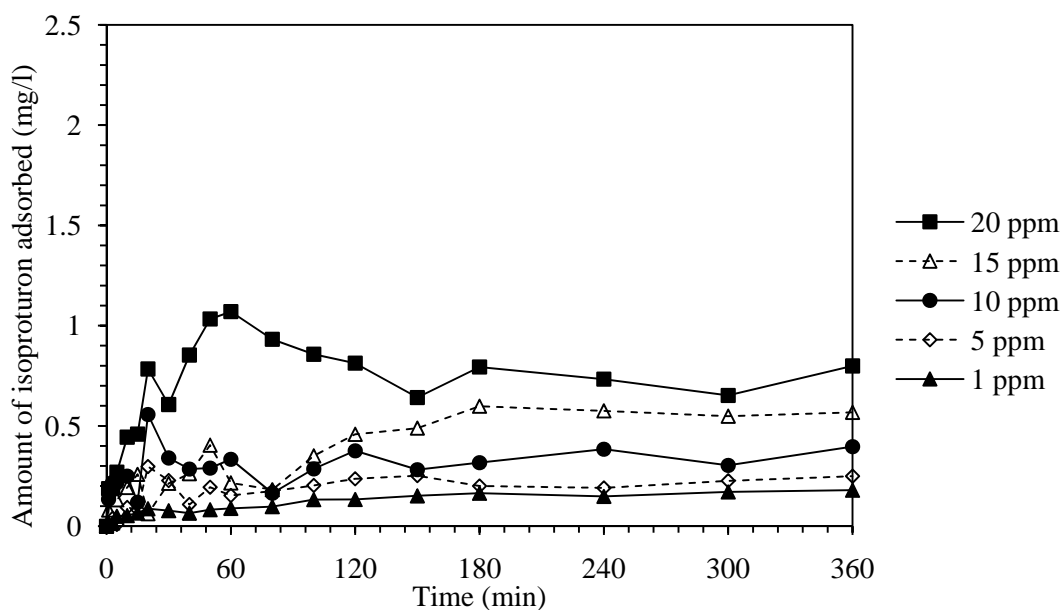


**Figure 4.12** Adsorption of isotroturon on the surface of synthesized zinc oxide when the initial concentration was 1, 5, 10, 15 and 20 ppm.

The sorption ability of the photocatalyst can be investigated from the adsorption isotherm. The adsorption isotherms of isotroturon on commercial titanium dioxide, commercial zinc oxide and synthesized zinc oxide at room temperature are shown in Figure

4.13. It is found that the amount of isoproturon adsorbed at equilibrium increases with the concentration of isoproturon for all catalysts.

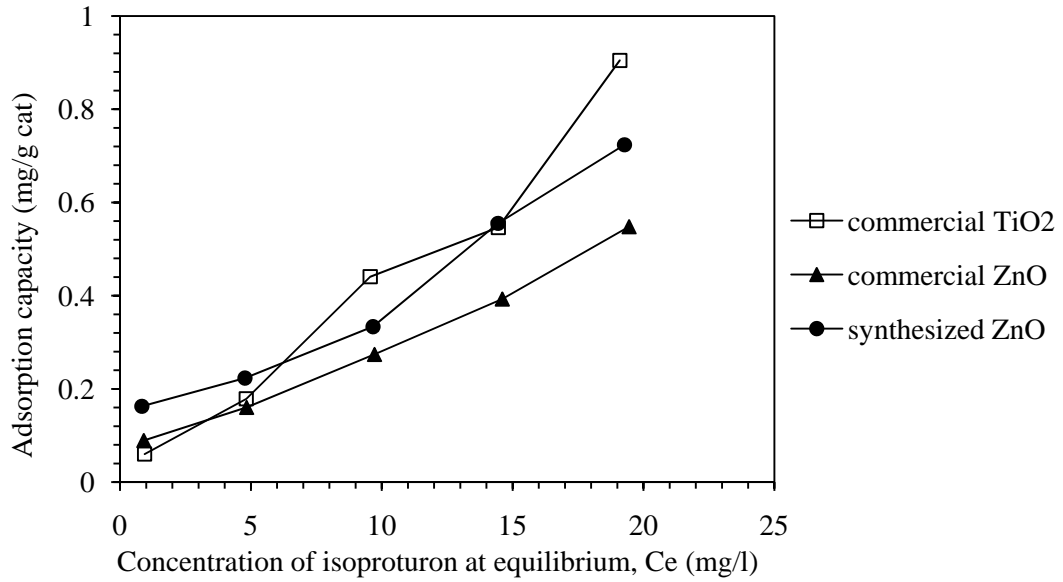


**Figure 4.13** Adsorption isotherm of isoproturon onto the surface of commercial titanium dioxide, commercial zinc oxide and synthesized zinc oxide at room temperature.

The adsorption isotherm can provide information about the nature of the physico-chemical interaction involved in the adsorption process [47]. In this study, Langmuir and Freundlich isotherm models were used to describe the adsorption process of isoproturon on the catalyst surfaces. The Langmuir isotherm has been used for monolayer adsorption. The linearized form of the Langmuir isotherm model is [44]:

$$\frac{1}{q_e} = \frac{1}{q_{\max}} + \frac{1}{bq_{\max}} \frac{1}{C_e} \quad (4.4)$$

where  $q_e$  is amount of adsorbate on adsorbent at equilibrium (mg/g),  $q_{\max}$  is maximum adsorption capacity (mg/g),  $C_e$  is equilibrium concentration (mg/l), and  $b$  is Langmuir's equilibrium constant related to energy of the sorption system (l/mg).

For the Freundlich isotherm, it is used for a system with heterogeneous surface energy to describe multilayer adsorption. The Freundlich isotherm is represented in logarithmic form as follow [44, 46]:

$$\ln q_e = \ln K_f + \frac{1}{n} \ln C_e \quad (4.5)$$

where  $q_e$  is amount of adsorbate on adsorbent at equilibrium (mg/g),  $C_e$  is equilibrium concentration (mg/l),  $1/n$  is adsorption intensity and  $K_f$  is Freundlich constant related to adsorption capacity ( $\text{mg/g}(\text{mg/l})^{-1/n}$ ).

Figure 4.14 (a) - (f) show the fitting of the experimental data against the Langmuir and Freundlich models of the adsorption isoproturon on commercial titanium dioxide, commercial zinc oxide and synthesized zinc oxide. The fitted parameters derived from these plots are presented in Table 4.2. The results reveal that the adsorption behaviors of isoproturon onto titanium dioxide and zinc oxide are different, as observed from  $R^2$ . The adsorption of isoproturon onto the surface of titanium dioxide is well represented by the Langmuir isotherm model, which is based on the assumption of monolayer adsorption. On the other hand, for the adsorption on zinc oxide, both of commercial zinc oxide and synthesized zinc oxide, it shows a better fit with the Freundlich isotherm model that describes the multilayer adsorption.

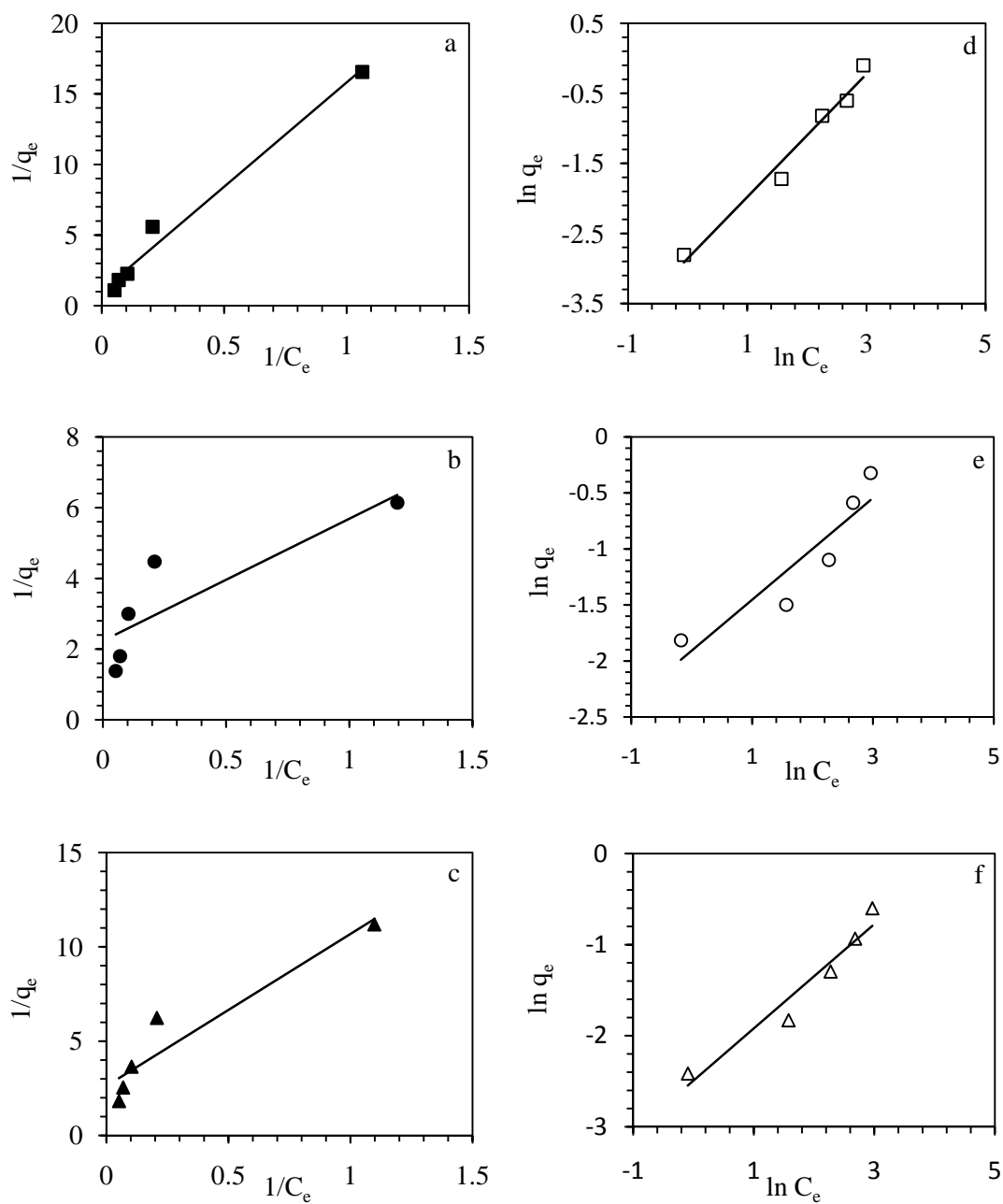


**Figure 4.14** Langmuir isotherm (a-c) and Freundlich isotherm (d-f) for adsorption of isotipuron on: (■) commercial titanium dioxide, (●) commercial zinc oxide and (▲) synthesized zinc oxide.

**Table 4.2** Parameters of Langmuir and Freundlich isotherm models for adsorption of isoproturon on commercial TiO<sub>2</sub>, commercial ZnO and synthesized ZnO.

Models	Parameters	Catalyst		
		Commercial TiO <sub>2</sub>	Commercial ZnO	Synthesized ZnO
Langmuir isotherm model	$q_{max}$	0.9550	0.3808	0.4475
	$b$	0.0709	0.3257	0.6472
	$R^2$	0.9824	0.9000	0.7390
Freundlich isotherm model	$K_f$	0.0573	0.0827	0.1485
	$n$	1.1392	1.7461	2.2036
	$R^2$	0.9756	0.9408	0.8440

The essential characteristic of the Langmuir isotherm can be expressed in terms of a dimensionless equilibrium parameter, separation factor  $r$  was calculated by following equation [44, 45]:

$$r = \frac{1}{1 + bC_0} \quad (4.6)$$

Value of  $r > 1$  represents unfavorable adsorption condition, and value of  $0 < r < 1$  represents favorable adsorption conditions [44, 45]. In this case,  $r$  value is between 0 and 1 (0.5851 for commercial titanium dioxide), suggesting that the sorption is favorable for isoproturon on titanium dioxide.

For Freundlich's parameter relates to the mean energy of adsorption. A very weak adsorbent/adsorbate interaction occurs at values of  $n < 1$ , while  $n > 1$  suggests a strong adsorbent/adsorbate interaction. At value of  $n = 1$ , it is assumed that all sites are energetically similar [29]. In this case, value of  $n > 1$  for adsorption of isoproturon on both of commercial zinc oxide and synthesized zinc oxide, It indicated strong isoproturon and catalyst interaction. This was confirmed by the values of Freundlich's constant,  $K_f$ , which also relates to the adsorption capacity.

### 4.3 Photodegradation of Isoproturon

In recent year, the photocatalytic degradation process has been extensively proposed as an attractive alternative for the treatment of contaminated ground, surface, and wastewater containing pesticides or non-biodegradable organic [2], such as isoproturon. This process is generally based on the generation of hydroxyl radicals which interact with organic pollutants leading to progressive degradation and subsequently complete mineralization. The degradation of isoproturon can be expressed by the following reaction [2, 3]:



The complete mineralization is expressed by the following equation:



In this work, the photodegradation of isoproturon in an aqueous solution using commercial titanium dioxide, commercial zinc oxide and synthesized zinc oxide as the photocatalyst was conducted in a 600 ml pyrex reactor in which 550 ml of isoproturon solution. The content of the photocatalyst was kept at 1 mg of the catalyst per 10 ml of the solution (initial isoproturon concentration of 10 ppm.). Prior to the start of the reaction, the mixture was kept in dark for 30 min under continuously stirring to allow the complete adsorption of isoproturon on to the surface of catalysts. The photodegradation of isoproturon solution was investigated for 6 hours of UV-A irradiation. The photocatalytic activities of photocatalysts were determined from the photodegradation of isoproturon. The results are shown in Figure 4.15 compared with the photolysis result. It can be observed that the degradation of isoproturon in absence of catalyst is 14% after 6 hours of UV irradiation, which is much slower than photocatalytic degradation of isoproturon on catalysts. Thus it can be inferred that there is no significant degradation when the isoproturon solution is irradiated in the absence of photocatalysts.



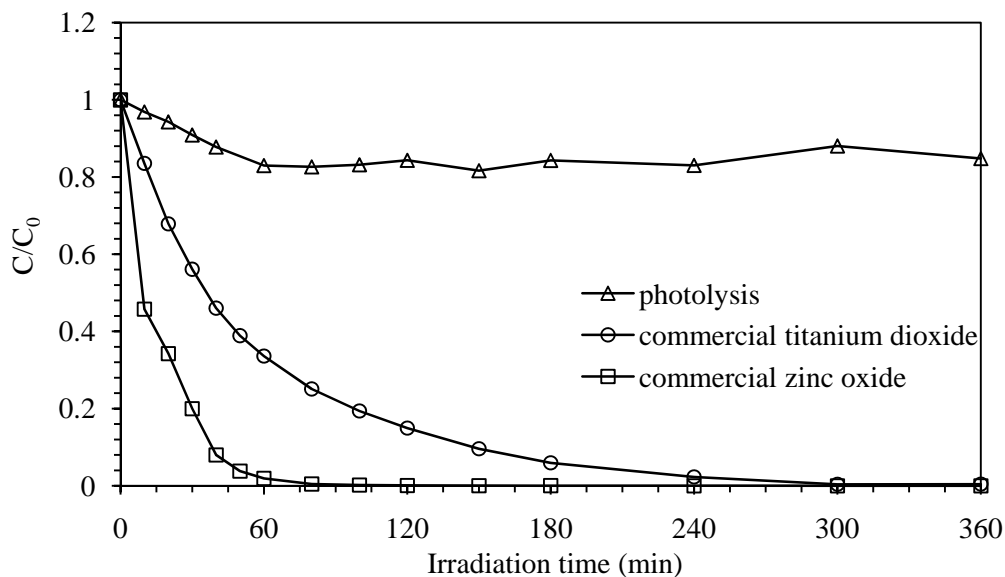


**Figure 4.15** Concentration of isoproturon with respect to the initial isoproturon concentration ( $C/C_0$ ) during the photocatalytic degradation on: ( $\Delta$ ) photolysis, ( $\circ$ ) commercial titanium dioxide and ( $\square$ ) commercial zinc oxide.

#### 4.3.1 Comparative Study of Photocatalytic Degradation of Isoproturon on Commercial Titanium Dioxide and Commercial Zinc Oxide

Concentration of isoproturon during the photocatalytic degradation with respect to the initial isoproturon concentration ( $C/C_0$ ) when the commercial titanium dioxide and zinc oxide were used as catalyst are shown in Figure 4.15. The results show that the degradation of isoproturon on commercial titanium dioxide is about 99% within 6 hours while that on commercial zinc oxide can reach complete degradation within only 3 hours of UV-irradiation. In the other words, zinc oxide exhibits much higher photocatalytic activity than titanium dioxide.

According to many researchers, kinetic of the photodegradation of many organic pollutants is described by the pseudo-first order kinetic.

$$r = -\frac{dC}{dt} = k_r KC = k_{ap} C \quad (4.7)$$

where  $r$  is the rate of isoproturon degradation,  $C$  is the concentration of the isoproturon being degraded,  $k_{ap}$  is the apparent rate constant of a pseudo first order model,  $t$  is the irradiation time. For batch operation, Eq. (4.7) can be integrated to Eq. (4.8) when  $C_0$  is an initial concentration of isoproturon.

$$\ln \frac{C_0}{C} = k_{ap} t \quad (4.8)$$

Kinetics studies were assessed by monitoring the change in the concentration of isoproturon at certain interval of time. The apparent rate constants have been used to calculate degradation rate for the degradation of isoproturon on commercial titanium dioxide and zinc oxide. The results are shown in Figure 4.16. The apparent rate constant ( $k_{ap}$ ) can be determined from the slope of the curve obtained. The apparent rate constants for commercial titanium dioxide and zinc oxide are shown in Table 4.3.

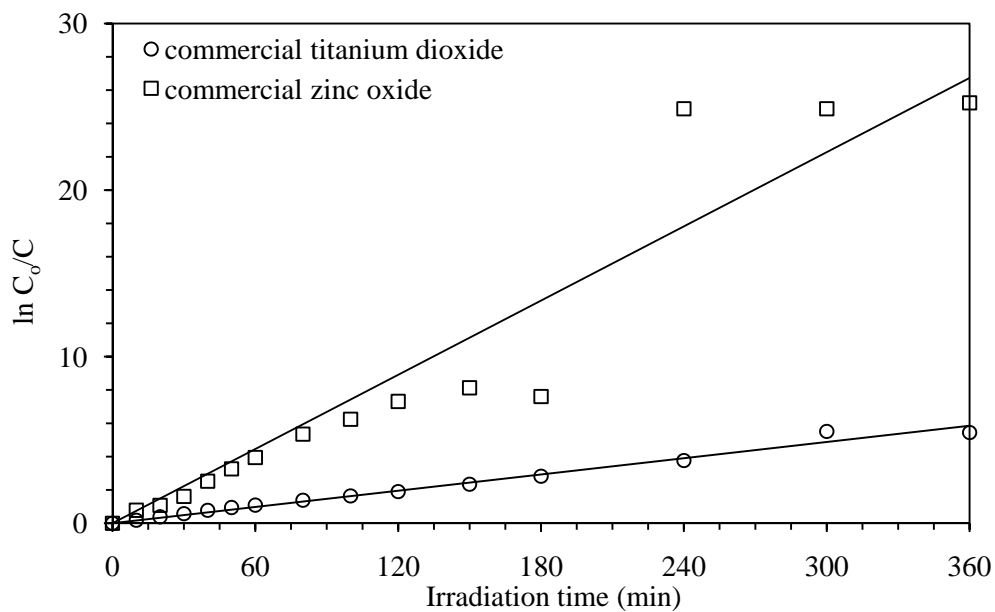


**Figure 4.16** First-order linear transforms plot of the photocatalytic degradation on: (○) commercial titanium dioxide, (□) commercial zinc oxide.

Moreover, the Langmuir – Hinshelwood kinetic model is also suitable for representing photocatalytic reaction, it is assumed that the reaction occurs on the surface and the rate of reaction ( $r$ ) is proportional to the fraction of surface covered by the substrate ( $\theta$ ) [42]:

$$r = -\frac{dC}{dt} = k_r \theta = k_r \frac{KC}{1 + KC} \quad (4.9)$$

This equation can be integrated, becoming:

$$\ln\left(\frac{C_0}{C}\right) + K(C_0 - C) = k_r K t \quad (4.10)$$

where  $C_0$  is the initial concentration of the organic substrate,  $C$  is the concentration of the substance being degraded,  $K$  is the constant of adsorption equilibrium,  $k_r$  is true rate constant and  $t$  is the irradiation time.

From the experiment data, it was observed that the first-order kinetics does not provide a good fit to the experimental data. On the other hand, the degradation results were well fitted in the Langmuir-Hinshelwood (L-H) kinetic model when the commercial titanium dioxide and commercial zinc oxide were used as the catalyst. The fitted results, i.e. the reaction rate constants ( $k_r$ ), and the adsorption constants ( $K$ ) are shown in Table 4.3.

**Table 4.3** The apparent rate constant ( $k_{ap}$ ), reaction rate constants ( $k_r$ ), and the adsorption constant ( $K$ ) for the photocatalytic degradation of isotroturon using commercial titanium dioxide and commercial zinc oxide as catalyst.

Catalyst	Pseudo-first order kinetic model		Langmuir-Hinshelwood (L-H) kinetic model		
	$k_{ap}$ ( $\text{min}^{-1}$ )	$R^2$	$k_r$ (ppm/min)	$K$ ( $\text{ppm}^{-1}$ )	$R^2$
Commercial TiO <sub>2</sub>	0.0163	0.9846	0.6155	0.0298	0.9873
Commercial ZnO	0.0743	0.9074	4.6383	0.0149	0.9737

Comparison of commercial titanium dioxide and commercial zinc oxide, it is observed that the reaction rate constant of the commercial zinc oxide is much higher than that of the commercial titanium dioxide thus, the reaction of isotroturon occur on commercial zinc oxide is faster than the synthesized zinc oxide. While the adsorption constant of the commercial titanium dioxide is higher than that of the commercial zinc oxide due to commercial titanium dioxide has much higher specific surface area which is adsorb more isotroturon on the surface. The adsorption constant is in accordance with the results from adsorption experiment moreover, the results show that the degradation rate is much more than adsorption rate.

The decrease of TOC (Total Organic Carbon) as a result of mineralization of isoproturon was also observed during the degradation process. Figure 4.17 shows the depletion in TOC as a function of time on irradiation of an aqueous solution of isoproturon. From the result, although isoproturon can be degraded using commercial titanium dioxide and commercial zinc oxide as catalyst, TOC reduction in the photocatalytic degradation for commercial titanium dioxide and commercial zinc oxide were decreased only by 40% at the end of degradation (within 6 hours) which confirms that the photocatalytic degradation process can decompose isoproturon and generates reaction intermediates during the degradation of isoproturon. Moreover, TOC results can be observed that the decreasing of TOC on commercial zinc oxide is lower than that on commercial titanium dioxide although commercial zinc oxide shows higher degradation than commercial titanium dioxide due to quantity of intermediates which are generated during the reaction on commercial zinc oxide is much higher than that on commercial titanium dioxide in addition, the structure of intermediates may be more complex and then it cannot degraded later.

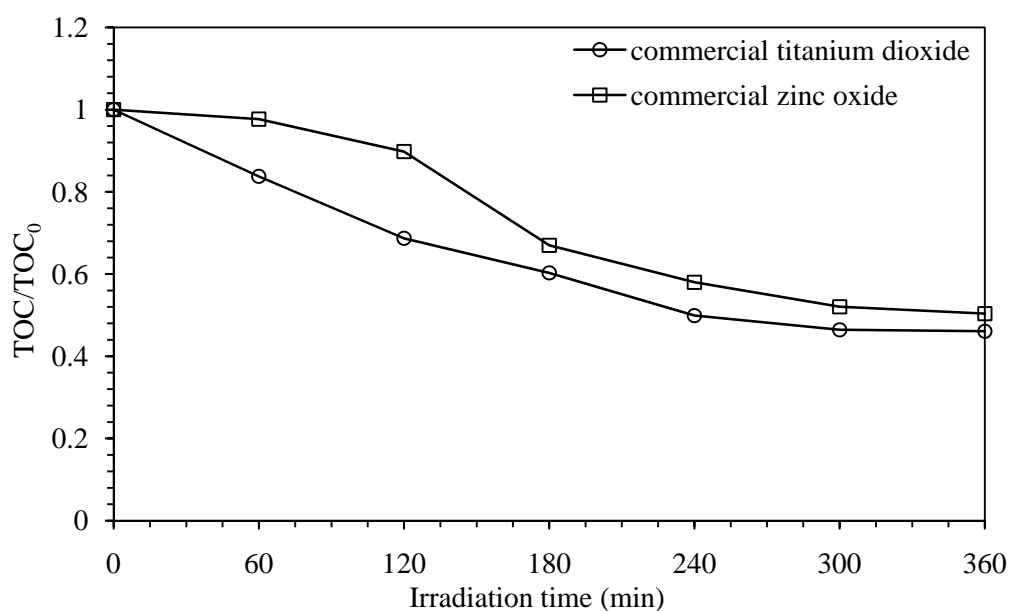


**Figure 4.17** Total organic carbon (TOC) with respect to the initial TOC of isoproturon solution ( $\text{TOC}/\text{TOC}_0$ ) during the photocatalytic degradation on: (○) commercial titanium dioxide and (□) commercial zinc oxide.

From the experiment results, both titanium dioxide and zinc oxide have been known to be capable of producing of radicals upon the exposure with UV light. On the other hand, it was found that the catalytic activity of commercial zinc oxide is greater than that of

commercial titanium dioxide in degradation of isoproturon although, the specific surface area of zinc oxide is one order of magnitude lower than that of titanium dioxide. It is indicated that the surface area is not the major factor affecting the extent of decomposition. The band energy position of photocatalysts may be a reason for greater photocatalytic activity of commercial zinc oxide. Although energy band gaps of zinc oxide and titanium dioxide are relatively the same, the band position of zinc oxide and titanium dioxide are different. The band position of titanium dioxide and zinc oxide are shown in Table 4.4. The valence band energy for zinc oxide is lower than that of titanium dioxide, which infers that the valence holes of zinc oxide (and the hydroxyl radicals) should have greater oxidizing power ( $2\text{H}_2\text{O} \rightarrow \text{O}_2 + 4\text{H}^+ + 4\text{e}^-$ ;  $E^0=1.23\text{ V}$ ) [48]. The conduction band energy of titanium dioxide is close to the potential required to electrolytically reduce water to hydrogen gas ( $2\text{H}_2\text{O} + 2\text{e}^- \rightarrow \text{H}_2 + 2\text{OH}^-$ ;  $E^0=0\text{ V}$ ), while that of zinc oxide is higher, which means that zinc oxide has higher reducing power. Hence, zinc oxide has higher oxidizing power and reducing power. Therefore, zinc oxide can drive the very important reaction involving the electrolytic reduction of molecular oxygen ( $\text{O}_2$ ) to superoxide ( $\text{O}_2^-$ ). Superoxide has been found to be almost as important as the holes and hydroxyl radicals in breaking down organic compounds [40].

**Table 4.4** Band energy position of titanium dioxide and zinc oxide in aqueous solution [49].

Semiconductor	Valence band (V vs. NHE)	Conduction band (V vs. NHE)
Titanium dioxide	+3.1	-0.1
Zinc oxide	+3.0	-0.2

#### 4.3.1 Comparative Study of Photocatalytic Degradation of Isoproturon on Commercial Zinc Oxide and Synthesized Zinc Oxide

Figure 4.18 shows the change in concentration of isoproturon during the photocatalytic degradation with respect to the initial isoproturon concentration ( $C/C_0$ ) when the commercial zinc oxide and synthesized zinc oxide were used as catalyst. The results reveal that the commercial zinc oxide showed higher efficiency in degrading isoproturon than the synthesized zinc oxide. The photocatalytic degradation of isoproturon on commercial zinc oxide is complete within only 3 hours while that on synthesized zinc oxide can reach 88%

degradation within 6 hours of UV-irradiation. The fact that the photocatalytic efficiency of commercial and synthesized zinc oxide are different may come from the different of isoproturon adsorption on catalyst which may result from the rearrangement of  $Zn^{+}$  and  $O^{-}$  on surface are different (It can be notice on the difference of point of zero charge). Moreover, the effect of size on the photodegradation efficiency can be ascribed that when the size of zinc oxide crystals is decreased, the amount of the dispersion particles per volume in the solution is increased, resulting in the enhancement of the photon absorbance [50].

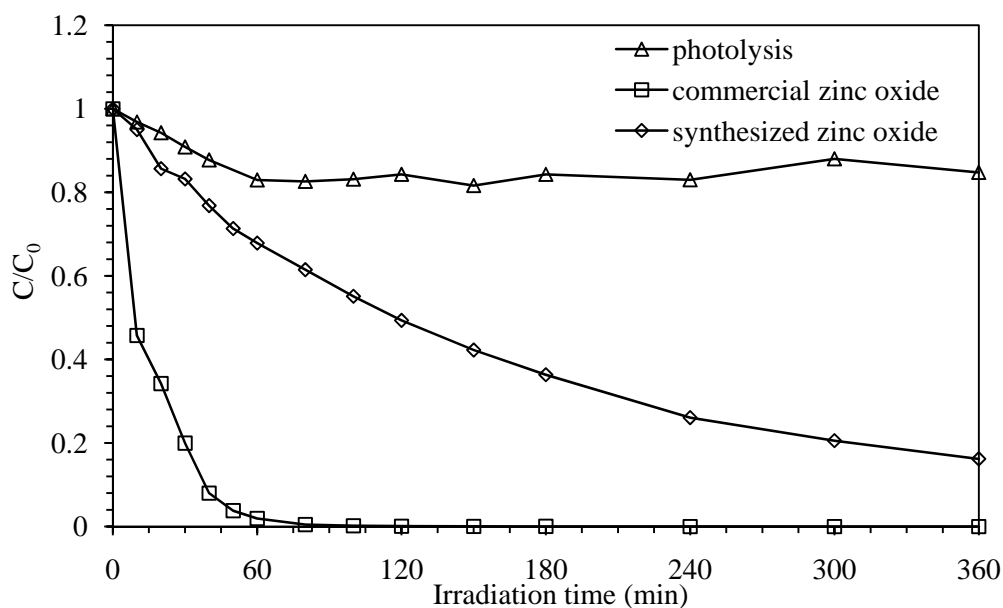


**Figure 4.18** Concentration of isoproturon with respect to the initial isoproturon concentration ( $C/C_0$ ) during the photocatalytic degradation on: ( $\Delta$ ) photolysis, ( $\square$ ) commercial zinc oxide and ( $\diamond$ ) synthesized zinc oxide.

From the degradation data, the first-order linear transform were plotted as shown in Figure 4.19. The apparent rate constants ( $k_{ap}$ ) for commercial and synthesized zinc oxide were determined from the slopes of curves and represented in Table 4.5. The data were also better fitted in the Langmuir-Hinshelwood kinetic model than the first-order kinetics as indicated by the high  $R^2$  value. All parameters, i.e. the reaction rate constants ( $k_r$ ), and the adsorption constants ( $K$ ), are shown in Table 4.5.

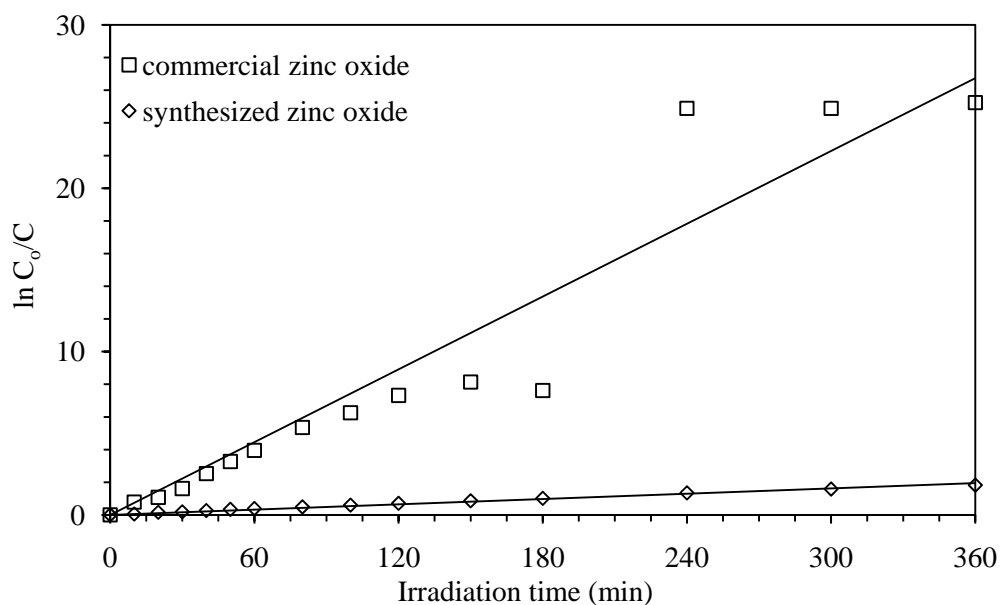


**Figure 4.19** First-order linear transforms plot of the photocatalytic degradation on: (□) commercial zinc oxide, (◇) synthesized zinc oxide.

**Table 4.5** The apparent rate constant ( $k_{ap}$ ), reaction rate constants ( $k_r$ ), and the adsorption constant ( $K$ ) for the photocatalytic degradation of isoproturon using commercial zinc oxide and synthesized zinc oxide as catalyst.

Catalyst	Pseudo-first order kinetic model		Langmuir-Hinshelwood (L-H) kinetic model		
	$k_{ap}$ ( $\text{min}^{-1}$ )	$R^2$	$k_r$ (ppm/min)	$K$ ( $\text{ppm}^{-1}$ )	$R^2$
Commercial ZnO	0.0743	0.9074	4.6383	0.01485	0.9737
Synthesized ZnO	0.0054	0.9897	0.4013	0.01550	0.9948

In comparison of commercial zinc oxide and synthesized zinc oxide, it is observed that the reaction rate constant of the commercial zinc oxide is much higher than that of the synthesized zinc oxide. On the other hand, the adsorption constant is not much different. The adsorption constant of synthesized zinc oxide is slightly higher than that of commercial zinc oxide which is in accordance with the results from adsorption experiments. Thus, the reaction of isoproturon occur on commercial zinc oxide is faster than the synthesized zinc oxide.

Figure 4.20 shows the depletion of TOC as a function of irradiation time during photocatalytic degradation of isoproturon using commercial and synthesized zinc oxide as catalyst. It is found that the mineralization of isoproturon by commercial and synthesized zinc oxide is not complete even after 6 hours of irradiation, which indicates that the photodegradation process generates reaction intermediates during the degradation of isoproturon, especially synthesized zinc oxide. The TOC of isoproturon on synthesized zinc oxide is lower than that on commercial zinc oxide due to the fact that the degradation of isoproturon is low as the result in the amount of isoproturon still remains in reaction system.

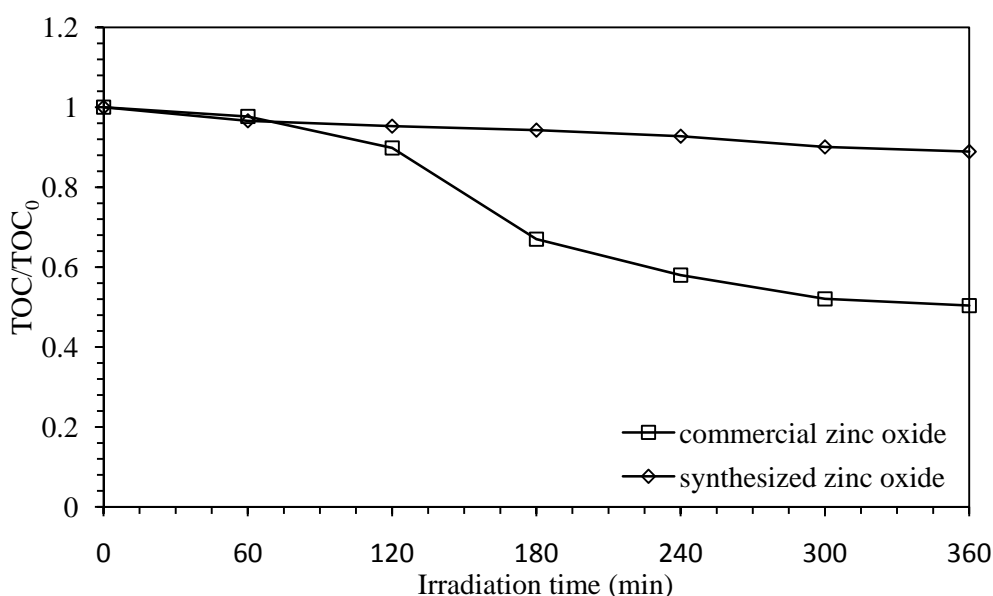


**Figure 4.20** Total organic carbon (TOC) with respect to the initial TOC of isoproturon solution ( $\text{TOC}/\text{TOC}_0$ ) during the photocatalytic degradation on: ( $\square$ ) commercial zinc oxide and ( $\diamond$ ) synthesized zinc oxide.

#### 4.4 Intermediate Products of the Photodegradation of Isoproturon

Even though the efficiency of the photocatalytic decomposition of isoproturon was assessed, the intermediate products were formed during the process. It should be noted that the intermediates can be even more toxic or greater persistent than the parent herbicides [51]. Therefore, identification of intermediate products is useful to understand a basic mechanism of this process.



#### 4.4.1 Effect of Type of Photocatalysts

In this research, identification of intermediate compounds formed from the photocatalytic degradation of isotroturon using different photocatalyst was investigated. It has been known that the intermediate products are formed from the reaction between radicals formed from the photocatalysts and isotroturon. The isotroturon structure is shown in Figure 4.21.

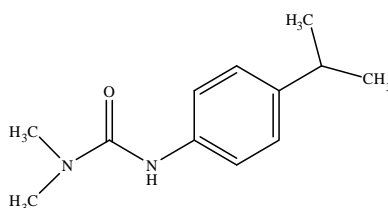


**Figure 4.21** Chemical structure of isotroturon.

During the photocatalytic degradation of isotroturon, the preliminary HPLC results reported several kinds of the degradation intermediates. The peak height of intermediates generated during photocatalytic degradation of isotroturon on commercial titanium dioxide, commercial zinc oxide and synthesized zinc oxide are shown in Figure 4.21-4.23. It should be noted that, the actual concentration of intermediates were not determined to since there is no standard reference available.

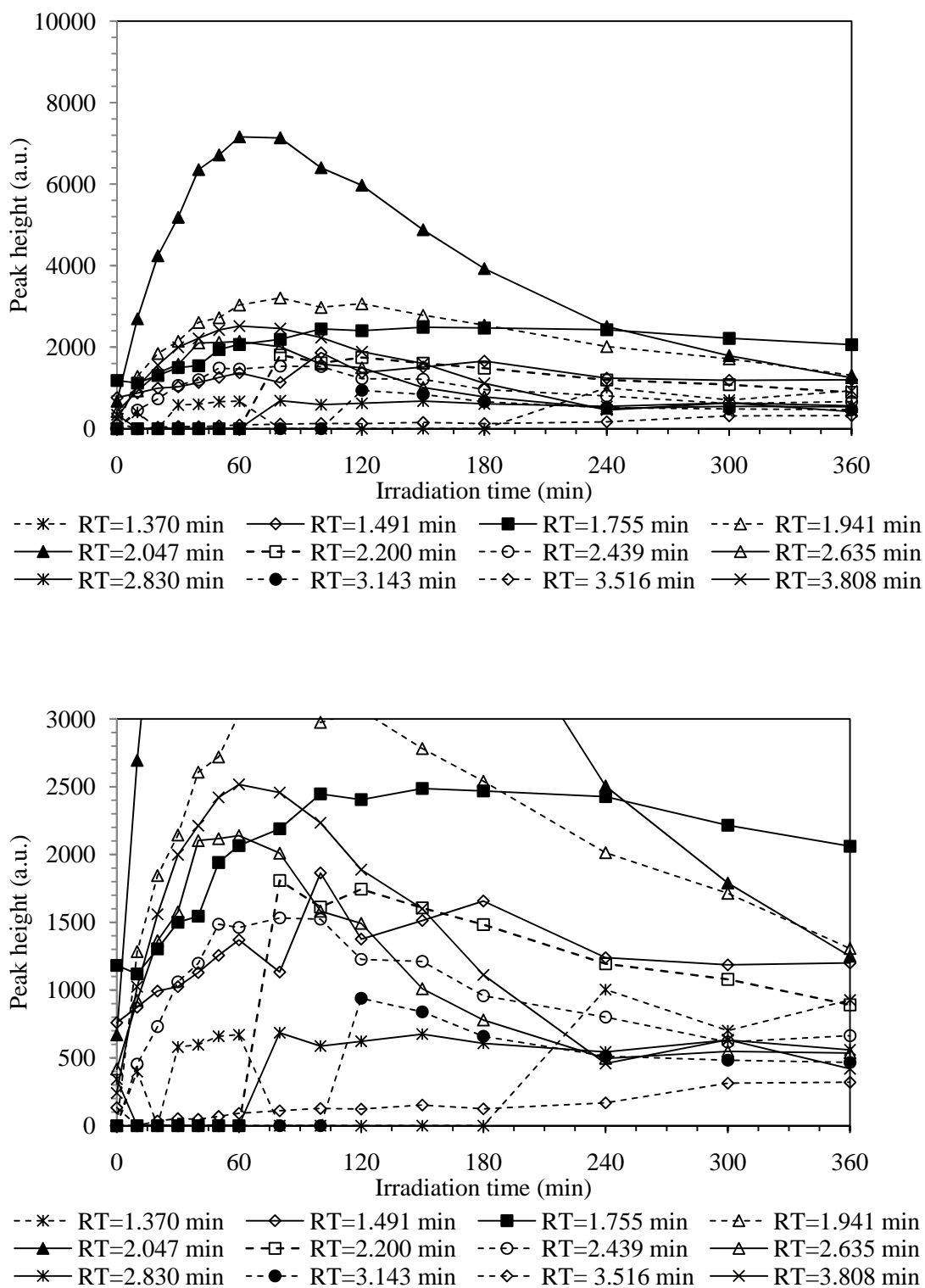


**Figure 4.22** (a) HPLC peak height of intermediates generated during photocatalytic degradation of isotroturon on commercial titanium dioxide and (b) enlargement of (a).

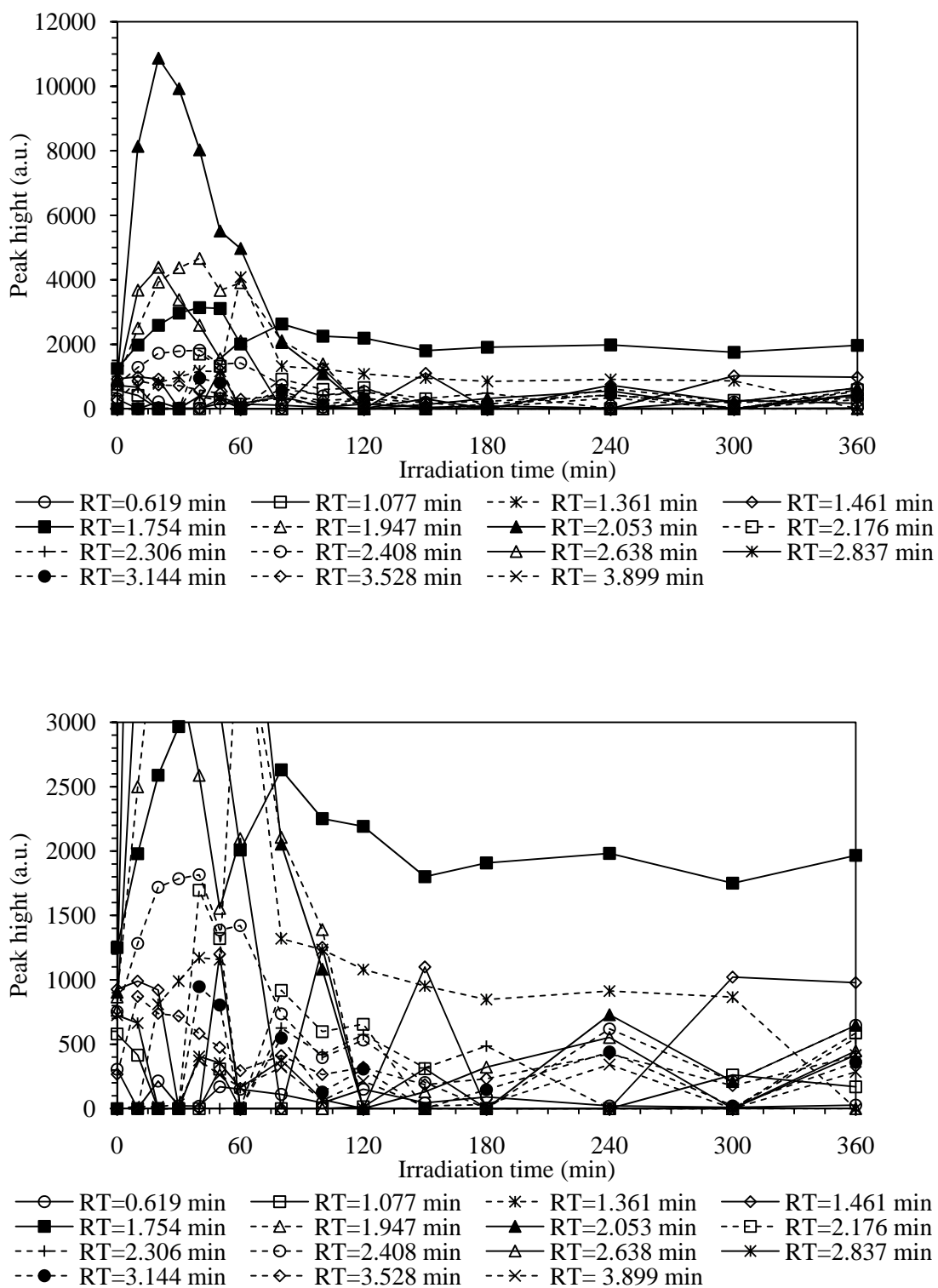


**Figure 4.23** (a) HPLC peak height of intermediates generated during photocatalytic degradation of isotreturon on commercial zinc oxide and (b) enlargement of (a).

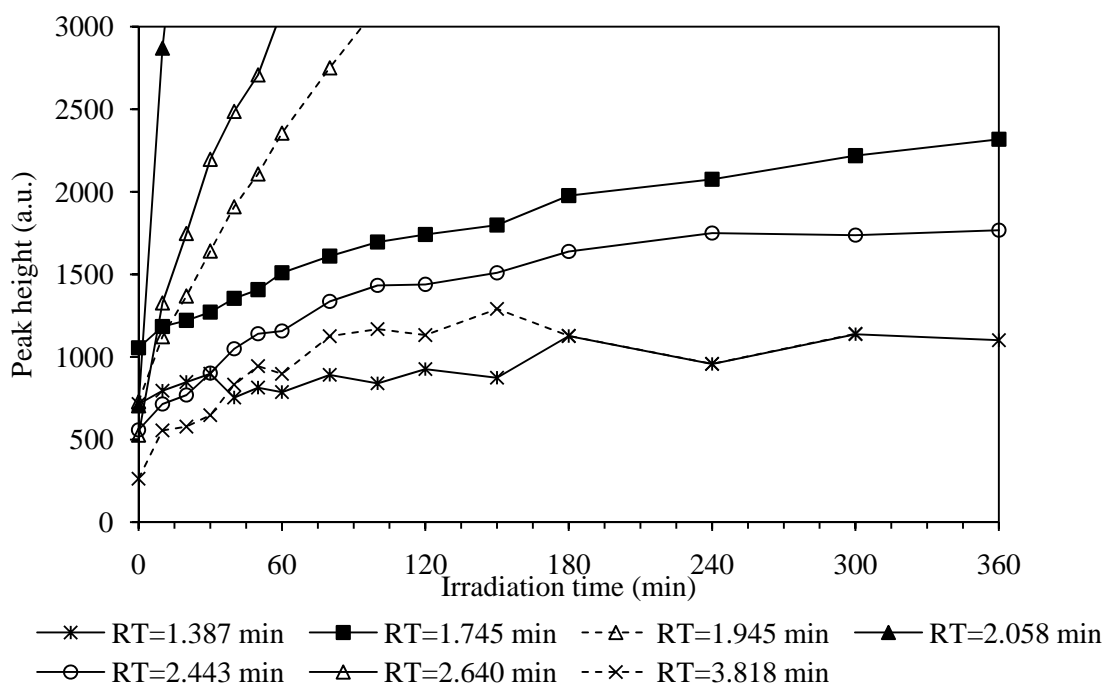
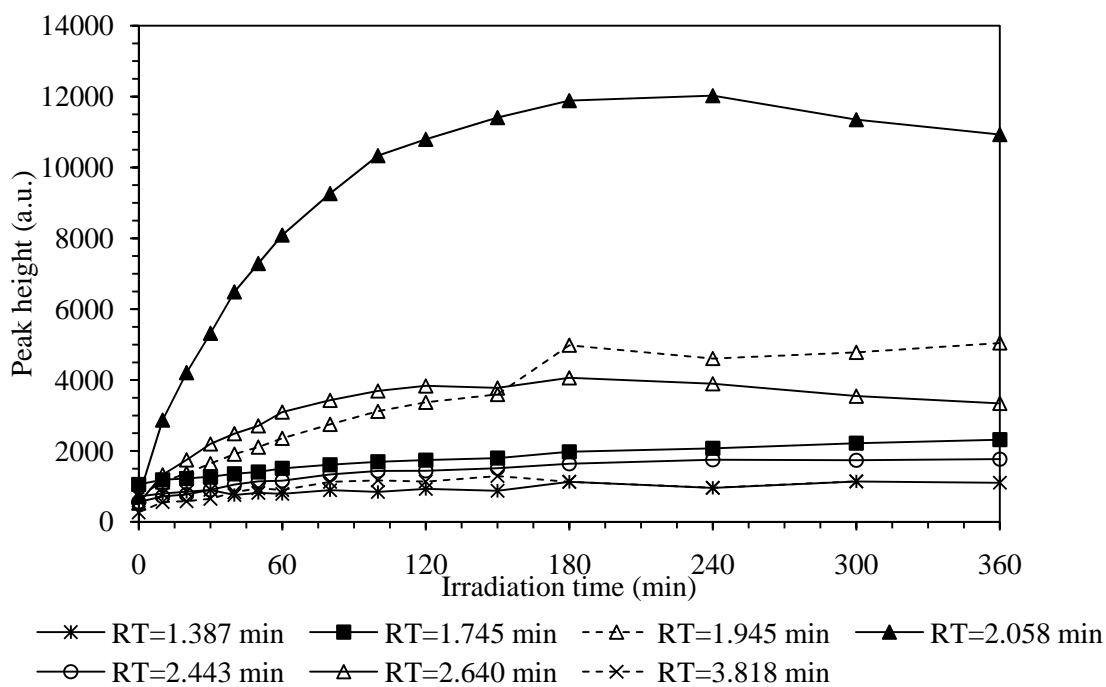


**Figure 4.24** (a) HPLC peak height of intermediates generated during photocatalytic degradation of isoproturon on synthesized zinc oxide and (b) enlargement of (a).

In Figure 4.22, all intermediates are formed at the highest concentration within the first 60 min of the photodegradation using commercial titanium dioxide as catalyst. For commercial zinc oxide, all intermediates are formed at the highest concentration within the first 30 min of reaction as shown in Figure 4.23. Some intermediates decrease as the irradiation time progresses. However, some intermediates remain stable at low concentration even after 6 h of the reaction. For peak height of the intermediates generated during the photocatalytic degradation of isoproturon on synthesized zinc oxide as shown in Figure 4.24, the results reveal that the longer irradiation time would lead to the increase in concentration of the intermediates thus it shows that the degradation of isoproturon on synthesized zinc oxide requires much longer time than 6 h to achieve complete mineralization. When the reaction rate constant is high, the degradation of isoproturon is fast which in turn generates a lot of intermediates. So the intermediates which are formed using commercial zinc oxide ( $k_r = 4.6383$ ) as the catalyst are generated faster than commercial titanium dioxide ( $k_r = 0.6155$ ) and synthesized zinc oxide ( $k_r = 0.4013$ ).

The intermediates generated during the degradation process were detected and identified by LC-MS/MS in order to obtain structural information, MS/MS spectra. For Isoproturon peak, it was observed as reported in literature at m/z of 207 in positive ion mode. The proposed intermediated structures of the intermediate product as well as the main fragmentations are summarized in Table 4.6. The results indicate that the degradation isoproturon during the photocatalytic process leads to other products, the main intermediate products which were identified in this process are the same as detected by other authors [5, 51-53].

**Table 4.6** Main fragments obtained from MS/MS spectra in positive mode and proposed structures of intermediates generated from photodegradation of isoproturon on commercial titanium dioxide, commercial zinc oxide and synthesized zinc oxide.

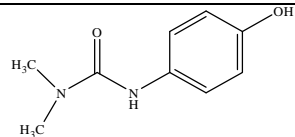
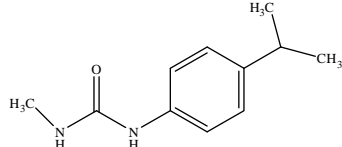
MW (m/z)	MS/MS fragmentation	Proposed structure	Commercial TiO <sub>2</sub>	Commercial ZnO	Synthesized ZnO
181 [5, 52]	165, 136, 72		✓		
193 [5, 51, 53]	151, 136, 95		✓	✓	

Table 4.6 (continued).

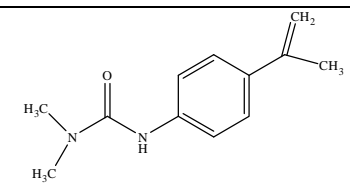
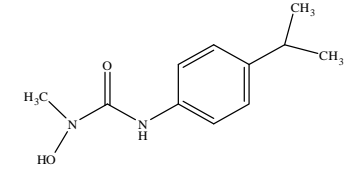
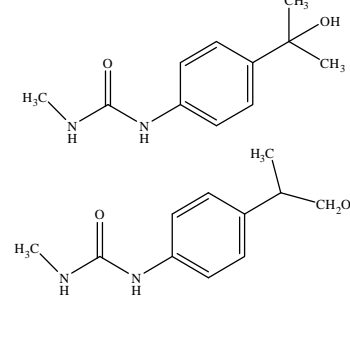
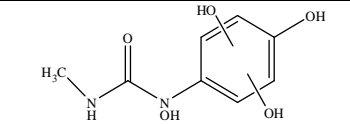
MW (m/z)	MS/MS fragmentation	Proposed structure	Commercial TiO <sub>2</sub>	Commercial ZnO	Synthesized ZnO
205 [53]	163, 72			✓	✓
209 [5, 53]	191, 165			✓	
	191, 151			✓	
215	213		✓	✓	

Table 4.6 (continued).

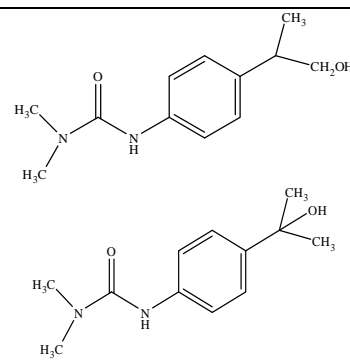
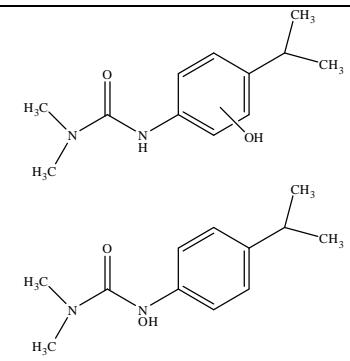
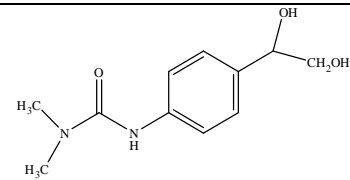
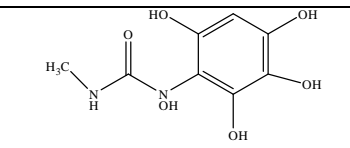
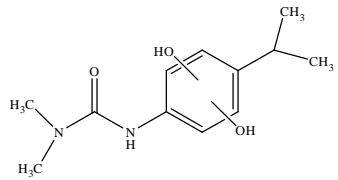
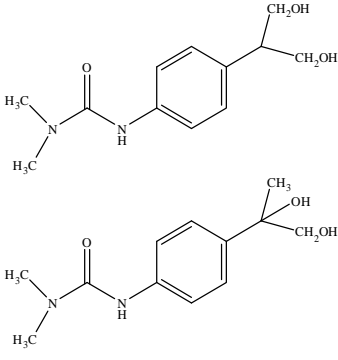
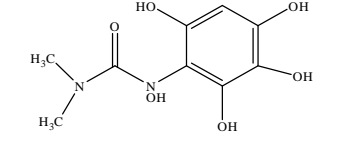
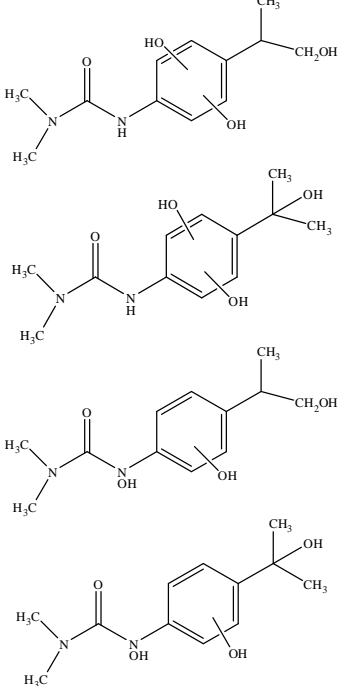
MW (m/z)	MS/MS fragmentation	Proposed structure	Commercial TiO <sub>2</sub>	Commercial ZnO	Synthesized ZnO
223 [5, 51- 53]	205,165,160		✓	✓	✓
	181, 178, 72		✓	✓	✓
225 [5]	193			✓	
231	229, 200			✓	

Table 4.6 (continued).

MW (m/z)	MS/MS fragmentation	Proposed structure	Commercial TiO <sub>2</sub>	Commercial ZnO	Synthesized ZnO
239 [5, 51]	221, 192, 146		✓	✓	✓
	207, 176, 165		✓	✓	✓
245	200		✓	✓	✓
255 [5]	223, 181				✓



**Table 4.6** (continued).

MW (m/z)	MS/MS fragmentation	Proposed structure	Commercial TiO <sub>2</sub>	Commercial ZnO	Synthesized ZnO
261	243, 229, 214		✓	✓	✓
275	230			✓	
277	230		✓	✓	✓

From the results, the LC-MS/MS analysis could not detect some intermediate which has molecular weight lower than 70 so the intermediates which is aliphatic was not detect. Comparison of the intermediates formed, when different photocatalyst was used, shows that some intermediates were detected when all catalysts were used. However, the intermediates that are specific to one particular catalyst were also observed. In addition, some intermediates of which the structure could not be identified were also found. For example, the intermediate with  $m/z=235$  was found in presence of all catalysts and  $m/z=203$  is presented in commercial titanium dioxide. The difference in the intermediate products may result from the different interaction between the catalyst surface and the adsorbed isoproturon, which leads to different mechanism of the reaction. Although the detailed mechanism of isoproturon degradation on titanium dioxide and zinc oxide are different, the main photocatalytic degradation pathways remain the same. The degradation reaction involves mainly hydroxylation, dealkylation, dehydrogenation and decarboxylation.

The sites for hydroxyl radical ( $\text{OH}\cdot$ ) to attack can be divided into two regions, the aromatic ring and the alkyl group. From the identified intermediates, a potential mechanism involving the reaction with the aromatic ring is shown as follows [39]:

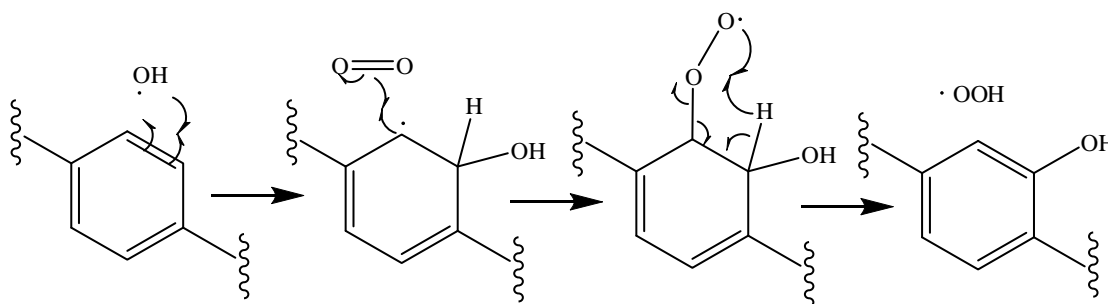


**Figure 4.25** Hydroxylation reaction.

The attack of hydroxyl radical on the carbon of methyl group through hydrogen atom abstraction is energetically favorable. The oxidation of methyl group yields an alcohol, and subsequently gets further oxidized to yield aldehyde and carboxylic acid, which then undergoes decarboxylation as shown in Figure 4.26 [39].

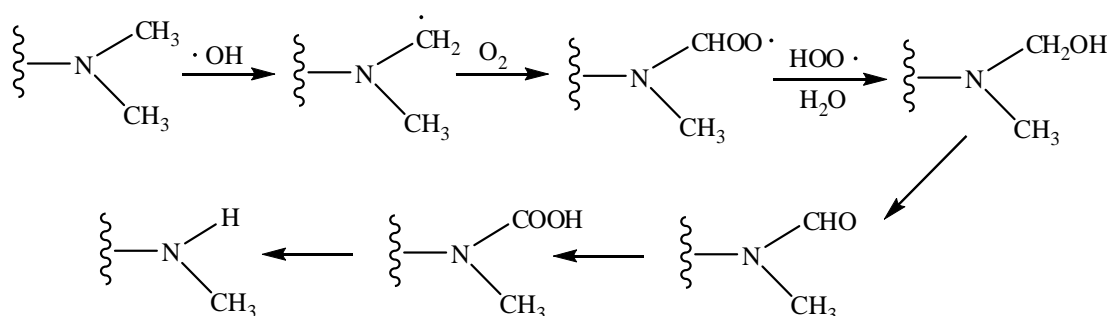


**Figure 4.26** Decarboxylation reaction.

From the proposed structures of all intermediated products, the intermediate compounds which are formed by hydroxylation of the aromatic ring or an alkyl group (isopropyl and methyl), are those with  $m/z = 223, 239, 255$ . By demethylation reaction, the result is intermediate with  $m/z = 193$  and dehydrogenation is that with  $m/z = 205$ .

#### 4.5 Effect of pH of Isoproturon Solution

The pH of solution is an important parameter in the photocatalytic reaction, since it affects the surface charge of the photocatalyst and therefore the adsorption of the isoproturon solution on the surface of catalysts. Therefore, the effect of pH of the isoproturon solution on the photocatalytic degradation was studied. The pH value of the isoproturon solution was

adjusted before irradiation to the desired value in the range of 3 to 10 by 0.1 M of HCl or NaOH and it is not controlled during the course of the reaction. For the study of this parameter, the amount of photocatalyst was added into the solution at the ratio of 1 mg to 10 ml of the solution. The photodegradation were conducted by UV-A irradiation.

#### 4.5.1 Effect of pH of isotroturon solution on commercial titanium dioxide

The results of the photodegradation of isotroturon using commercial titanium dioxide as catalyst at pH 3, 5 and 10 are illustrated in Figure 4.27. The data were fitted against the Langmuir-Hinshelwood kinetic model, as shown in Table 4.7.

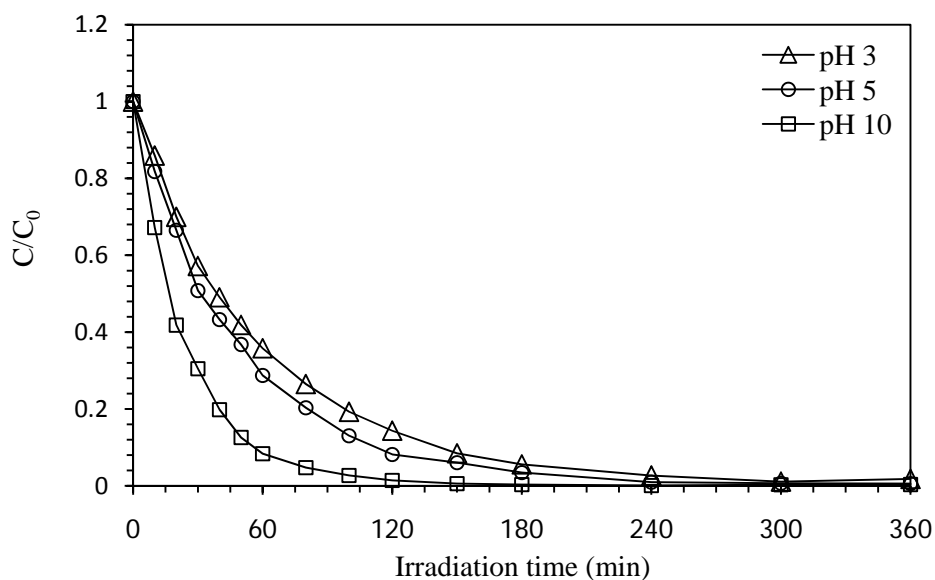
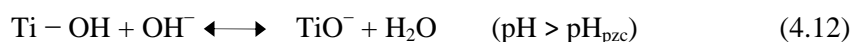


**Figure 4.27** Effect of pH of the solution on photodegradation of isotroturon using commercial titanium dioxide as catalyst: ( $\Delta$ ) pH 3, ( $\circ$ ) pH 5 and ( $\square$ ) pH 10.

**Table 4.7** The reaction rate constants ( $k_r$ ), and the adsorption constant ( $K$ ) for the photocatalytic degradation of isoproturon using commercial titanium dioxide as catalyst at pH 3, pH 5 and pH 10.

pH of solution	Langmuir-Hinshelwood (L-H) kinetic model		
	$k_r$ (ppm/min)	$K$ (ppm <sup>-1</sup> )	$R^2$
pH 3	0.5822	0.02931	0.9792
pH 5	0.6550	0.03316	0.9840
pH 10	0.8449	0.04329	0.9306

The results indicate that the photodegradation rate is increased with increasing pH from 3 to 10. The solution pH influences the degradation process due to the strong pH dependence of the charged state of semiconductor surface. The point of zero charge ( $\text{pH}_{\text{pzc}}$ ) is the pH values at which the surface charge of catalyst is zero. For commercial titanium dioxide, the point of zero charge ( $\text{pH}_{\text{pzc}}$ ) is 5.7 (see appendix B). The surface of titanium dioxide particle will be positively charged at  $\text{pH} < \text{pH}_{\text{pzc}}$ , negatively charged at  $\text{pH} > \text{pH}_{\text{pzc}}$ , and neutral at  $\text{pH} = \text{pH}_{\text{pzc}}$  [54]:



where  $\text{TiOH}^{2+}$ ,  $\text{TiOH}$ , and  $\text{TiO}^-$  are the positive, neutral, and negative surface hydroxyl groups, respectively. When pH of solution is lower than  $\text{pK}_a$  of the reactant, reactant is mainly present in neutral molecular form; conversely, at pH greater than  $\text{pK}_a$  the reactant exists in ionic form [50, 54] and the  $\text{pK}_a$  of isoproturon solution is 4.85 [55]. For pH 5 and pH 10, it can be indicated that pH of solution is higher than  $\text{pK}_a$  then isoproturon is present in ionic form. At pH 10, the surface of titanium dioxide is present as negative charged by adsorbed  $\text{OH}^-$  ions. The presence of large quantities of  $\text{OH}^-$  ions on the particle surface as well as in the reaction medium favors the formation of  $\text{OH}^\bullet$  radical, which is widely accepted as principal oxidizing species responsible for decomposition process at neutral or high pH levels and results in enhancement of the efficiency of the process [49, 56]. So the results indicated that the formation of hydroxyl radicals is more important parameter than the electrostatic interaction force.

Figure 4.28 shows progress of intermediates formation with respect to the irradiation time, using commercial titanium dioxide at different pH. The intermediates concentration are expected to be very low, since the intensities of the HPLC peak for the intermediates are much lower than that of isoproturon.

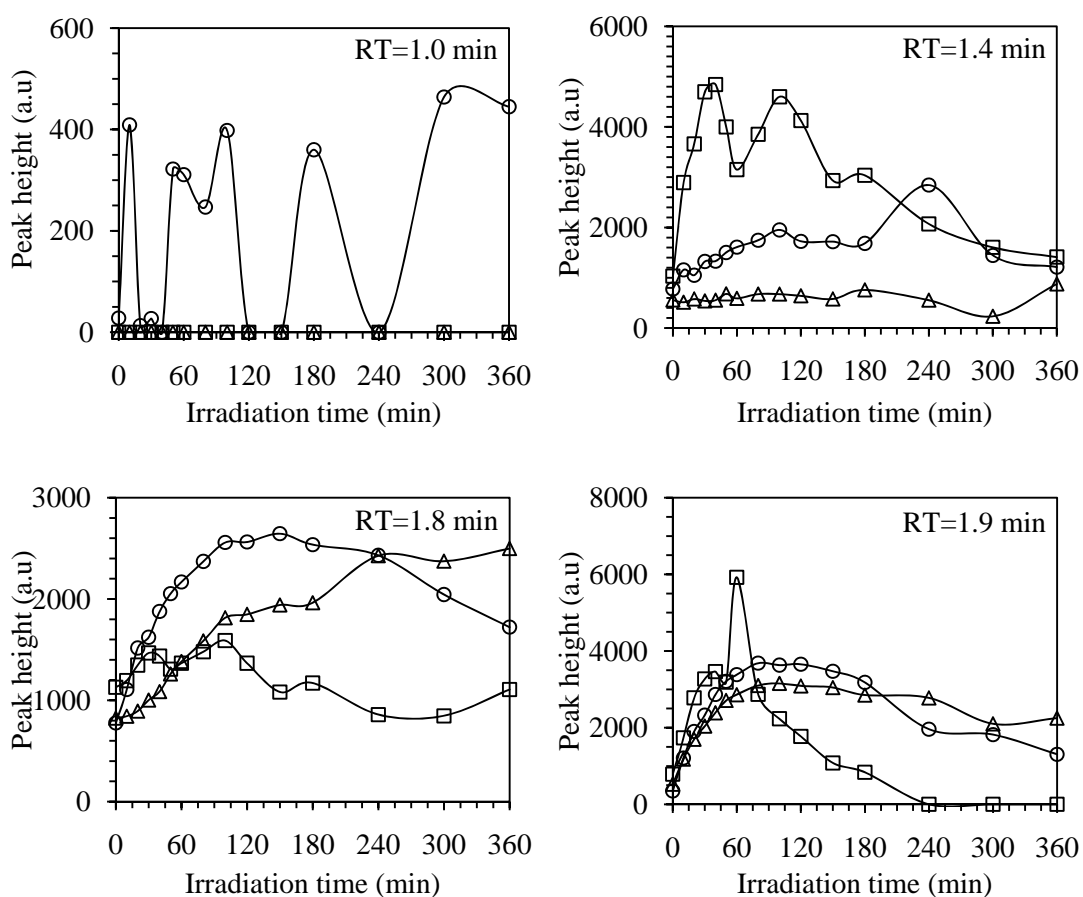


**Figure 4.28** HPLC peak height of intermediates generated during photocatalytic degradation of isoproturon on commercial titanium dioxide at different retention time in pH of solution is ( $\Delta$ ) pH 3, ( $\circ$ ) pH 5 and ( $\square$ ) pH10.

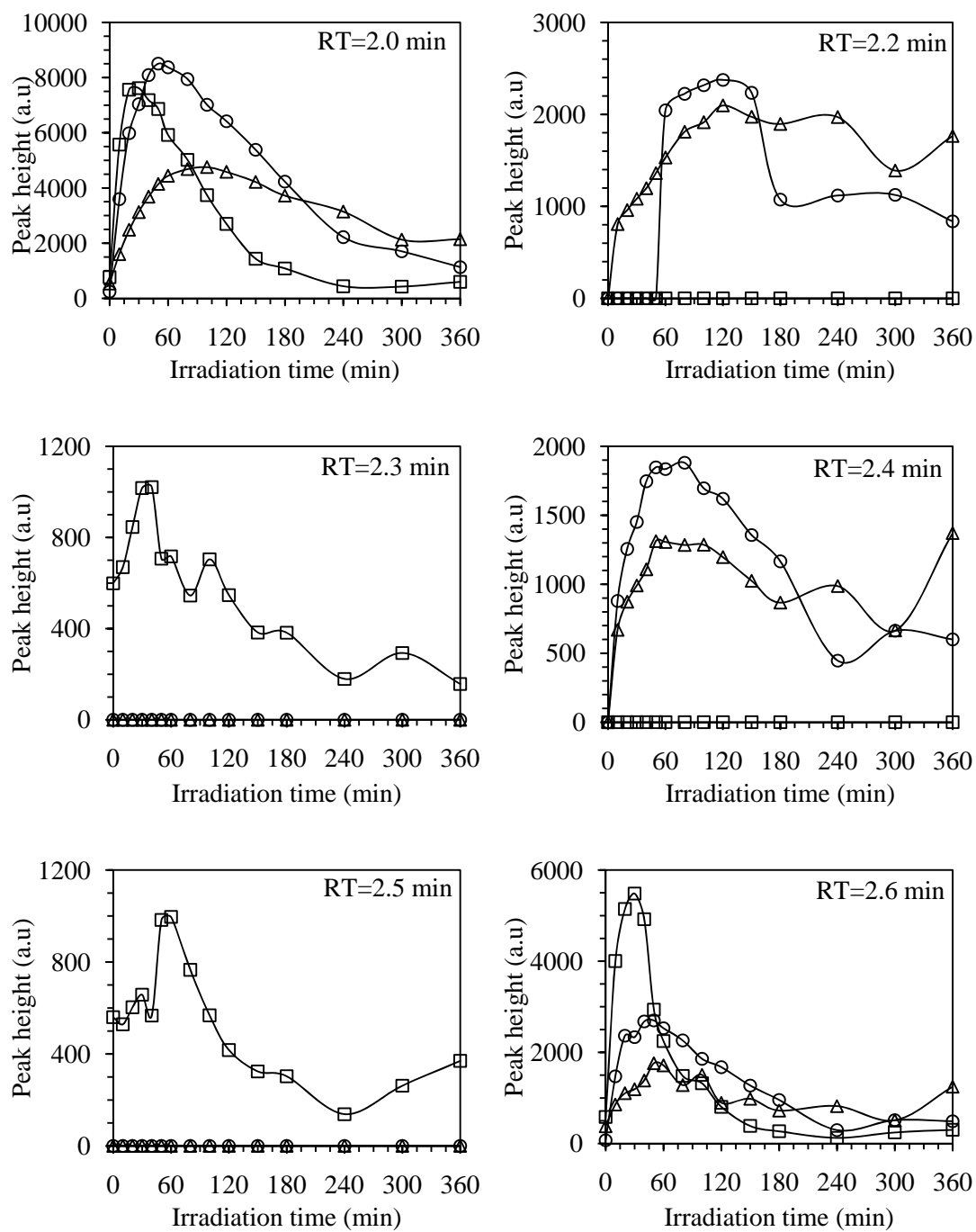


Figure 4.28 (continued).

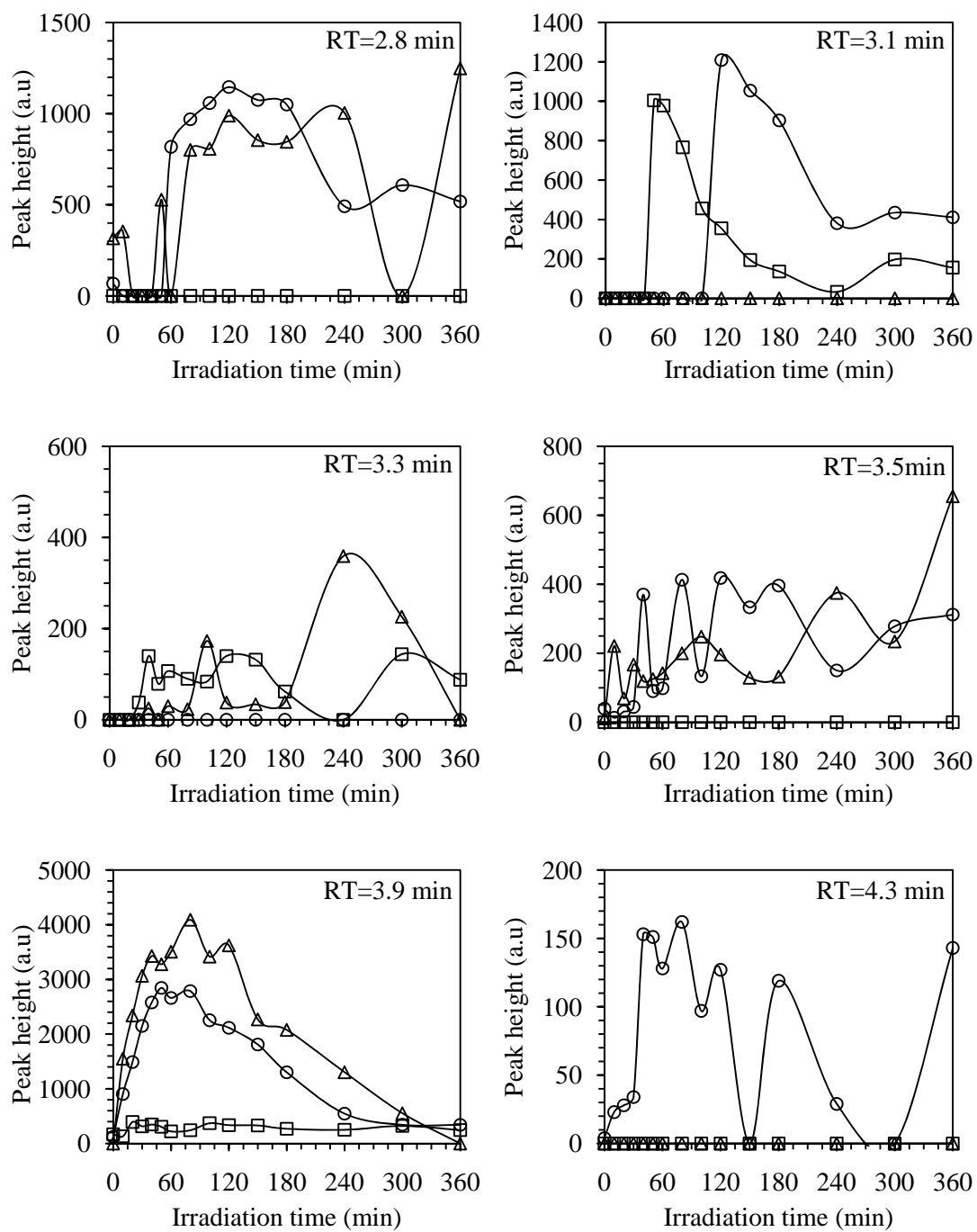


Figure 4.28 (continued).

From the HPLC peak height, it shows that the intermediates which are formed at retention time of 1.4, 1.8, 1.9, 2.0, 2.6 and 3.9 min occurred in all pHs of solution (3, 5 and 10) and almost formed at the highest concentration in the first period of the reaction after which they are decreased continuously. Furthermore, some intermediates occurred only in specific pH. For the example, the intermediates at retention time of 1.0 and 4.3 min. were found only in pH 5 and at retention time = 2.3 and 2.5 min. were found only in pH 10. It can be indicated that some intermediates are different when the pH of solution was changed. For identification of possible intermediated structures, the intermediates were detected and identified though LC-MS/MS analysis. The proposed intermediated structures of intermediated product as well as the main fragmentations are summarized in Table 4.8.

**Table 4.8** Main fragments obtain from MS/MS spectra in positive mode and proposed structures of intermediates generated from photodegradation of isoproturon on different pH of commercial titanium dioxide.

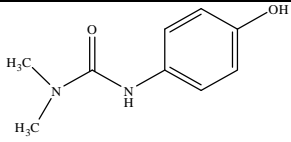
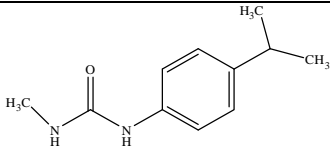
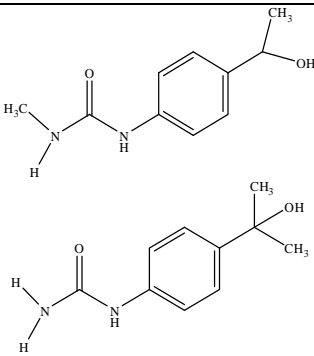
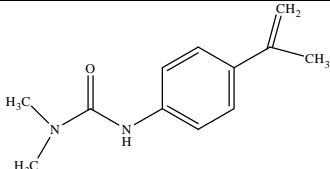
MW (m/z)	MS/MS fragmentation	Proposed structure	pH 3	pH 5	pH 10
181 [5, 52]	179, 163		✓		
193 [5, 51, 53]	151, 136, 95		✓		✓
195 [53]	177				✓
205 [53]	160, 72		✓		



Table 4.8 (continued).

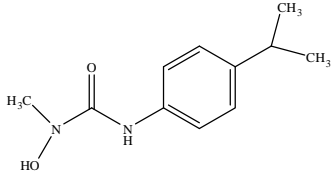
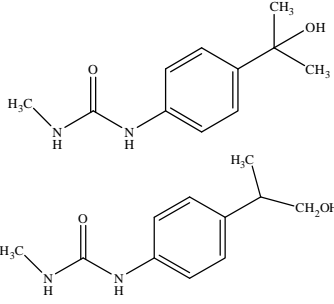
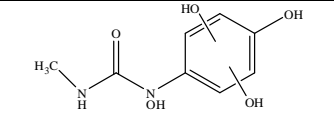
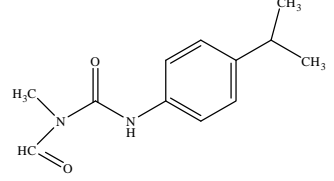
MW (m/z)	MS/MS fragmentation	Proposed structure	pH 3	pH 5	pH 10
209 [5, 53]	191, 165		✓		✓
	191, 151		✓		✓
215	213				✓
221 [51]	219, 162		✓		

Table 4.8 (continued).

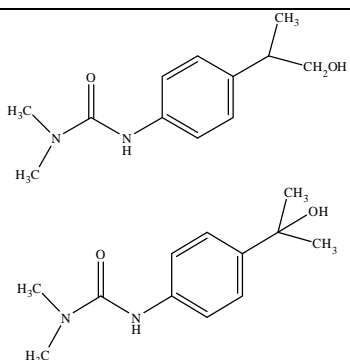
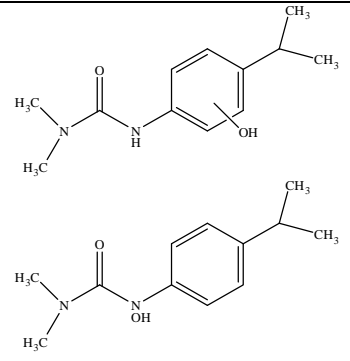
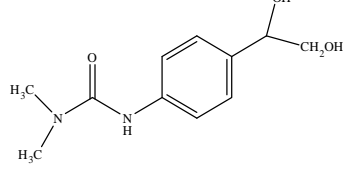
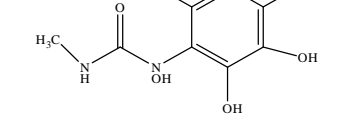
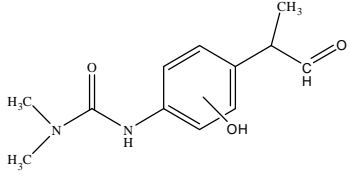
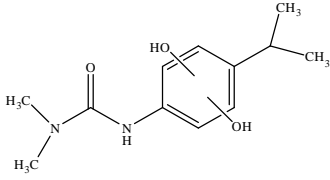
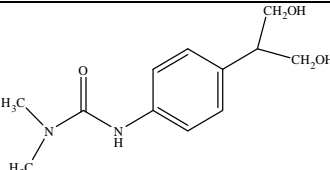
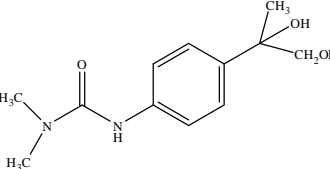
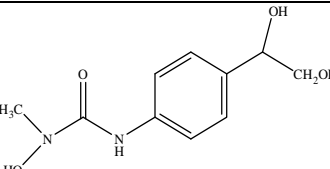
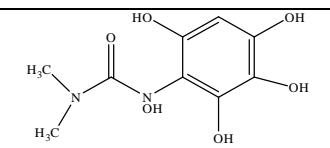
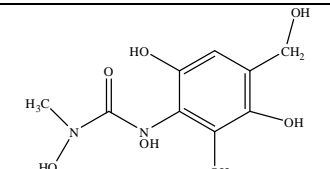
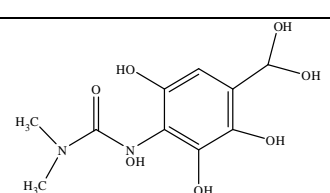
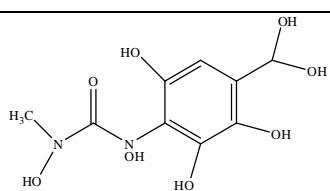
MW (m/z)	MS/MS fragmentation	Proposed structure	pH 3	pH 5	pH 10
223 [5, 51-53]	205, 165, 160		✓	✓	✓
	181, 178, 72		✓	✓	✓
225 [5]	193		✓	✓	
231	229, 213, 200				✓
237 [51]	219, 149		✓		

Table 4.8 (continued).

MW (m/z)	MS/MS fragmentation	Proposed structure	pH 3	pH 5	pH 10
239 [5, 51]	221, 192, 146		✓	✓	✓
	207, 176, 165	 	✓	✓	✓
243	225		✓		
245	200		✓	✓	✓
261	243, 229			✓	✓
275	230				✓
277	230			✓	✓

Apart from the proposed structure in Table 4.8, some intermediates cannot be identified like  $m/z=235$  which are found in all pHs and  $m/z=253$  in pH 3 and 10. The proposed intermediated products from photodegradation of isotroturon on titanium dioxide show that the distribution of products depends on the pH of the solution. In acid solution, the hydroxyl radicals mainly attack on methyl group while in basic solution, the hydroxylation of aromatic ring is favored.

#### 4.5.2 Effect of pH of isotroturon solution on commercial zinc oxide

Figure 4.29 shows the changes of isotroturon concentration during the photocatalytic degradation with respect to the initial isotroturon concentration ( $C/C_0$ ) when the commercial zinc oxide as catalyst at pH 3, 5 and 10. The result was fitted against the Langmuir-Hinshelwood kinetic model, as shown in Table 4.9.

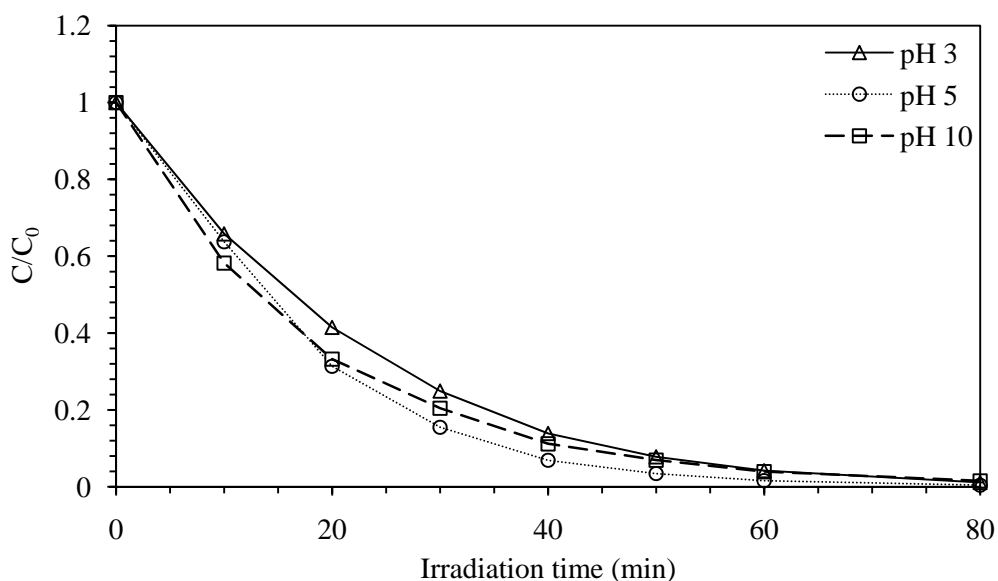


**Figure 4.29** Effect of pH of the solution on photodegradation of isotroturon using commercial zinc oxide as catalyst: ( $\Delta$ ) pH 3, ( $\circ$ ) pH 5 and ( $\square$ ) pH 10.

**Table 4.9** The reaction rate constants ( $k_r$ ), and the adsorption constant ( $K$ ) for the photocatalytic degradation of isotroturon using commercial zinc oxide as catalyst at pH 3, pH 5 and pH 10.

pH of solution	Langmuir-Hinshelwood (L-H) kinetic model		
	$k_r$ (ppm/min)	$K$ (ppm <sup>-1</sup> )	$R^2$
pH 3	4.617	0.01076	0.9441
pH 5	4.644	0.01105	0.8847
pH 10	4.628	0.01060	0.9524

Generally, the effect of pH on organic degradation assisted by the semiconductor oxides has been related to the establishment of acid-base equilibria governing the surface chemistry of metal oxides in water, as shown in the following reactions [50].



The point of zero charge for commercial zinc oxide is 6.3 (see appendix B). When the solution pH is lower than pKa of the reactant, reactant is mainly present in neutral molecular form; conversely, at pH greater than pKa the reactant exists in ionic form [48, 49]. It has been reported that the pKa for isotroturon is 4.85 [55]. The effect of pH on the photocatalytic performance can be explained in terms of electrostatic interaction between the catalyst surface and the target substrate [50]. From the results, it was found that at solution pH 3 which is lower than pKa, isotroturon is mainly in neutral molecular form while at pH 5 and 10, the isotroturon reactant are present in ionic forms. So, at solution pH 5 and 10, the photodegradation rate is greater than pH 3 and the optimal conditions were found at  $\text{pKa} < \text{pH} < \text{pH}_{\text{pzc}}$  at which the positive charged zinc oxide and negative charged isotroturon should attract each other [50].

Figure 4.30 shows the intermediate profiles which are generated during photocatalytic degradation of isotroturon on commercial zinc oxide at different retention time by varying pH of solution (3, 5 and 10). From the HPLC peak height, concentrations of these intermediates are very low, since the intensities of the HPLC signals for the intermediate are much lower than that of isotroturon. Moreover, it shows that at retention time of 1.5, 1.8, 1.9,

2.0, 2.4 and 2.6 min, the intermediates are formed in solution of all pHs. Most intermediates are formed to highest concentration within 30 minutes of irradiation time. Moreover, intermediates which are formed at retention time of 2.1, 2.3, 2.8, 3.1 and 3.5 min occurred in acid pHs while the intermediates at retention time of 1.6, 2.2, 2.5 and 3.4 min are occurred in basic pH. It can be inferred that pH of the solution affect on formation of intermediates.

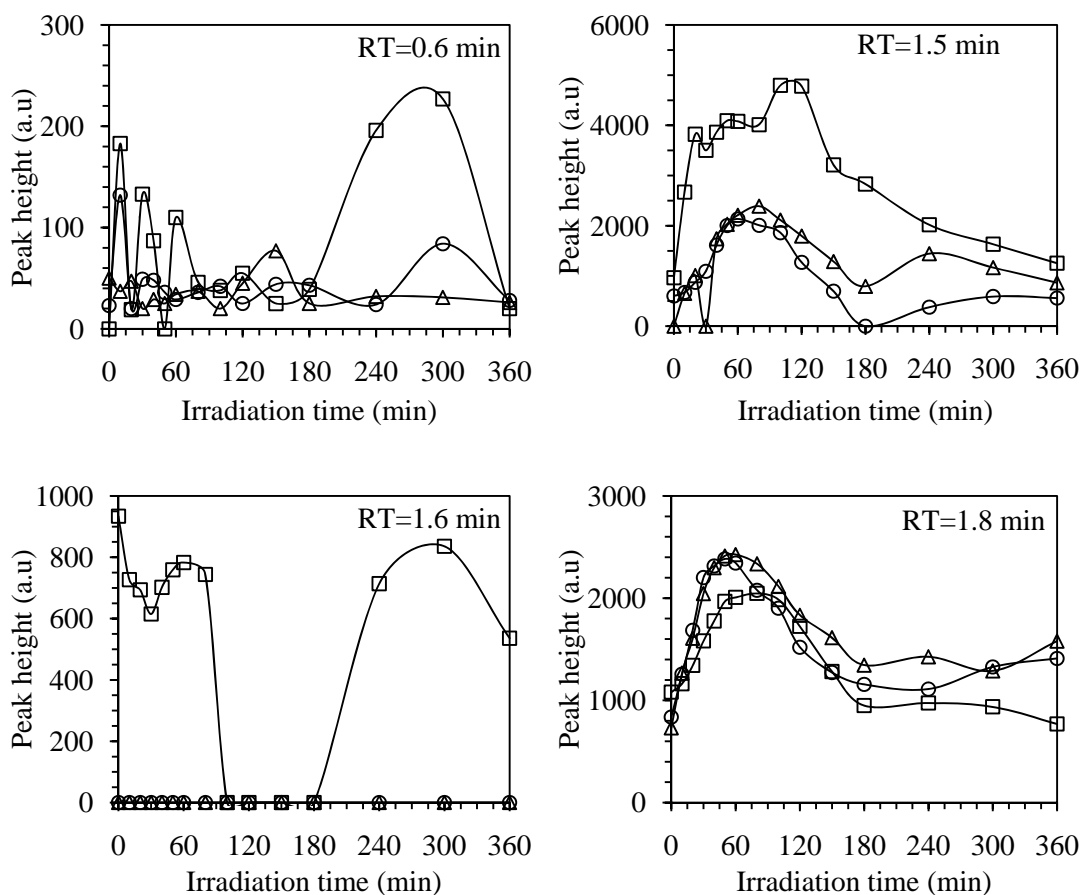


**Figure 4.30** HPLC peak height of intermediates generated during photocatalytic degradation of isoproturon on commercial zinc oxide at different retention time in pH of solution is ( $\Delta$ ) pH 3, ( $\circ$ ) pH 5 and ( $\square$ ) pH10.

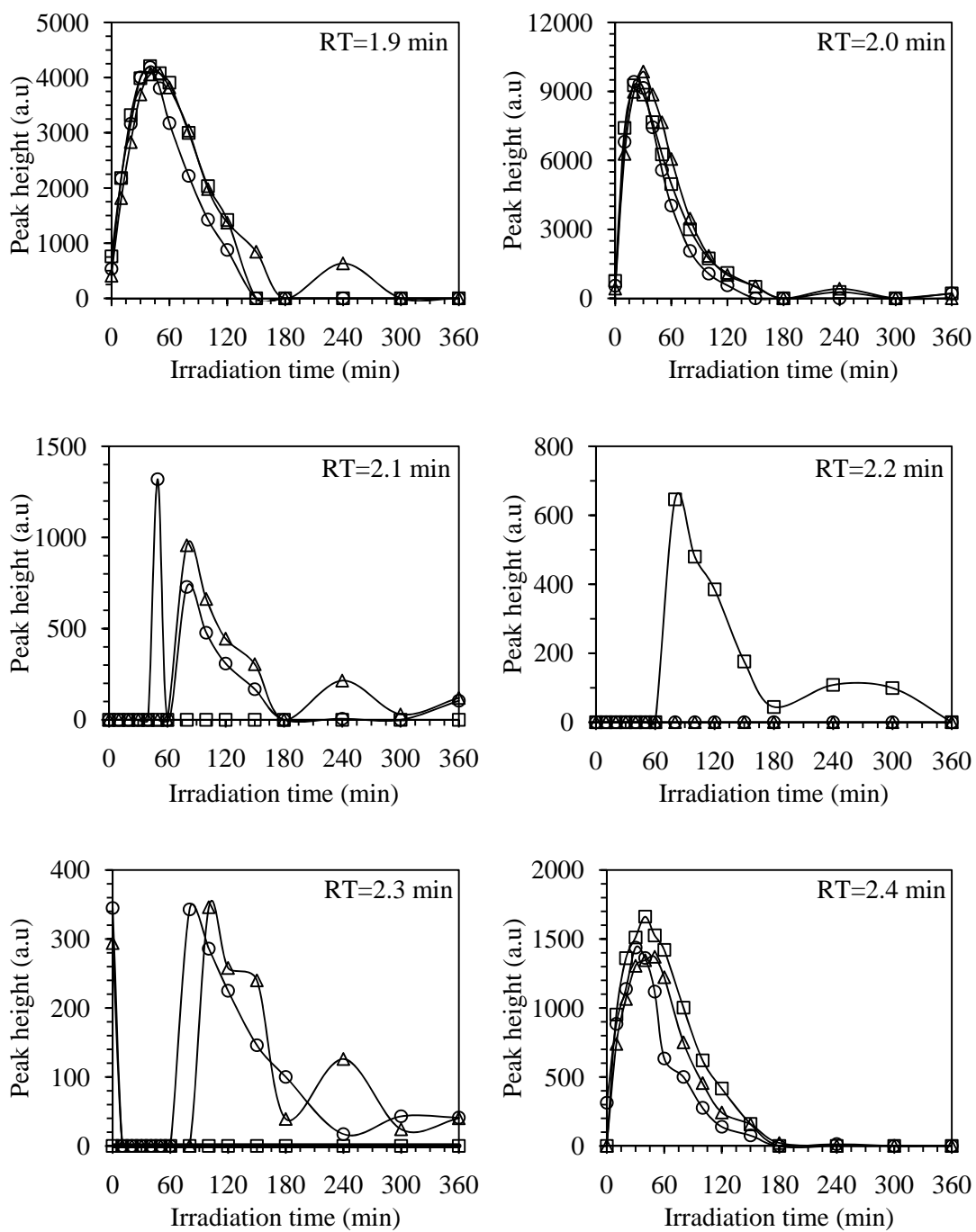


Figure 4.30 (continued).

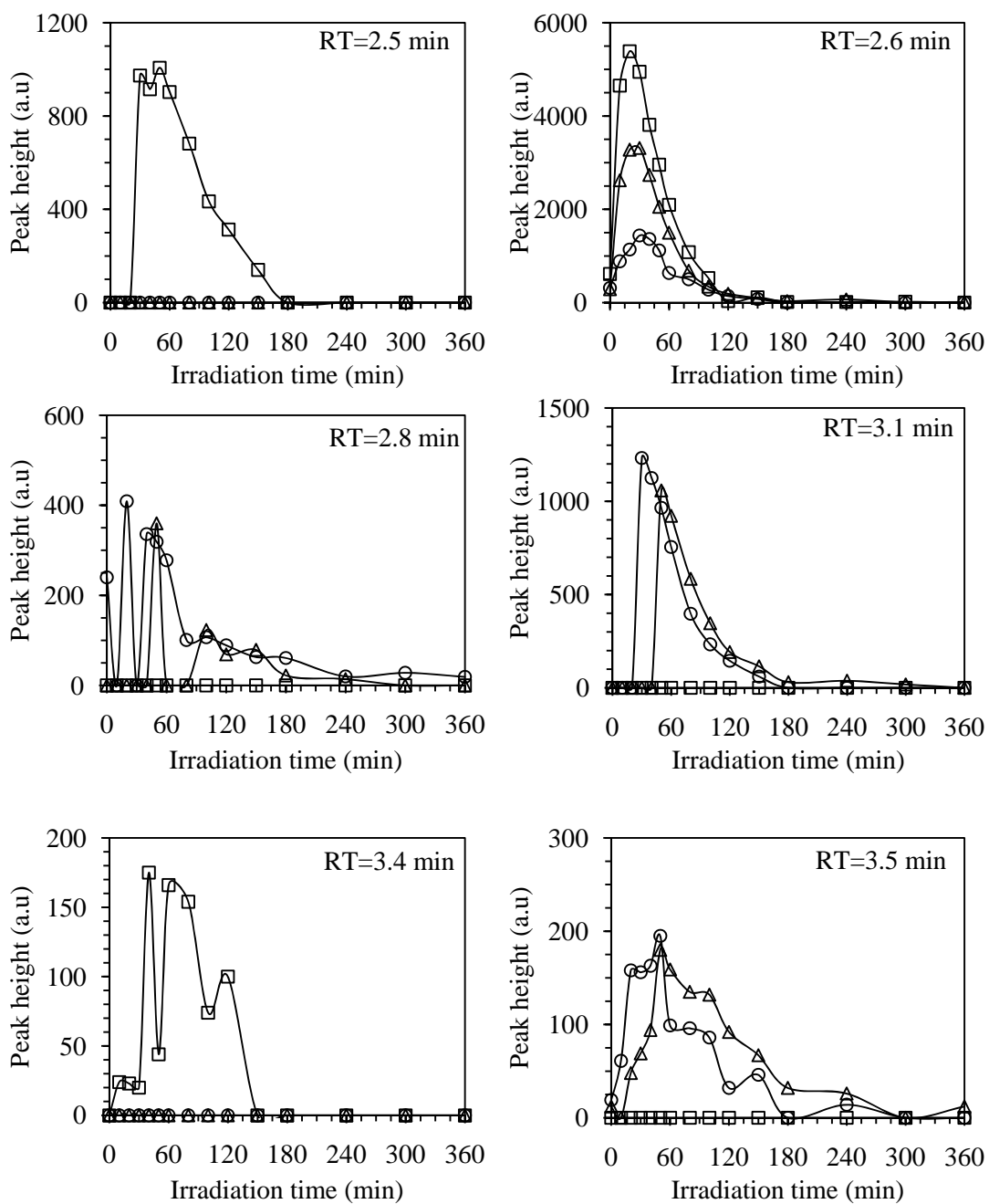
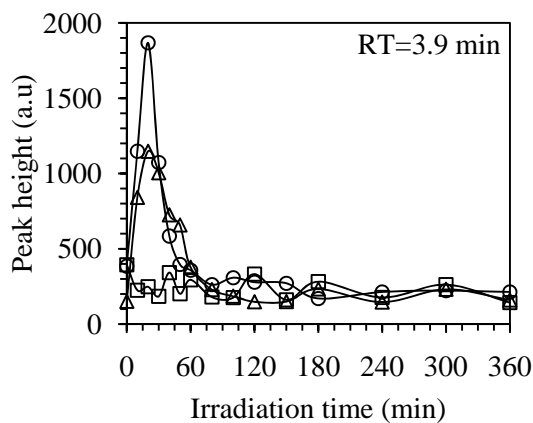


Figure 4.30 (continued).





**Figure 4.30** (continued).

For identification, the intermediate products were identified through LC-MS analysis and the structures of all intermediates are proposed in Table 4.10.

**Table 4.10** Main fragments obtain from MS/MS spectra in positive mode and proposed structures of intermediates generated from photodegradation of isoproturon on different pH of commercial zinc oxide.

MW (m/z)	MS/MS fragmentation	Proposed structure	pH 3	pH 5	pH 10
193 [5, 53]	151, 136, 95			✓	✓
205 [53]	163, 72			✓	
209 [5, 53]	191, 151				✓

Table 4.10 (continued).

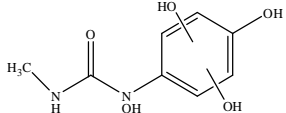
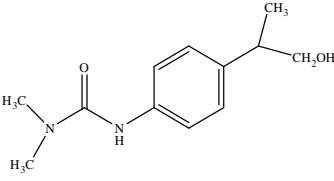
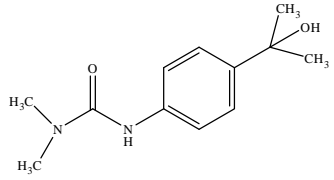
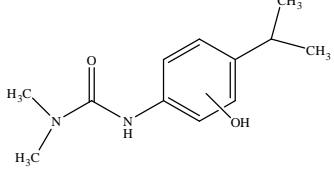
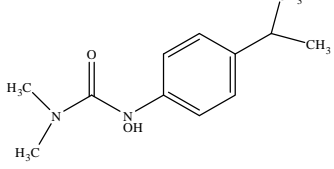
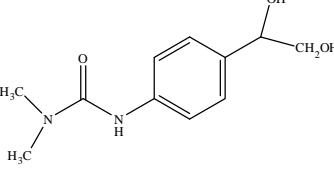
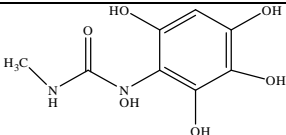
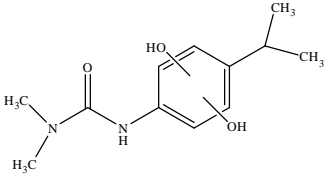
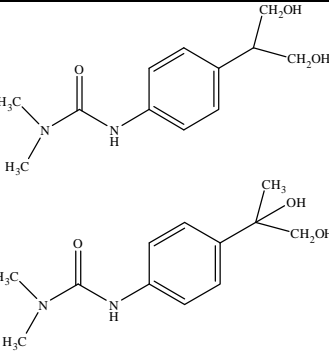
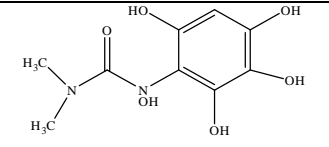
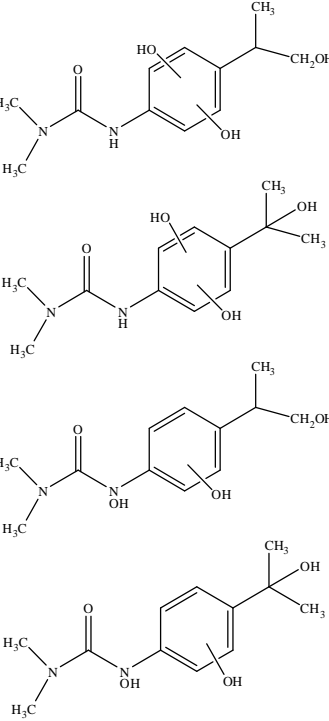
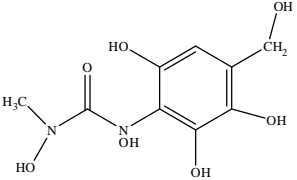
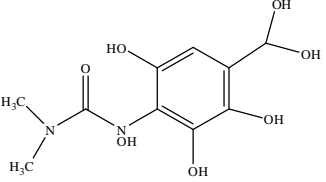
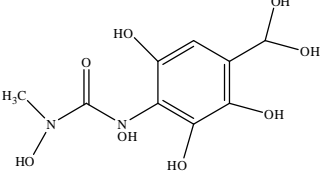
MW (m/z)	MS/MS fragmentation	Proposed structure	pH 3	pH 5	pH 10
215	213			✓	✓
223 [5, 51-53]	205, 165, 160	 	✓	✓	✓
223 [5, 51-53]	181, 178, 72	 	✓	✓	✓
225 [5]	193		✓	✓	
231	229, 200				✓

Table 4.10 (continued).

MW (m/z)	MS/MS fragmentation	Proposed structure	pH 3	pH 5	pH 10
239 [5, 51]	221, 192, 146		✓	✓	✓
	207, 176, 165		✓	✓	✓
245	200		✓	✓	✓
255 [5]	239			✓	

**Table 4.10** (continued).

MW (m/z)	MS/MS fragmentation	Proposed structure	pH 3	pH 5	pH 10
261	243, 229, 213		✓	✓	✓
275	230				✓
277	230			✓	✓

Moreover, It is found that some intermediated which generate during photodegradation at various pH of solution on commercial zinc oxide cannot be identified such as  $m/z=295$  in pH 5 of solution,  $m/z=116, 141, 157$  in pH 10,  $m/z=265$  in pH 3 and pH 5 and  $m/z=235$  in all pHs. The result indicated that the pH of solution is an effect on the generated intermediates since the pH values change the surface charge properties and then result to the different adsorption of isotroturon.

#### 4.5.3 Effect of pH of isotroturon solution on synthesized zinc oxide

When synthesized zinc oxide was used as the catalyst in photodegradation process at different pH of solution, the results of degradation are shown in Figure 4.31. The experiment data were fitted in Langmuir-Hinshelwood kinetic model and the parameters were calculated and represent in Table 4.11.

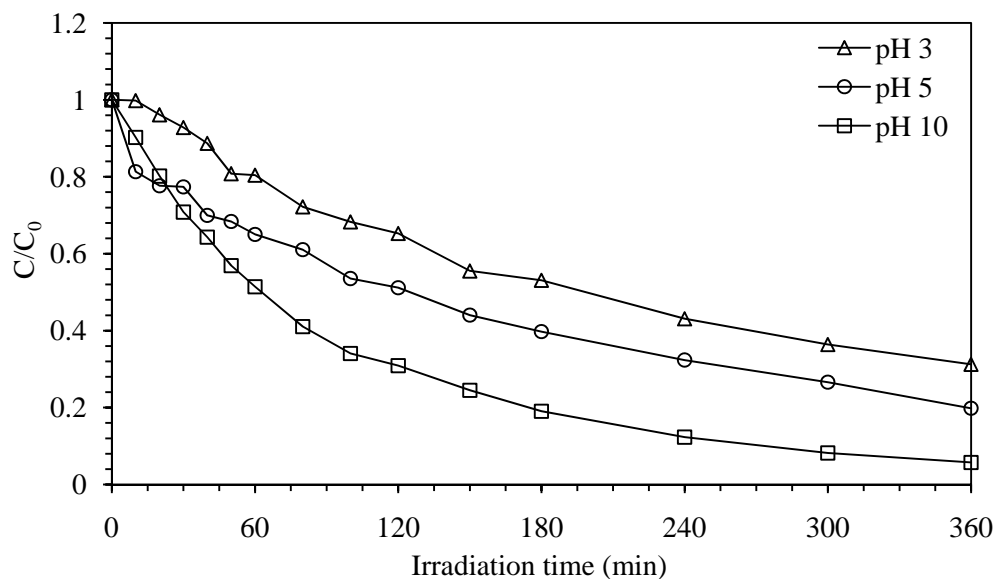


**Figure 4.31** Effect of pH of the solution on photodegradation of isotroturon using synthesized zinc oxide as catalyst: ( $\Delta$ ) pH 3, ( $\circ$ ) pH 5 and ( $\square$ ) pH 10.

**Table 4.11** The reaction rate constants ( $k_r$ ), and the adsorption constant ( $K$ ) for the photocatalytic degradation of isotroturon using synthesized zinc oxide as catalyst at pH 3, pH 5 and pH 10.

pH of solution	Langmuir-Hinshelwood (L-H) kinetic model		
	$k_r$ (ppm/min)	$K$ (ppm <sup>-1</sup> )	$R^2$
pH 3	0.2759	0.01389	0.9884
pH 5	0.3457	0.01583	0.9262
pH 10	0.4806	0.02071	0.9732

As the same results, the pH of solution is an important parameter which effect to surface charge properties of catalyst and result in adsorption of reactant. The point of zero charge ( $\text{pH}_{\text{pzc}}$ ) for synthesized zinc oxide is 7.6 (see appendix B) and  $\text{pK}_a$  of isotroturon is 4.85 [55]. The results are the same that on commercial titanium dioxide which the photodegradation rate is increased with increasing pH of solution (3 to 10). pH 3 is lower than  $\text{pK}_a$  of isotroturon, then at this pH, isotroturon is present in neutral form while pH 5 and 10 are higher than  $\text{pK}_a$ , the reactant is an ionic form, so the photodegradation are greater in pH 3.

Although, at pH 10, the surface charge of catalyst is present in negative charge and isoproturon is in ionic form, the greater performance is in pH 10 of solution. It may be result from the basic pH range favors the formation of more OH radical in basic solution which will be enhance the photocatalytic degradation of isoproturon significantly [49, 56].

The intermediate profiles which are formed during the photodegradation on synthesized zinc oxide at different retention time by varying pH (3, 5 and 10), are shown in Figure 4.32. The results show that the intermediates which are formed at retention time of 1.7, 2.0, 2.4, 2.6 and 3.9 min occurred at all pHs of solution (3, 5 and 10). Moreover, most of generated intermediates are increased in concentration when increased irradiation time. Thus the degradation of isoproturon on synthesized zinc oxide for all pHs requires much longer time than 6 h to achieve complete mineralization.

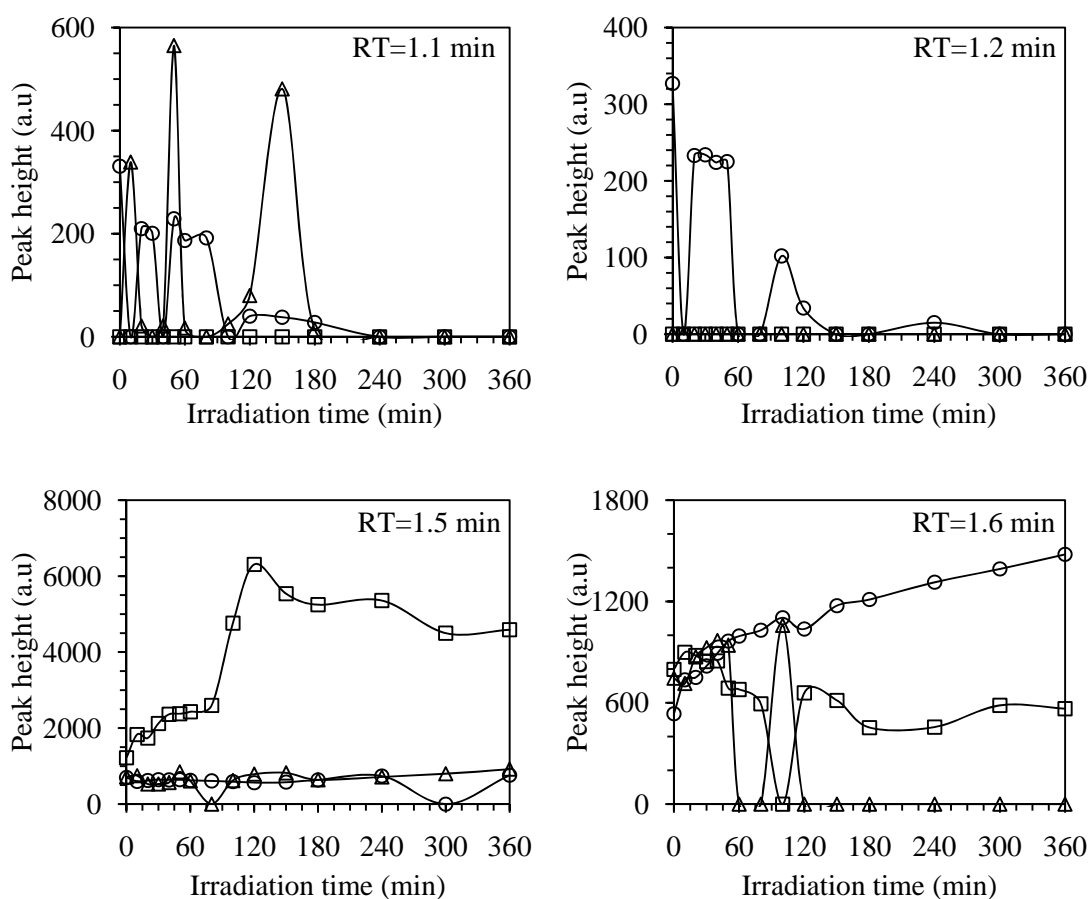


**Figure 4.32** HPLC peak height of intermediates generated during photocatalytic degradation of isoproturon on synthesized zinc oxide at different retention time in pH of solution is ( $\Delta$ ) pH 3, ( $\circ$ ) pH 5 and ( $\square$ ) pH10.

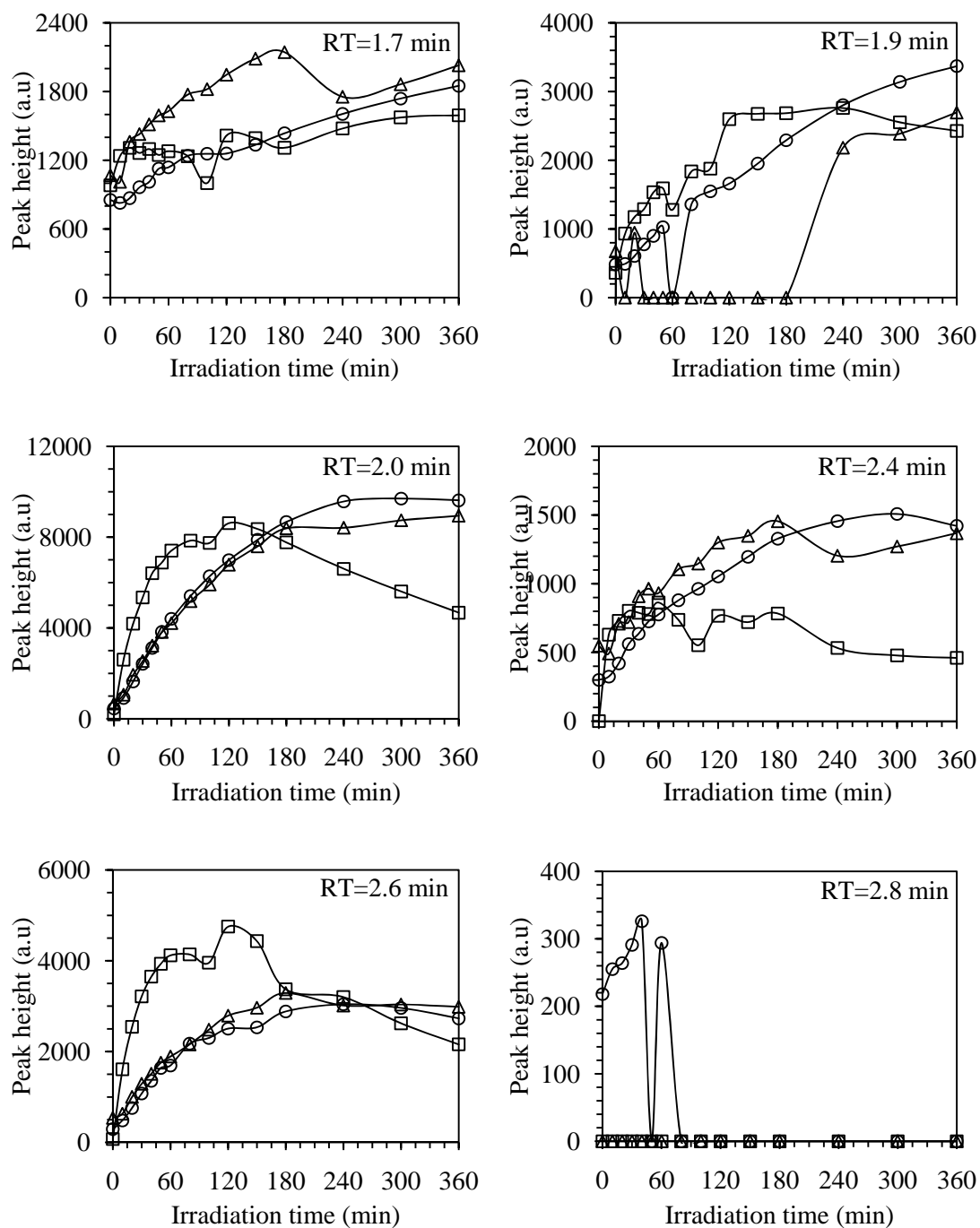
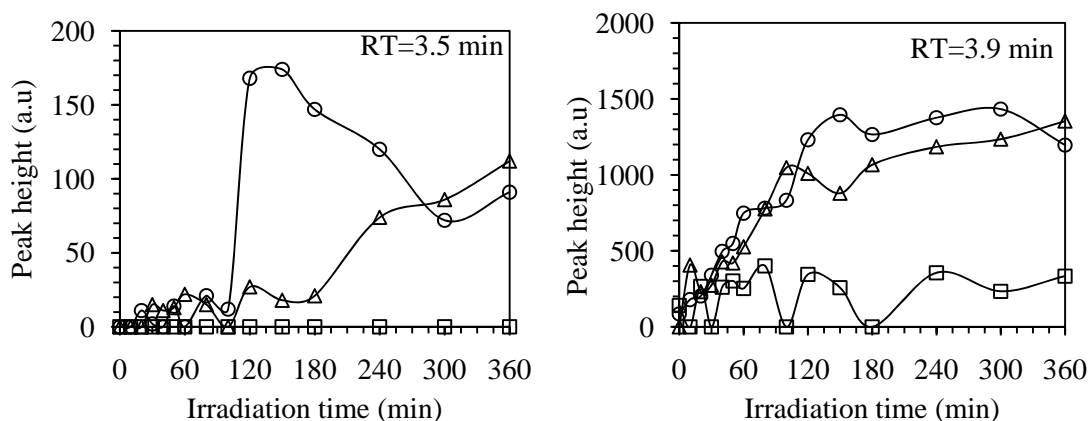


Figure 4.32 (continued).



**Figure 4.32** (continued).

The proposed structures of intermediated products which were identified through LC-MS analysis are shown in Table 4.12. Moreover, some intermediates were detected but cannot identify the structure i.e.,  $m/z = 289$  in pH3 and  $m/z = 235$  in all pH. The results show the different intermediate products may be result from the different adsorption of isoproturon on catalyst.

**Table 4.12** Main fragments obtain from MS/MS spectra in positive mode and proposed structures of intermediates generated from photodegradation of isoproturon on different pH of synthesized zinc oxide.

MW (m/z)	MS/MS fragmentation	Proposed structure	pH 3	pH 5	pH 10
181 [5, 52]	179, 165, 72		✓		✓
193 [5, 51, 53]	151, 136, 95			✓	✓



Table 4.12 (continued.)

MW (m/z)	MS/MS fragmentation	Proposed structure	pH 3	pH 5	pH 10
195 [53]	177				✓
205 [53]	163, 72		✓	✓	
209 [5, 53]	191, 165		✓		
	191, 151		✓		
213 [52]	195		✓		
215	198, 129, 79				✓

Table 4.12 (continued.)

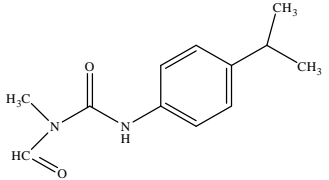
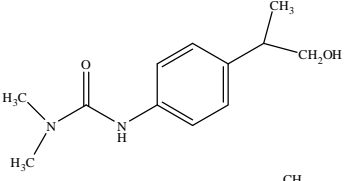
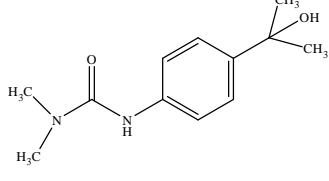
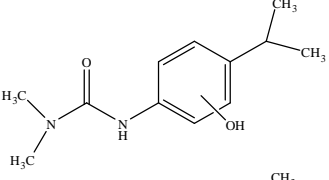
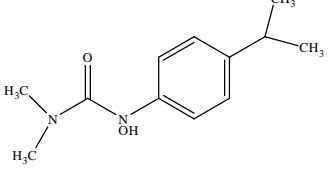
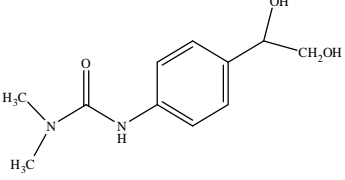
MW (m/z)	MS/MS fragmentation	Proposed structure	pH 3	pH 5	pH 10
221 [51]	132, 72		✓		
223 [5, 51-53]	205, 165, 160	 	✓	✓	✓
	181, 178, 72	 	✓	✓	✓
225 [5]	193, 72		✓		✓

Table 4.12 (continued.)

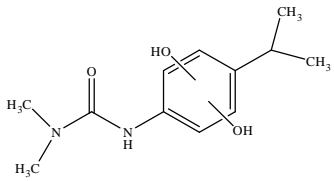
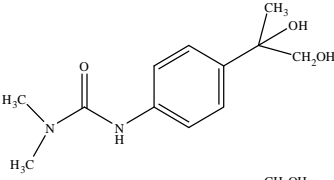
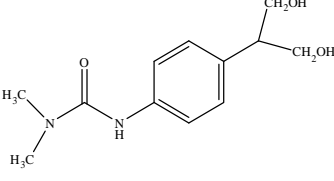
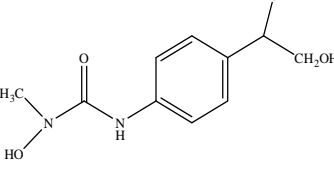
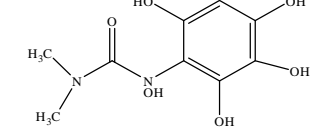
MW (m/z)	MS/MS fragmentation	Proposed structure	pH 3	pH 5	pH 10
239 [5, 51]	221, 192, 146		✓	✓	✓
	207, 176, 165	 	✓	✓	✓
243	225		✓		
245	200		✓	✓	✓

Table 4.12 (continued.)

MW (m/z)	MS/MS fragmentation	Proposed structure	pH 3	pH 5	pH 10
255 [5]	237, 210		✓		
257	239		✓		

**Table 4.12** (continued.)

MW (m/z)	MS/MS fragmentation	Proposed structure	pH 3	pH 5	pH 10
261	229, 214		✓	✓	✓
271	253		✓		
273	255		✓		
277	230		✓	✓	✓

From the pH effect, the photodegradation of isotroturon on commercial zinc oxide is most effective at pH 5 because the effect from electrostatic interaction force is more dominant than that from  $\text{OH}\cdot$  radical formation. On the other hand, the reactions on commercial titanium dioxide and synthesized zinc oxide are most effective at pH 10 due to the increased formation of  $\text{OH}\cdot$  radical. In addition, the characters of adsorption of isotroturon on commercial titanium dioxide, commercial zinc oxide and synthesized zinc oxide at various pH are different. It can be observed that isotroturon can be adsorbed onto commercial zinc oxide surface by electrostatic interaction while the adsorption of isotroturon onto commercial titanium dioxide and synthesized zinc oxide surface are done by the other adsorption.

Moreover, the pH of solution has an effect on the generated intermediates. It is observed that some intermediates are found for all pHs whereas some intermediates are found specific for one particular pH. It can be indicated that the pH of solution affects the surface

charge properties of catalysts and may be result to the different in interaction between the catalyst surface and the adsorbed isoproturon.

From the results, it can be indicated that the photocatalytic degradation of isoproturon on commercial zinc oxide is greater performance than that on commercial titanium dioxide and synthesized zinc oxide. In addition, the main mechanism is showed in Figure 4.33.

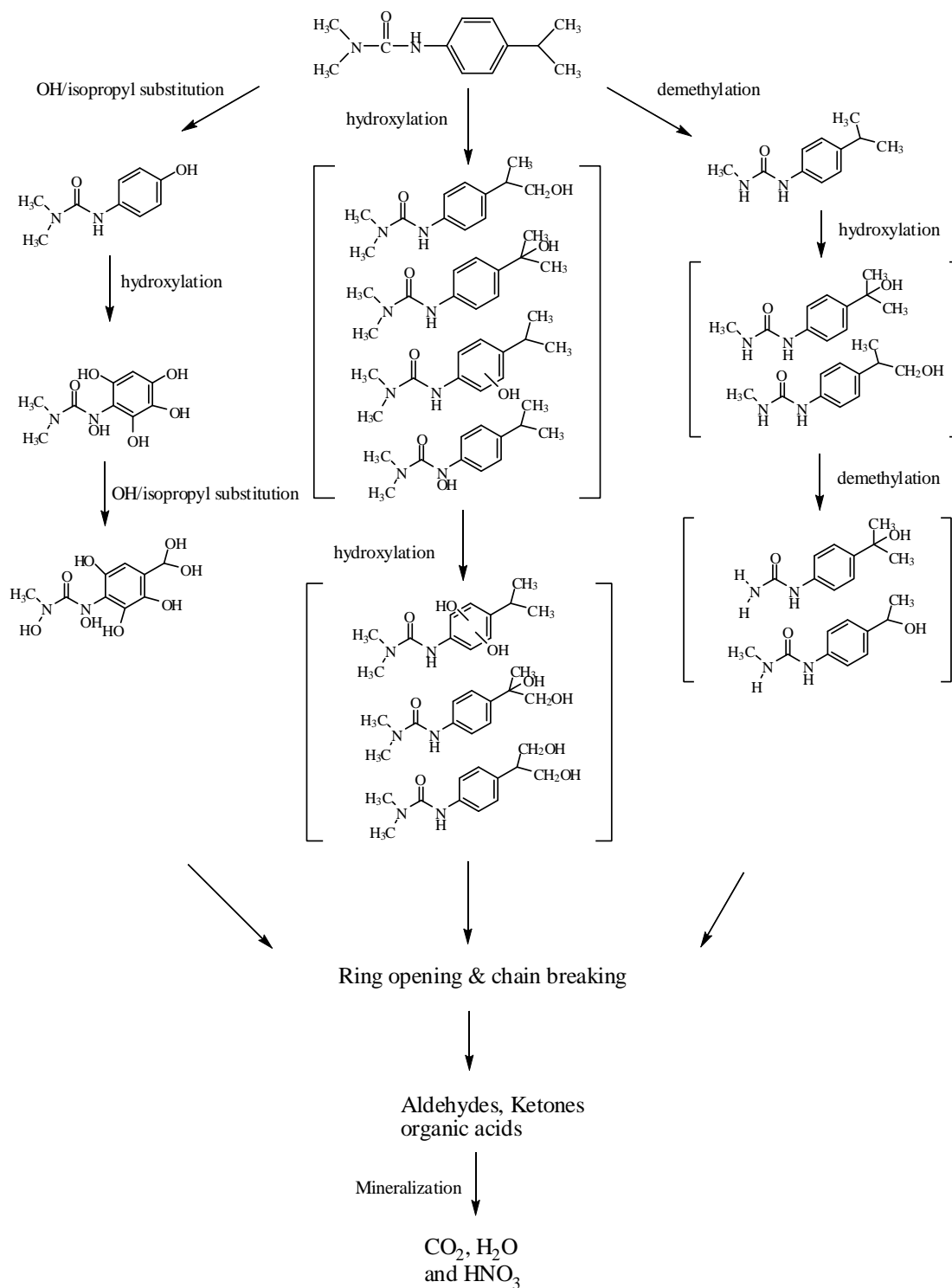


**Figure 4.33** Proposed mechanism of photodegradation of isoproturon.

## CHAPTER V

### CONCLUSIONS AND RECOMMENDATIONS

#### 5.1 Summary of Results

The summary of the results of the present research is the following:

1. Zinc oxide has higher performance in degrading isoproturon than titanium dioxide even though surface area of zinc oxide is much lower than that of titanium dioxide. Therefore, the surface area of the photocatalyst is not the major factor affecting the extent of decomposition in this process.
2. The different intermediates from photodegradation of isoproturon using different photocatalyst may be result from the different interaction between the catalyst surface and the adsorbed isoproturon.
3. The pH of isoproturon solution has an effect on the structure of intermediate products since the pH changes the surface charge of the photocatalyst and consequently affects the adsorption of isoproturon on the surface of the catalysts.
4. Photodegradation of isoproturon generates several intermediates. The degradation pathway is mainly consisted of hydroxylation, decarboxylation, and demethylation on the structure of isoproturon.

#### 5.2 Conclusions

Removal of residual isoproturon in water can be degraded via photocatalytic reaction using commercial titanium dioxide, commercial zinc oxide and synthesized zinc oxide as the catalyst. Although the degradation of isoproturon is induced, it generates lots of intermediates. Several degradation intermediates are generated by reactions of hydroxyl radical attacking to several sites of isoproturon structure during the photodegradation process. Moreover, the formation of intermediates depends upon the photocatalysts used and the pH of isoproturon solution. The difference in intermediates products is suggested to be the results from the difference in interaction between the catalyst surface and the adsorbed isoproturon.



### 5.3 Recommendations

Recommendations for the future work, based on the results of this work, are following.

1. Further identification of the adsorption of isoproturon on the catalyst surface by using NMR analysis (solid).
2. Monitor the concentration of the hydroxyl radical ( $\text{OH}^\bullet$ ).
3. Quantify concentration of the generated intermediates.

## REFERENCE

- [1]. Von, W., et al. Degradation of isoproturon in biobeds. Biology and Fertility of Soils, 33, 6 (2001): 535-540.
- [2]. Sharma, M.,K. Lalitha,V. Durgakumari and M. Subrahmanyam. Solar photocatalytic mineralization of isoproturon over TiO<sub>2</sub>/HY composite systems . Solar Energy Materials and Solar Cells, 92, 3 (2008): 332-342.
- [3]. Phanikrishna Sharma, M.V.,V. Durga Kumari and M. Subrahmanyam. Photocatalytic degradation of isoproturon herbicide over TiO<sub>2</sub>/Al-MCM-41 composite systems using solar light. Chemosphere, 72, 4 (2008): 644-651.
- [4]. Sharma, M.,V. Durgakumari and M. Subrahmanyam. Solar photocatalytic degradation of isoproturon over TiO<sub>2</sub>/H-MOR composite systems. Hazardous Materials, 160, (2008): 568-575.
- [5]. Amorisco, A.,I. Losito,F. Palmisano and P.G. Zambonin. Photocatalytic degradation of the herbicide isoproturon: characterisation of by-products by liquid chromatography with electrospray ionisation tandem mass spectrometry. Rapid Communications in Mass Spectrometry, 19, 11 (2005): 1507-1516.
- [6]. Farré, M.J.,S. Brosillon,X. Domènech and J. Peral. Evaluation of the intermediates generated during the degradation of Diuron and Linuron herbicides by the photo-Fenton reaction. Journal of Photochemistry and Photobiology A: Chemistry, 189, 2-3 (2007): 364-373.
- [7]. Haque, M.M. and M. Muneer. Heterogeneous photocatalysed degradation of a herbicide derivative, isoproturon in aqueous suspension of titanium dioxide. Journal of Environmental Management, 69, 2 (2003): 169-176.
- [8]. Phanikrishna Sharma, M.V.,G. Sadanandam,A. Ratnamala,V. Durga Kumari and M. Subrahmanyam. An efficient and novel porous nanosilica supported TiO<sub>2</sub> photocatalyst for pesticide degradation using solar light. Journal of Hazardous Materials, 171, 1-3 (2009): 626-633.
- [9]. Tian, J.,J. Wang,J. Dai,X. Wang and Y. Yin. N-doped TiO<sub>2</sub>/ZnO composite powder and its photocatalytic performance for degradation of methyl orange. Surface and Coatings Technology, 204, 5 (2009): 723-730.
- [10]. Dindar, B. and S. Içli. Unusual photoreactivity of zinc oxide irradiated by concentrated sunlight. Journal of Photochemistry and Photobiology A: Chemistry, 140, (2001): 263-268.
- [11]. Leyva, E.,C. Montalvo,E. Moctezuma and S. Leyva. Photocatalytic degradation of pyridine in water solution using ZnO as an alternative catalyst to TiO<sub>2</sub>. Journal of Ceramic Processing Research, 9, 5 (2008): 455-462.
- [12]. Lim, C.S. Synthesis and characterization of TiO<sub>2</sub>-ZnO nanocomposite by a two-step chemical method. Ceramic Processing Research, 11, 5 (2010): 631-635.

- [13]. Qamar, M. and M. Muneer. A comparative photocatalytic activity of titanium dioxide and zinc oxide by investigating the degradation of vanillin. Desalination, 249, 2 (2009): 535-540.
- [14]. Sakthivel, S., et al. Solar photocatalytic degradation of azo dye: comparison of photocatalytic efficiency of ZnO and TiO<sub>2</sub>. Solar Energy Materials and Solar Cells, 77, 1 (2003): 65-82.
- [15]. Chen, C.,B. Yu,Liu P.,Liu J.F. and W. L. Investigation of nano-sized ZnO particles fabricated by various synthesis routes. Journal of Ceramic Processing Research, 12, (2011): 420~425.
- [16]. Lee, J.,A.J. Easteal,U. Pal and D. Bhattacharyya. Evolution of ZnO nanostructures in sol-gel synthesis. Current Applied Physics, 9, 4 (2009): 792-796.
- [17]. Pelaez, M., et al. A review on the visible light active titanium dioxide photocatalysts for environmental applications. Applied Catalysis B: Environmental, 125, (2012): 331-349.
- [18]. Nolan, N.T.,M.K. Seery and S.C. Pillai. Spectroscopic investigation of the anatase-to-rutile transformation of sol-Gel synthesisedTiO<sub>2</sub> photocatalysts. Journal of Physical Chemistry C, (2009).
- [19]. Wetchakun, N.,B. Incessungvorn,K. Wetchakun and S. Phanichphant. Influence of calcination temperature on anatase to rutile phase transformation in TiO<sub>2</sub> nanoparticles synthesized by the modified sol-gel method. Materials Letters, 82, (2012): 195-198.
- [20]. M.W. Chase,J.L. Curnutt,H. Prophet,R.A. McDonald and A.N. Syverud. JANAF Thermochemical Tables, 1975 Supplement. J. Phys. Chem, 4, (1975).
- [21]. Rana S. and D. A. The photocatalytic degradation of priority pollutants. Master,Biotechnology and Environmental Sciences, Thapar University,2009
- [22]. Zhiyong Fan and J.G. Lu\*. Zinc Oxide Nanostructures: Synthesis and Properties. Department of Chemical Engineering and Materials Science & Department of Electrical Engineering and Computer Science, University of California,2005
- [23]. Akpan, U.G. and B.H. Hameed. The advancements in sol-gel method of doped-TiO<sub>2</sub> photocatalysts. Applied Catalysis A: General, 375, 1 (2010): 1-11.
- [24]. Prasad, K.,D.V. Pinjari,A.B. Pandit and S.T. Mhaske. Phase transformation of nanostructured titanium dioxide from anatase-to-rutile via combined ultrasound assisted sol-gel technique. Ultrasonics Sonochemistry, 17, 2 (2010): 409-415.
- [25]. Alias, S.S.,A.B. Ismail and A.A. Mohamad. Effect of pH on ZnO nanoparticle properties synthesized by sol-gel centrifugation. Journal of Alloys and Compounds, 499, 2 (2010): 231-237.

- [26]. Hayat, K.,M.A. Gondal,M.M. Khaled,S. Ahmed and A.M. Shemsi. Nano ZnO synthesis by modified sol gel method and its application in heterogeneous photocatalytic removal of phenol from water. Applied Catalysis A: General, 393, 1-2 (2011): 122-129.
- [27]. Li, Y.,L. Xu,X. Li,X. Shen and A. Wang. Effect of aging time of ZnO sol on the structural and optical properties of ZnO thin films prepared by sol-gel method. Applied Surface Science, 256, 14 (2010): 4543-4547.
- [28]. CHANG, H.T.,N.-M. WU and F. ZHU. A kinetic model for photocatalytic degradation of organic contaminants in a thin-film TiO<sub>2</sub> Catalyst. (1999).
- [29]. Valente, J.P.S.,P.M. Padilha and A.O. Florentino. Studies on the adsorption and kinetics of photodegradation of a model compound for heterogeneous photocatalysis onto TiO<sub>2</sub>. Chemosphere, 64, 7 (2006): 1128-1133.
- [30]. Zou, L.,Y. Luo,M. Hooper and E. Hu. Removal of VOCs by photocatalysis process using adsorption enhanced TiO<sub>2</sub>-SiO<sub>2</sub> catalyst. Chemical Engineering and Processing: Process Intensification, 45, 11 (2006): 959-964.
- [31]. Shao, M.,J. Han,M. Wei,D.G. Evans and X. Duan. The synthesis of hierarchical Zn-Ti layered double hydroxide for efficient visible-light photocatalysis. Chemical Engineering Journal, 168, 2 (2011): 519-524.
- [32]. Gouvea, C.A.K., et al. Semiconductor-assisted photocatalytic degradation of reactive. Chemosphere, 40, (1999): 443-440.
- [33]. Daneshvar, N.,D. Salari and A.R. Khataee. Photocatalytic degradation of azo dye acid red 14 in water: investigation of the effect of operational parameters. Journal of Photochemistry and Photobiology A: Chemistry, 157, 1 (2003): 111-116.
- [34]. Oyama, T., et al. Solar photocatalysis, photodegradation of a commercial detergent in aqueous TiO<sub>2</sub> dispersions under sunlight irradiation. Solar Energy, 77, 5 (2004): 525-532.
- [35]. Pourata, R.,A.R. Khataee,S. Aber and N. Daneshvar. Removal of the herbicide Bentazon from contaminated water in the presence of synthesized nanocrystalline TiO<sub>2</sub> powders under irradiation of UV-C light. Desalination, 249, 1 (2009): 301-307.
- [36]. Behnajady, M.,N. Modirshahla and R. Hamzavi. Kinetic study on photocatalytic degradation of C.I. Acid Yellow 23 by ZnO photocatalyst. Journal of Hazardous Materials, 133, 1-3 (2006): 226-232.
- [37]. Daneshvar, N.,M.H. Rasoulifard,A.R. Khataee and F. Hosseinzadeh. Removal of C.I. Acid Orange 7 from aqueous solution by UV irradiation in the presence of ZnO nanopowder. Journal of Hazardous Materials, 143, 1-2 (2007): 95-101.
- [38]. Mijin, D., et al. A study of the photocatalytic degradation of metamitron in ZnO water suspensions. Desalination, 249, 1 (2009): 286-292.

- [39]. Wannipa Pradittakan, E.S., Alisa S. Vangnai and V. Pavarajarn. Comparative Study on Mechanism of Photocatalytic Degradation of Diuron on Titanium Dioxide and Zinc Oxide. Master, Chemical Engineering, Chulalongkorn University, 2011
- [40]. Saowalux Sittichoktum and V. Pavarajarn. Photocatalytic Degradation of Linuron on Titania and Zinc Oxide. Master, Chemical Engineering, Chulalongkorn University, 2012
- [41]. Zhang, S., Z. Zheng, J. Wang and J. Chen. Heterogeneous photocatalytic decomposition of benzene on lanthanum-doped TiO<sub>2</sub> film at ambient temperature. Chemosphere, 65, 11 (2006): 2282-2288.
- [42]. Kumar, K.V., K. Porkodi and F. Rocha. Langmuir–Hinshelwood kinetics – A theoretical study. Catalysis Communications, 9, 1 (2008): 82-84.
- [43]. Gora, A., B. Toepfer, V. Puddu and G. Li Puma. Photocatalytic oxidation of herbicides in single-component and multicomponent systems: Reaction kinetics analysis. Applied Catalysis B: Environmental, 65, 1-2 (2006): 1-10.
- [44]. Annadurai, G., L.Y. Ling and J.-F. Lee. Adsorption of reactive dye from an aqueous solution by chitosan: isotherm, kinetic and thermodynamic analysis. Journal of Hazardous Materials, 152, 1 (2008): 337-346.
- [45]. Mittal, A., L. Kurup and J. Mittal. Freundlich and Langmuir adsorption isotherms and kinetics for the removal of Tartrazine from aqueous solutions using hen feathers. Journal of Hazardous Materials, 146, 1-2 (2007): 243-248.
- [46]. Kim, S.-H., H.H. Ngo, H.K. Shon and S. Vigneswaran. Adsorption and photocatalysis kinetics of herbicide onto titanium oxide and powdered activated carbon. Separation and Purification Technology, 58, 3 (2008): 335-342.
- [47]. Emmanuel Olajide Oyelude\* and U.R. Owusu. Adsorption of methylene blue from aqueous solution using acid modified calotropis procera leaf powder. Journal of Applied Sciences in Environmental Sanitation, 6, (2011): 477-484.
- [48]. Rao, Y.F. and W. Chu. Linuron decomposition in aqueous semiconductor suspension under visible light irradiation with and without H<sub>2</sub>O<sub>2</sub>. Chemical Engineering Journal, 158, 2 (2010): 181-187.
- [49]. Kansal, S., M. Singh and D. Sud. Studies on photodegradation of two commercial dyes in aqueous phase using different photocatalysts. Journal of Hazardous Materials, 141, 3 (2007): 581-590.
- [50]. Daneshvar, N., S. Aber, M.S. Seyed Dorraji, A.R. Khataee and M.H. Rasoulifard. Photocatalytic degradation of the insecticide diazinon in the presence of prepared nanocrystalline ZnO powders under irradiation of UV-C light. Separation and Purification Technology, 58, 1 (2007): 91-98.
- [51]. López-Muñoz, M.J., A. Revilla and J. Aguado. Heterogeneous photocatalytic degradation of isoproturon in aqueous solution: Experimental design and intermediate products analysis. Catalysis Today, 209, (2013): 99-107.

- [52]. Mascolo, G.,A. Lopez,H. James and M. Fielding. By-products formation during degradation of isoproturon in aqueous solution. I: ozonation. Water Research, 35, 7 (2001): 1695-1704.
- [53]. Constanze Pietsch,Eberhard Krause,B. Kent Burnison,Christian E.W. Steinberg and S. Pflugmacher. Effects and metabolism of the phenylurea herbicide isoproturon in the submerged macrophyte *Ceratophyllum demersum* L. Journal of Applied Botany and Food Quality, 80, (2006): 25 - 30.
- [54]. Lin, S.-H.,C.-H. Chiou,C.-K. Chang and R.-S. Juang. Photocatalytic degradation of phenol on different phases of TiO<sub>2</sub> particles in aqueous suspensions under UV irradiation. Journal of Environmental Management, 92, 12 (2011): 3098-3104.
- [55]. Jeevan L. KHURANA, et al. Characterization of the phenylurea hydrolases A and B: founding members of a novel amidohydrolase subgroup. Biochemical Journal, 418, (2009): 431-441.
- [56]. Akyol, A.,H.C. Yatmaz and M. Bayramoglu. Photocatalytic decolorization of Remazol Red RR in aqueous ZnO suspensions. Applied Catalysis B: Environmental, 54, 1 (2004): 19-24.

## **APPENDICE**

**APPENDIX A**  
**ISOPROTURON CARIBRATION CURVE**

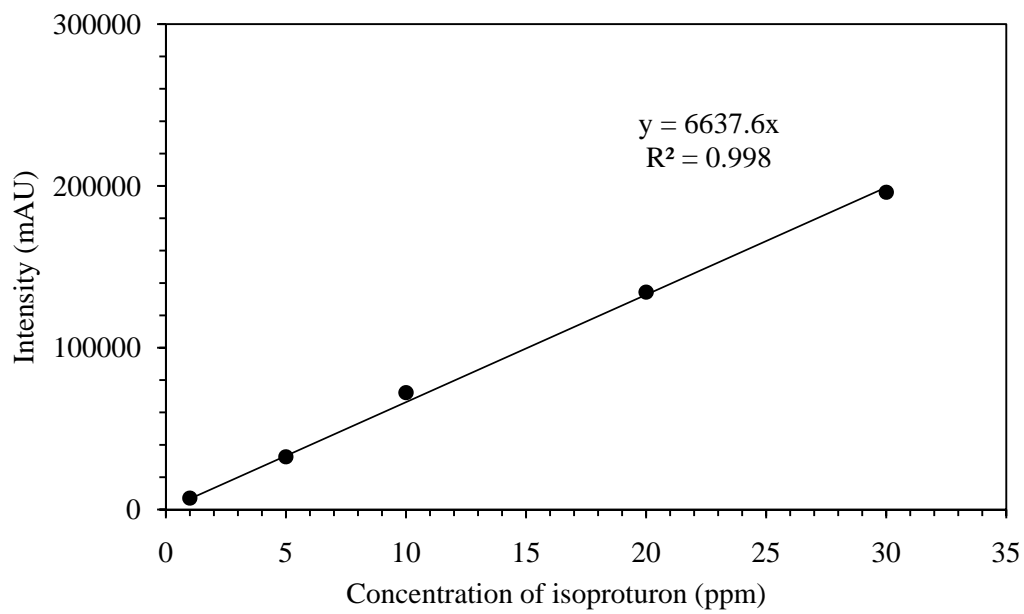


**Figure A.1** The calibration curve of isoproturon.



## APPENDIX B

### POINT OF ZERO CHARGE DETERMINATION

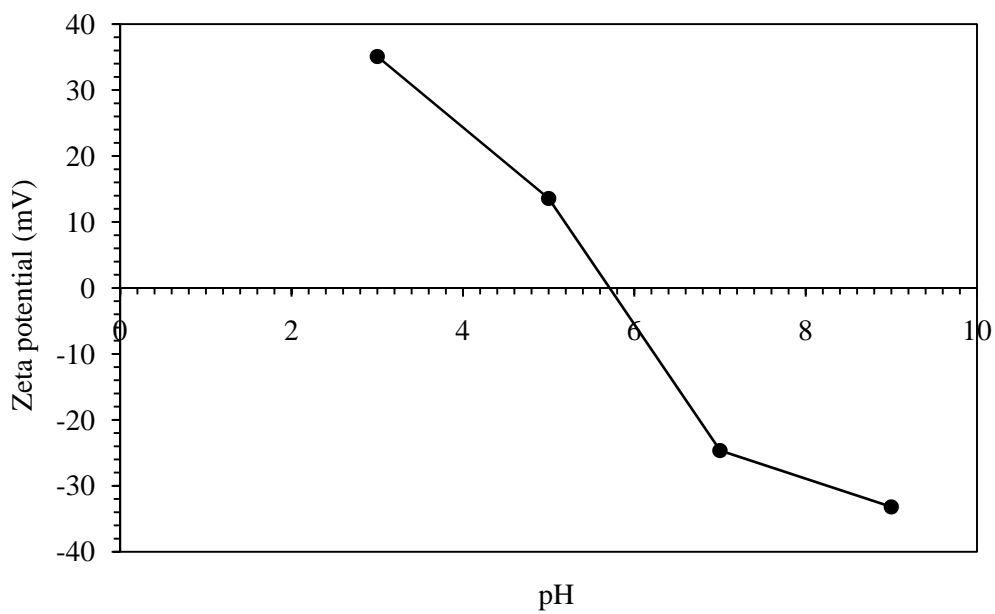


**Figure B.1** Determination of the point of zero charge of commercial titanium dioxide.

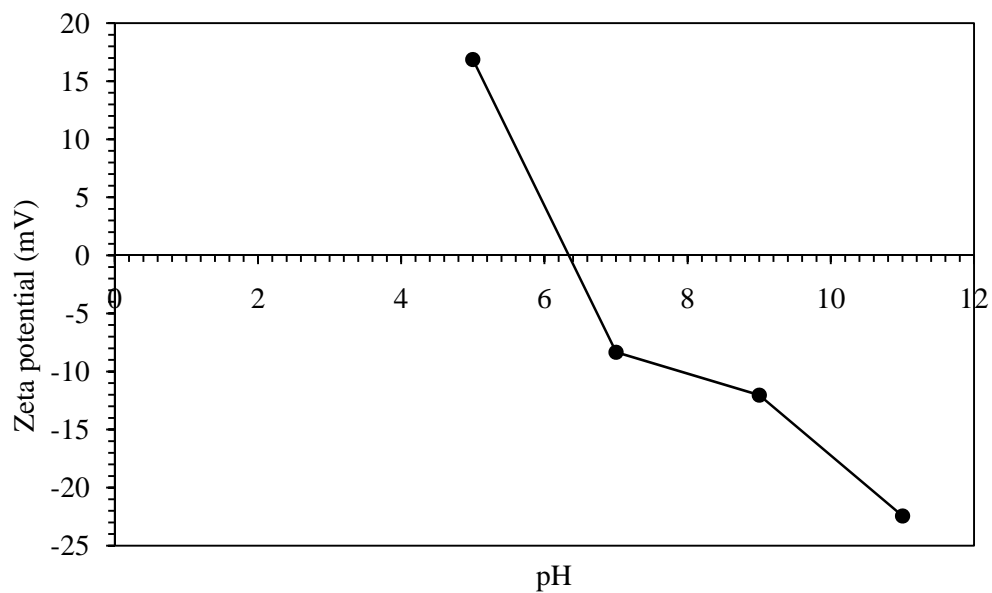


**Figure B.2** Determination of the point of zero charge of commercial zinc oxide.

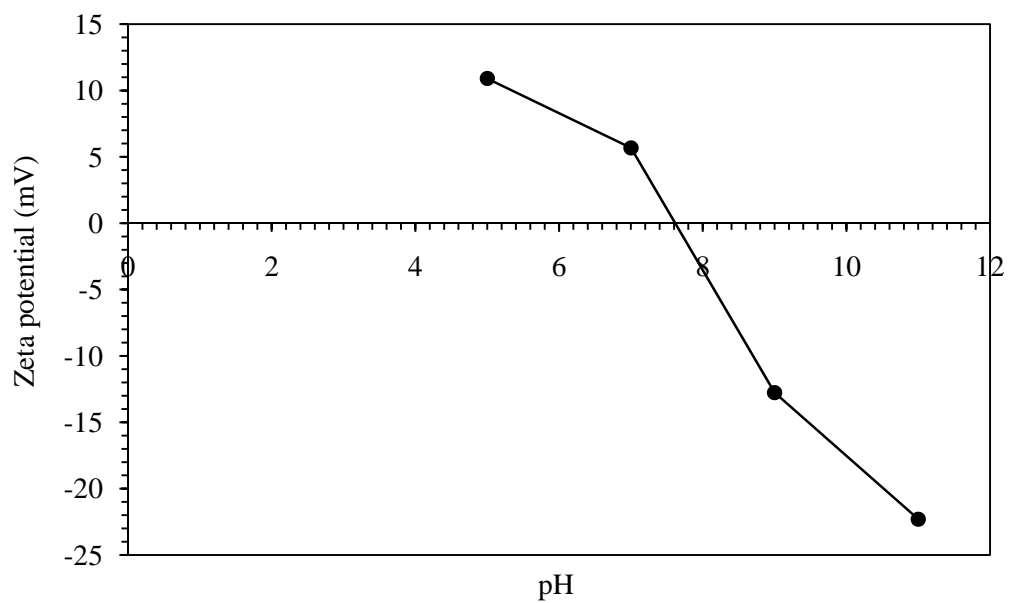


**Figure B.3** Determination of the point of zero charge of synthesized zinc oxide.

## APPENDIX C

### LC-MS/MS MASS SPECTRUM

All samples were sent for analysis at Scientific and Technological Research Equipment Centre. The mass spectrometer was equipped with phenyl column (Vertiseq UPS column, 2.1x100mm) and an ESI ion source operating in positive ion mode in the range 70-1,000 m/z. The mobile phase was 60% (v/v) acetonitrile mixed with 40% (v/v) deionized water and total flow rate was 0.2 ml/min.

#### C.1 Mass spectrum of isotroturon solution

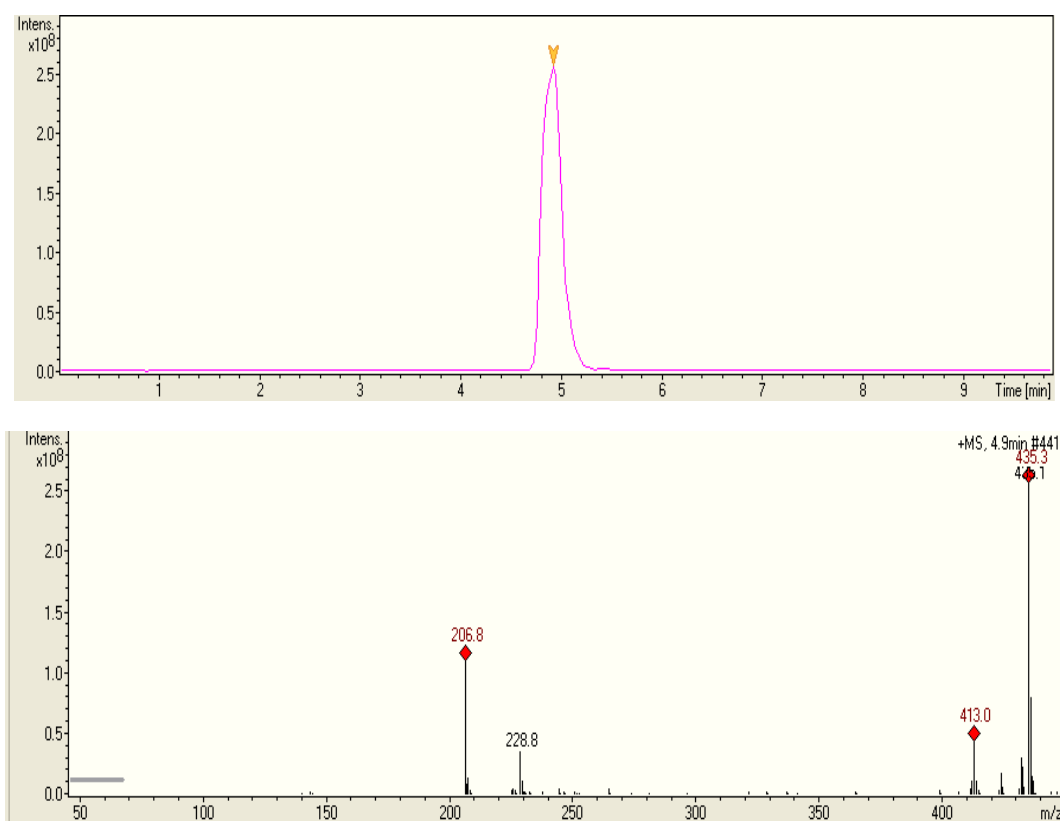


**Figure C.1** Chromatogram of isotroturon solution.

## C.2 MS/MS spectrum of isoproturon solution from photodegradation by commercial titanium dioxide.

### C2.1 At natural of solution

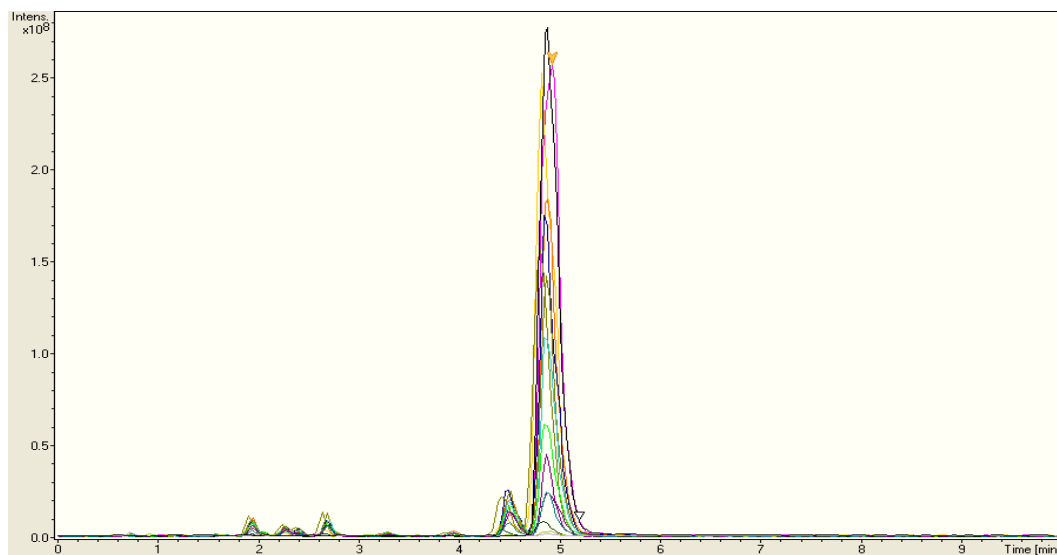
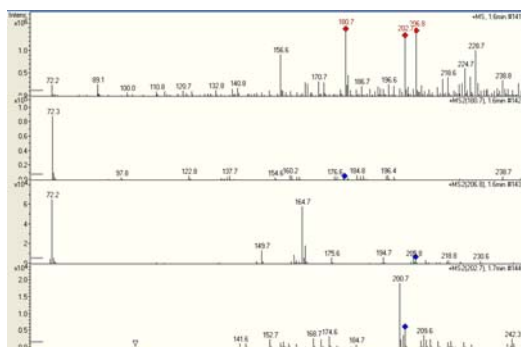
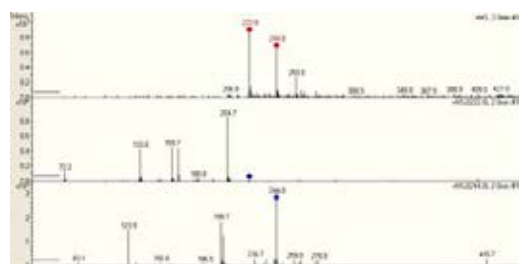


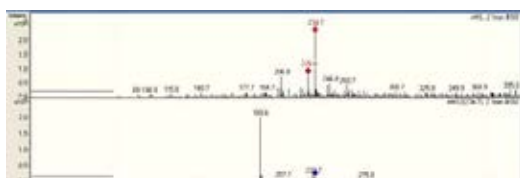
**Figure C.2** Chromatogram of isoproturon solution during photodegradation process using commercial titanium dioxide as catalyst at natural of solution (0-360 min during reaction process) are shown in (a). MS/MS spectrums at various retention times are display in (b)-(j).



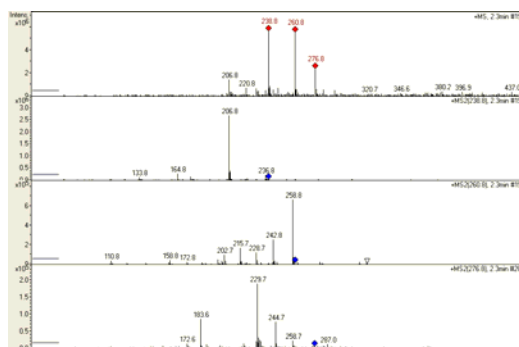
(b) Retention time 1.6 min



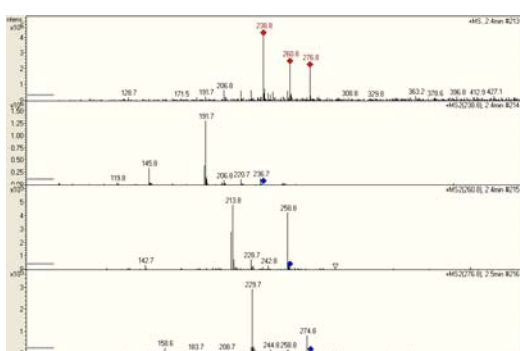
(c) Retention time 2.0 min



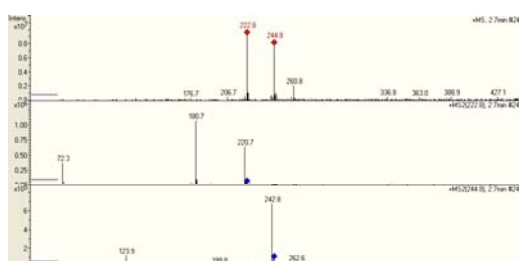
(d) Retention time 2.1 min



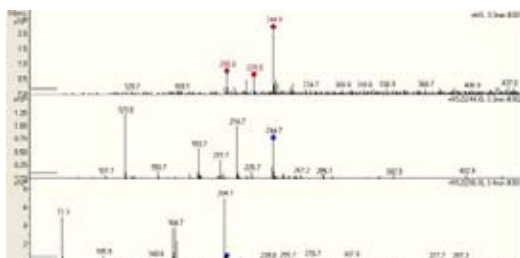
(e) Retention time 2.3 min



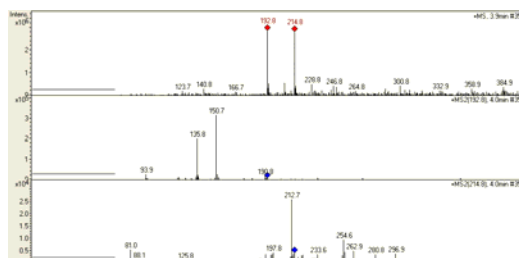
(f) Retention time 2.4 min



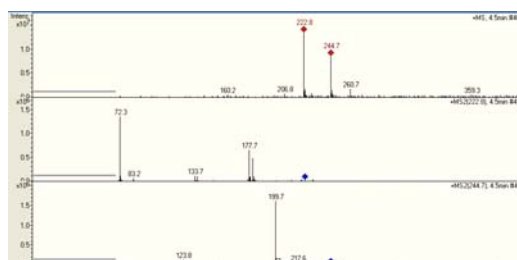
(g) Retention time 2.7 min



(h) Retention time 3.3 min



(i) Retention time 3.9 min



(j) Retention time 4.5 min

**Figure C.2** (continued).

## C2.2 At pH 3 of solution

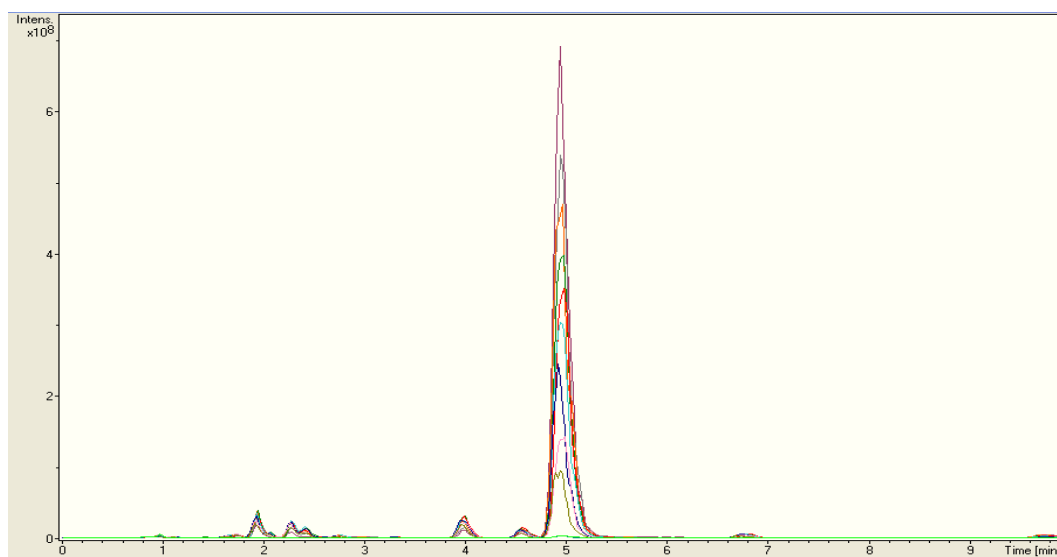
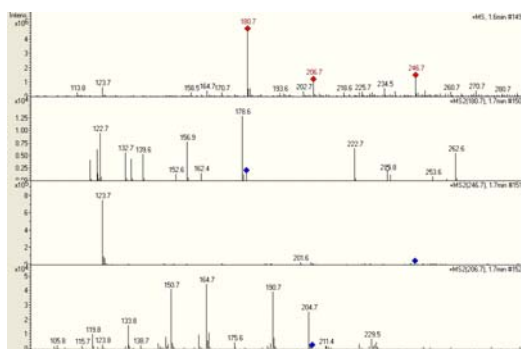
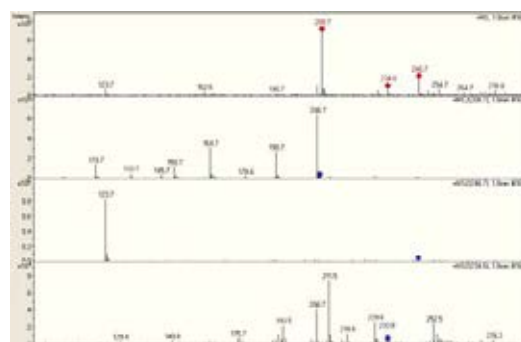


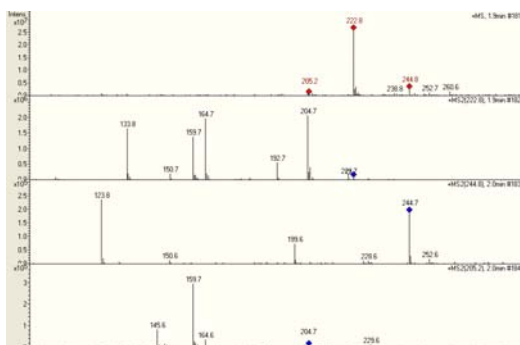
**Figure C.3** Chromatogram of isoproturon solution during photodegradation process using commercial titanium dioxide as catalyst at pH 3 of solution (0-360 min during reaction process) are shown in (a). MS/MS spectrums at various retention times are display in (b)-(k).



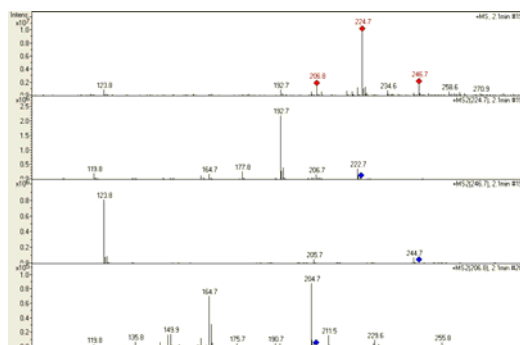
(b) Retention time 1.6 min



(c) Retention time 1.8 min



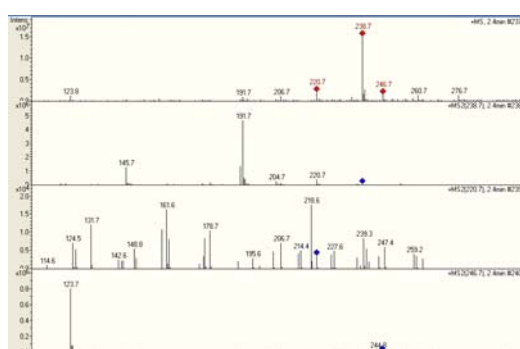
(d) Retention time 2.0 min



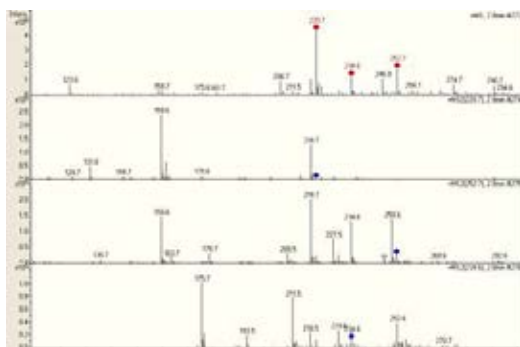
(e) Retention time 2.1 min



(f) Retention time 2.3 min



(g) Retention time 2.4 min



(h) Retention time 2.8 min



(i) Retention time 4.0 min

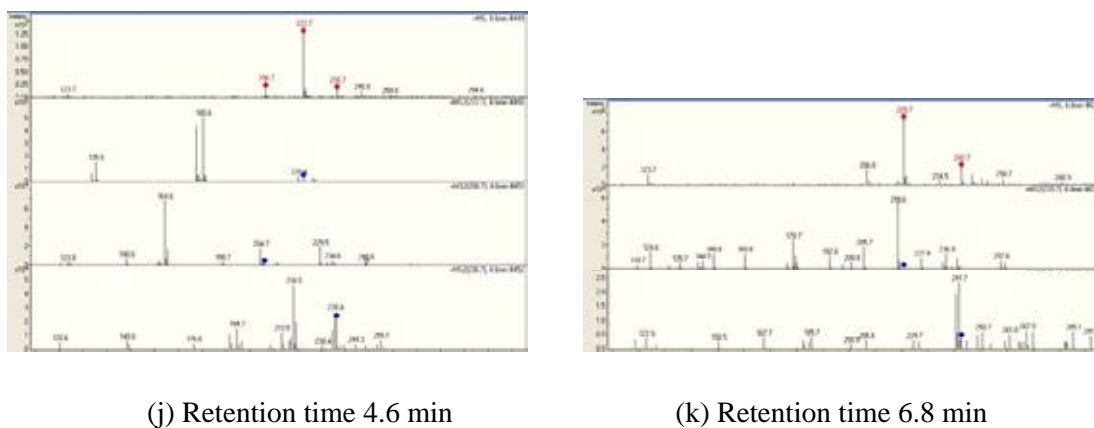


**Figure C.3** (continued).

### C2.3 At pH 5 of solution

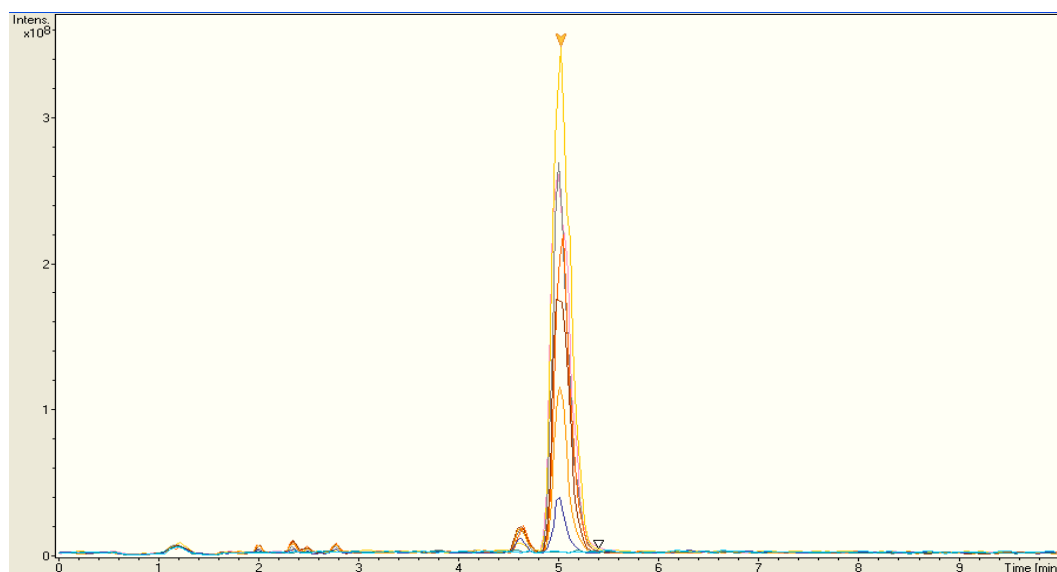
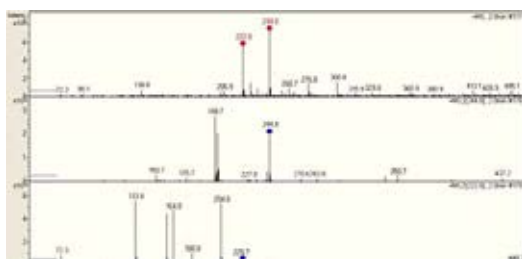
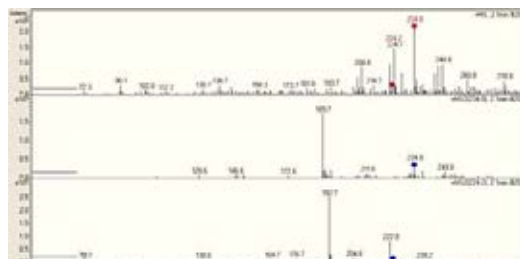


**Figure C.4** Chromatogram of isoproturon solution during photodegradation process using commercial titanium dioxide as catalyst at pH 5 of solution (0-360 min during reaction process) are shown in (a). MS/MS spectrums at various retention times are display in (b)-(g).

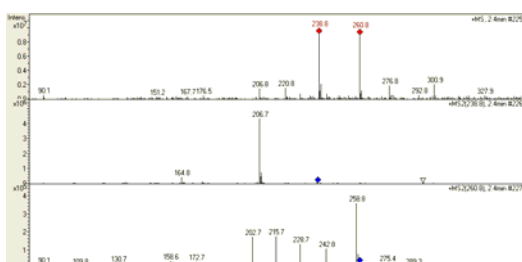




(b) Retention time 2.0 min



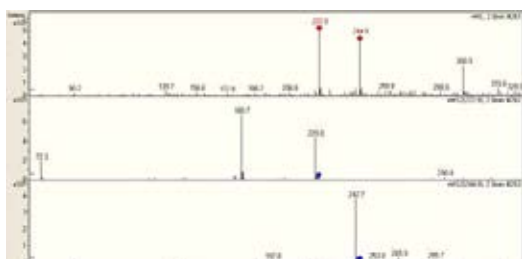
(c) Retention time 2.1 min



(d) Retention time 2.4 min



(e) Retention time 2.5 min



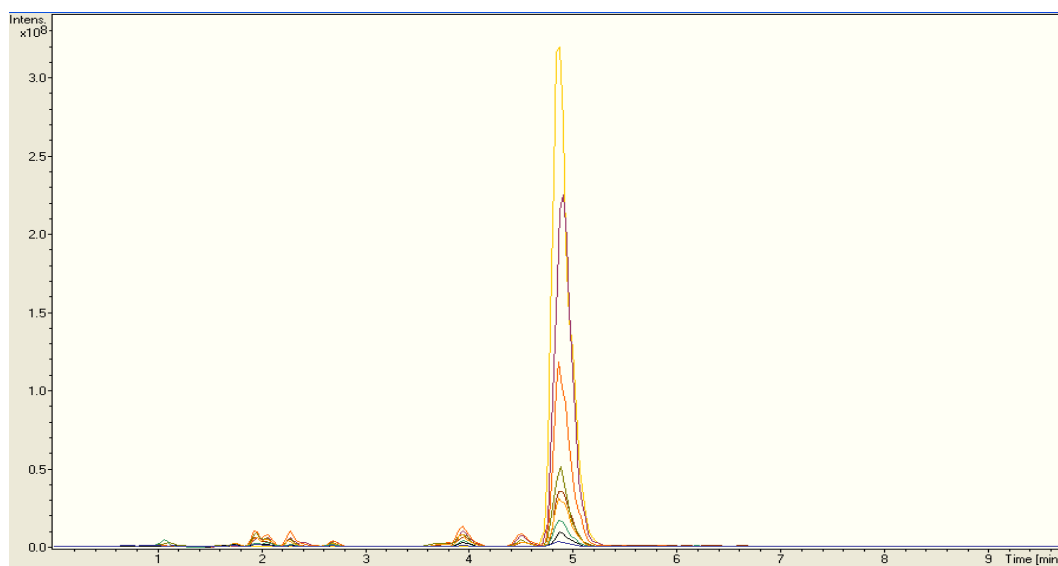
(f) Retention time 2.8 min



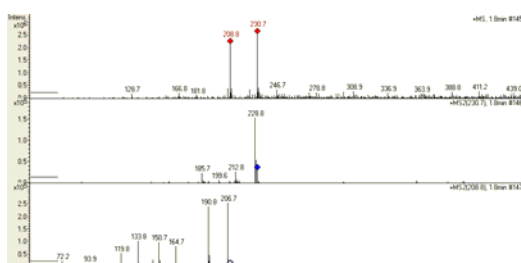
(g) Retention time 4.6 min

Figure C.4 (continued).

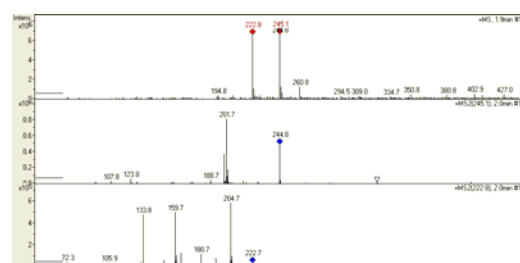
## C2.4 At pH 10 of solution



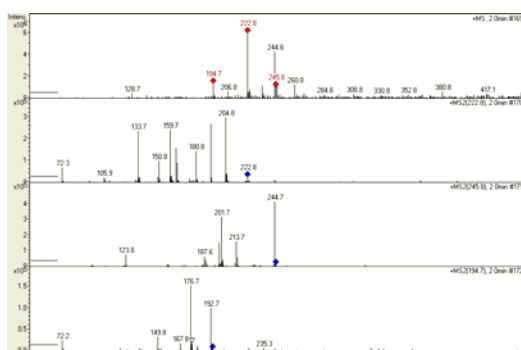
**Figure C.5** Chromatogram of isotiproturon solution during photodegradation process using commercial titanium dioxide as catalyst at pH 10 of solution (0-360 min during reaction process) are shown in (a). MS/MS spectrums at various retention times are display in (b)-(k).



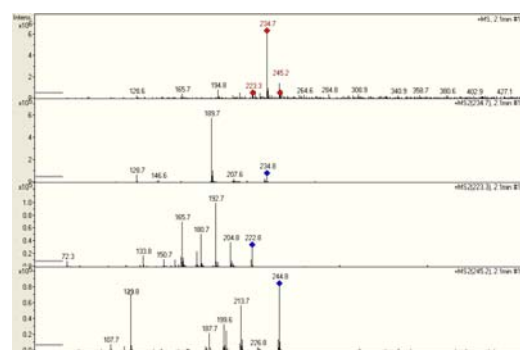
(b) Retention time 1.8 min



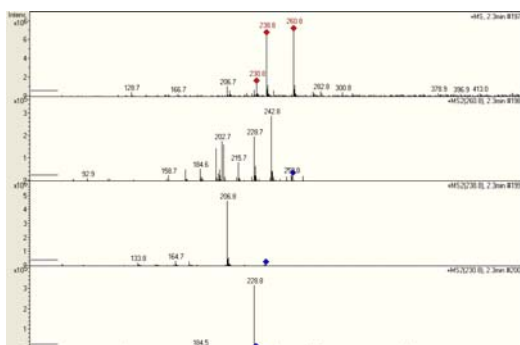
(c) Retention time 1.9 min



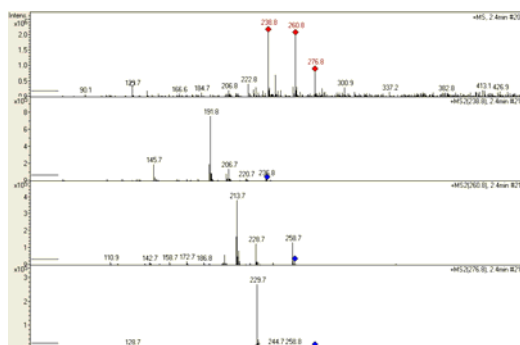
(d) Retention time 2.0 min



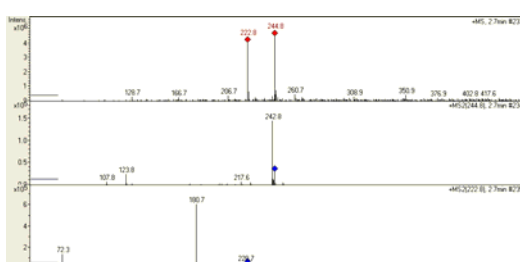
(e) Retention time 2.1 min



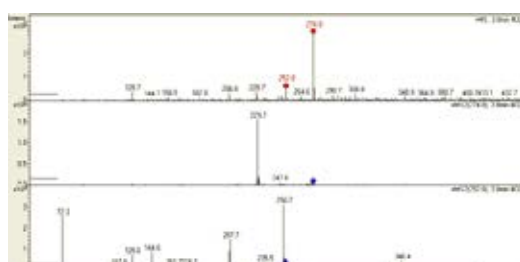
(f) Retention time 2.3 min



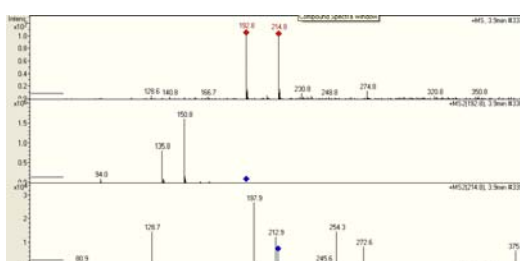
(g) Retention time 2.4 min



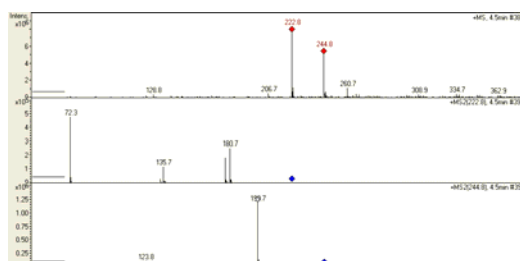
(h) Retention time 2.7 min



(i) Retention time 3.8 min



(j) Retention time 3.9 min



(k) Retention time 4.5 min

Figure C.5 (continued).

### C.3 MS/MS spectrum of isoproturon solution from photodegradation by commercial zinc oxide

#### C3.1 At natural of solution

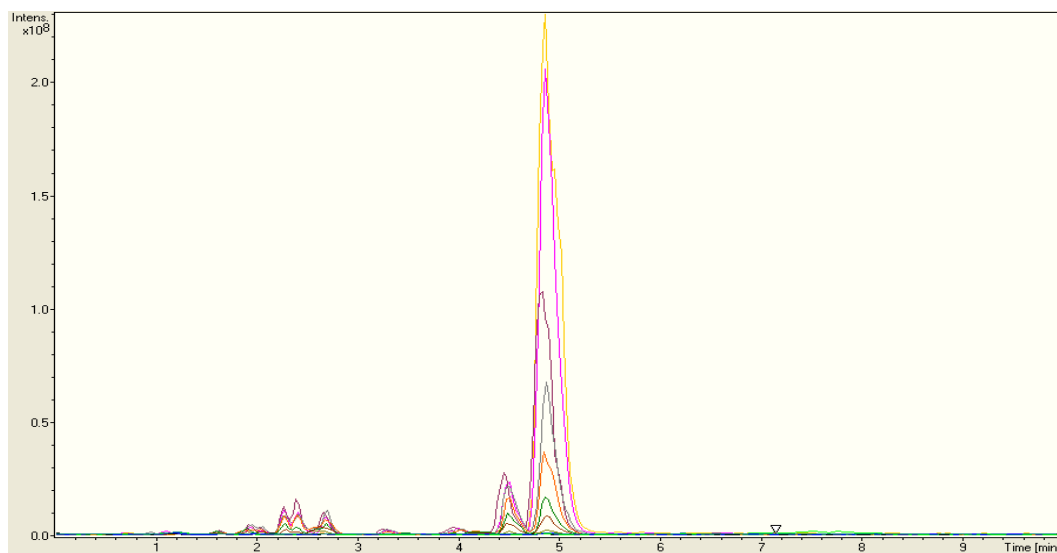
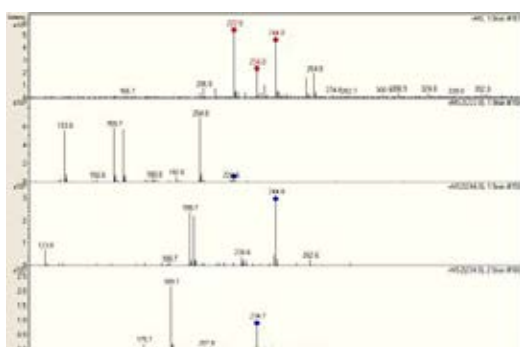


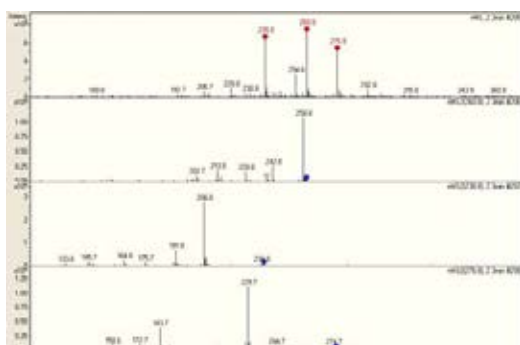
**Figure C.6** Chromatogram of isoproturon solution during photodegradation process using commercial zinc oxide as catalyst at natural of solution (0-360 min during reaction process) are shown in (a). MS/MS spectrums at various retention times are display in (b)-(k).



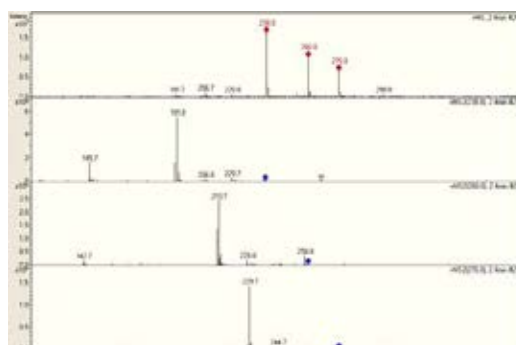
(b) Retention time 1.9 min



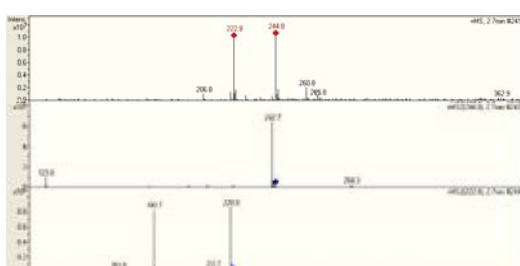
(c) Retention time 2.1 min



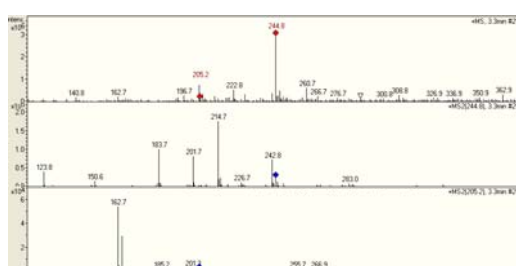
(d) Retention time 2.3 min



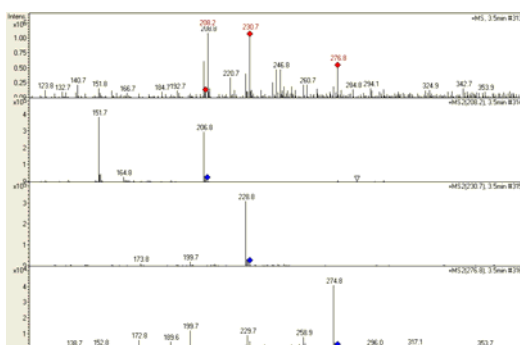
(e) Retention time 2.4 min



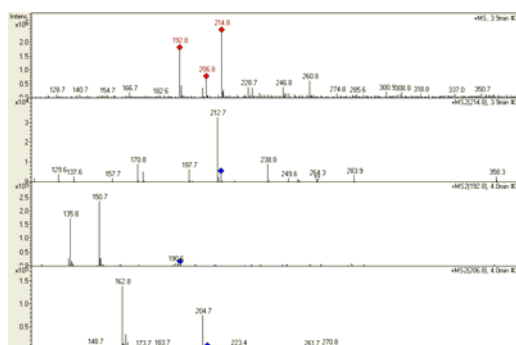
(f) Retention time 2.7 min



(g) Retention time 3.3 min

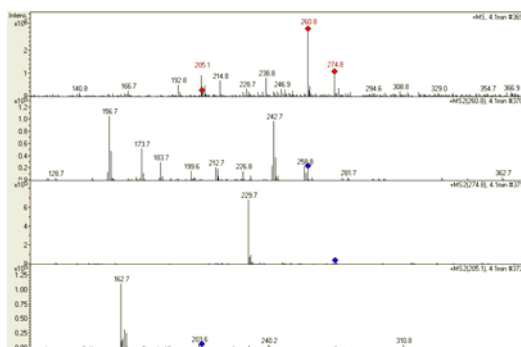


(g) Retention time 3.5 min

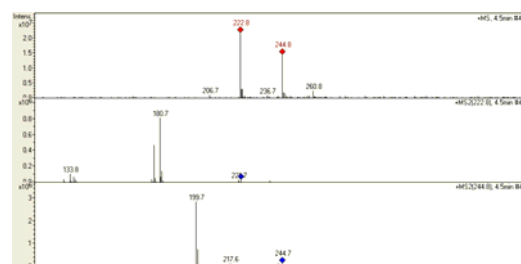


(i) Retention time 3.9 min

Figure C.6 (continued)



(j) Retention time 4.1 min



(k) Retention time 4.5 min

**Figure C.6** (continued)

### C3.2 At pH 3 of solution

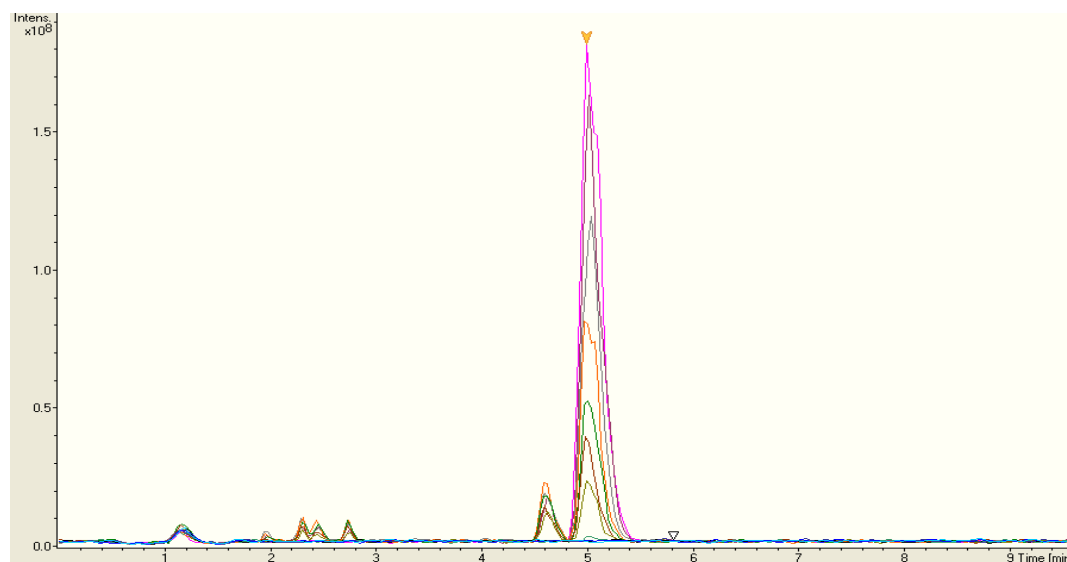
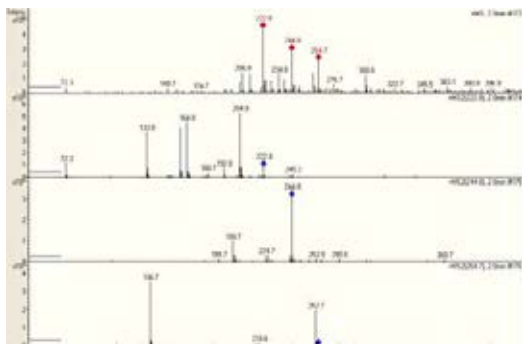
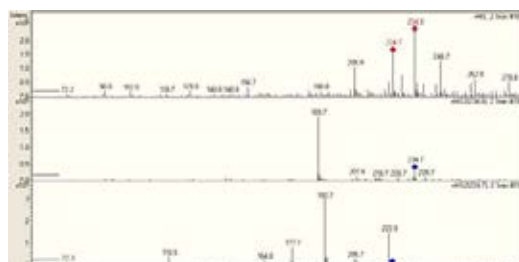


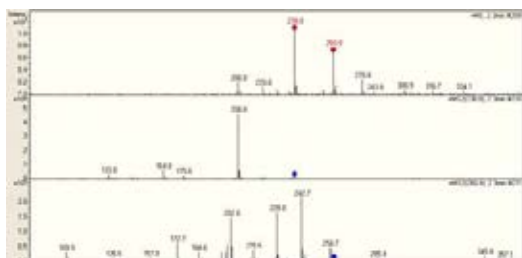
**Figure C.7** Chromatogram of isotproturon solution during photodegradation process using commercial zinc oxide as catalyst at pH 3 of solution (0-360 min during reaction process) are shown in (a). MS/MS spectrums at various retention times are display in (b)-(h).



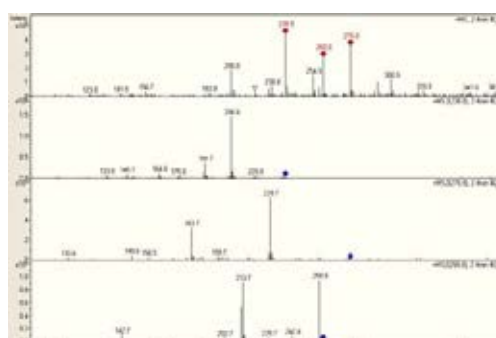
(b) Retention time 2.0 min



(c) Retention time 2.1 min



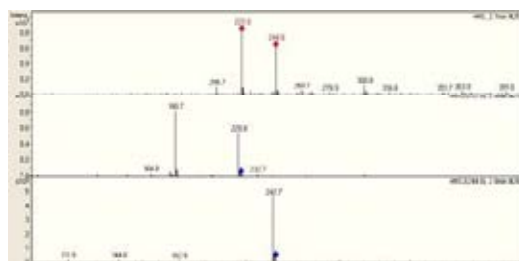
(d) Retention time 2.3 min



(e) Retention time 2.4 min

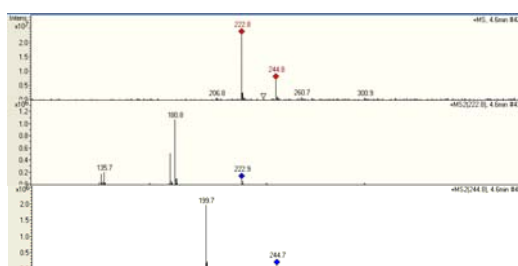


(f) Retention time 2.5 min



(g) Retention time 2.7 min

Figure C.7 (continued)



(h) Retention time 4.6 min

**Figure C.7** (continued)

### C3.3 At pH 5 of solution

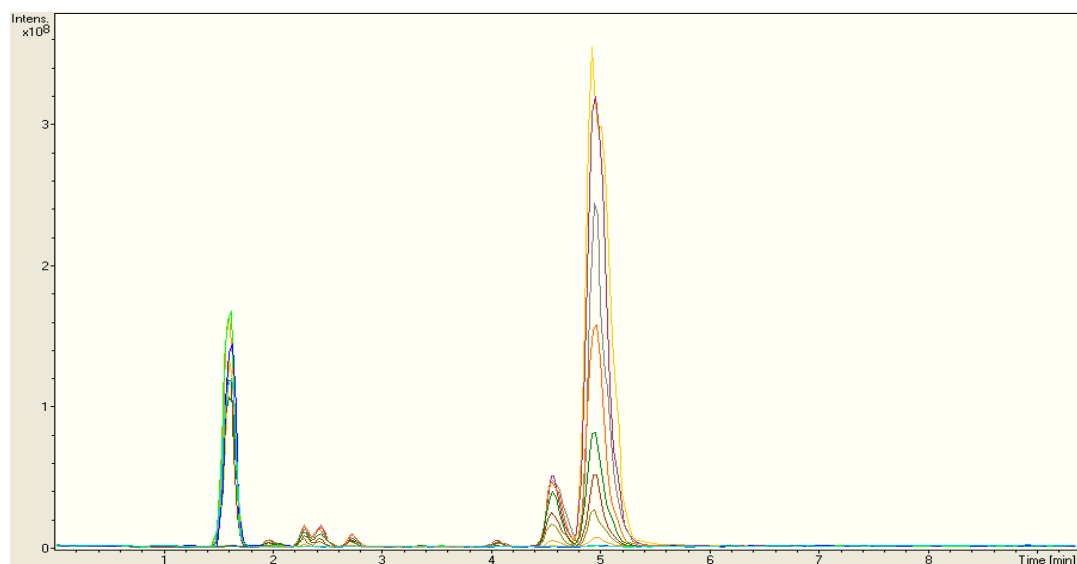
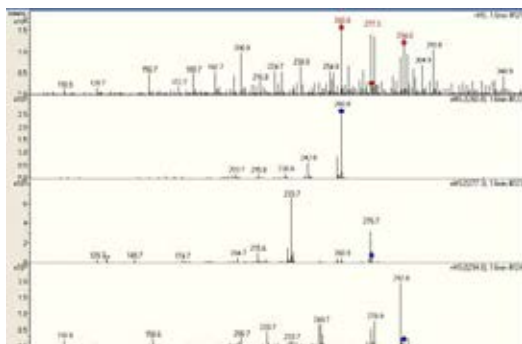


**Figure C.8** Chromatogram of isoproturon solution during photodegradation process using commercial zinc oxide as catalyst at pH 5 of solution (0-360 min during reaction process) are shown in (a). MS/MS spectrums at various retention times are display in (b)-(l).





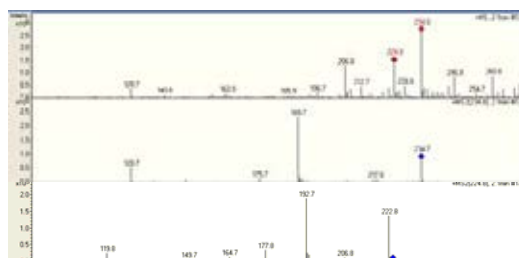
(b) Retention time 1.6 min



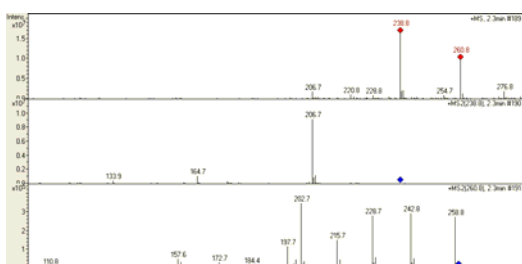
(c) Retention time 1.9 min



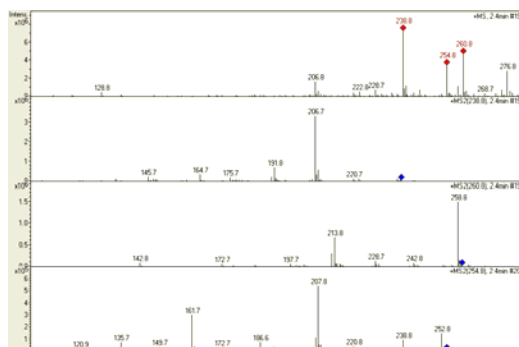
(d) Retention time 2.0 min



(e) Retention time 2.1 min



(f) Retention time 2.3 min

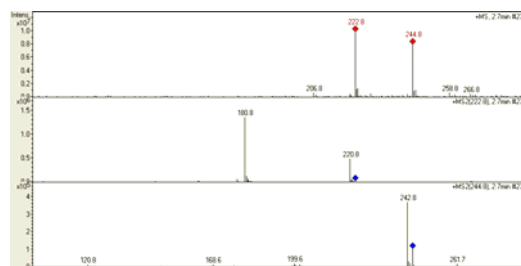


(g) Retention time 2.4 min

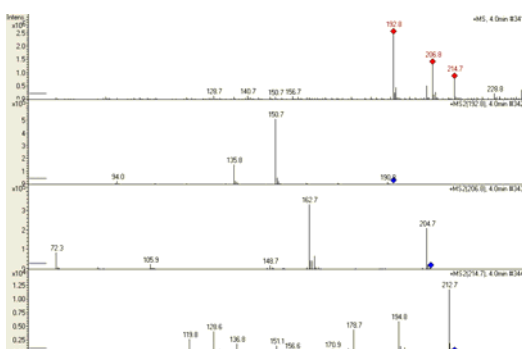
Figure C.8 (continued)



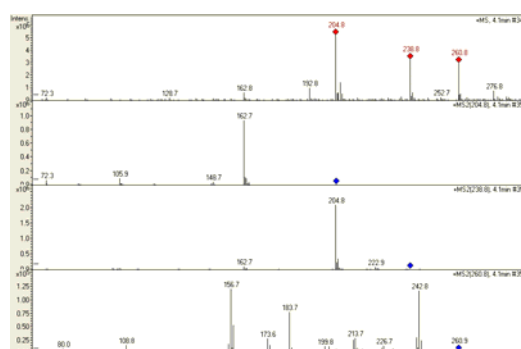
(h) Retention time 2.5 min



(i) Retention time 2.7 min



(j) Retention time 4.0 min



(k) Retention time 4.1 min



(l) Retention time 4.6 min

**Figure C.8** (continued)

## C3.3 At pH 10 of solution

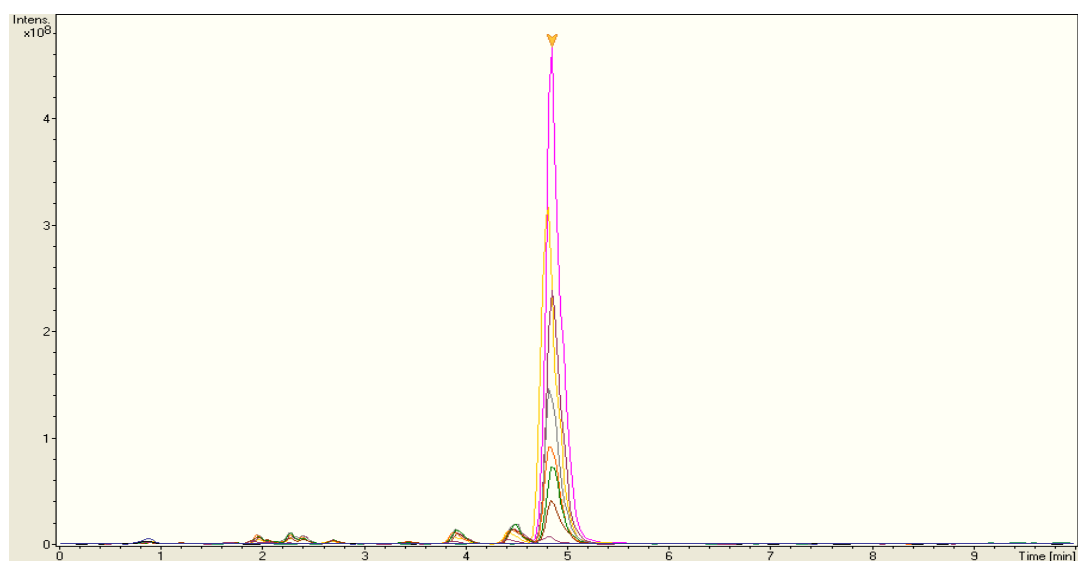
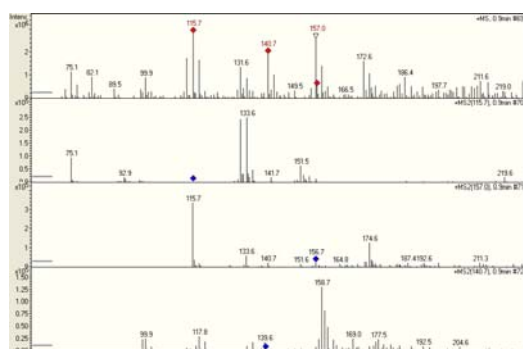
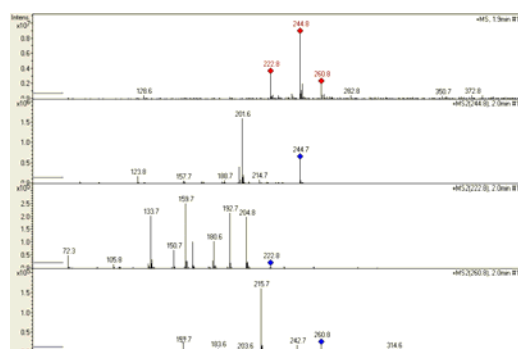


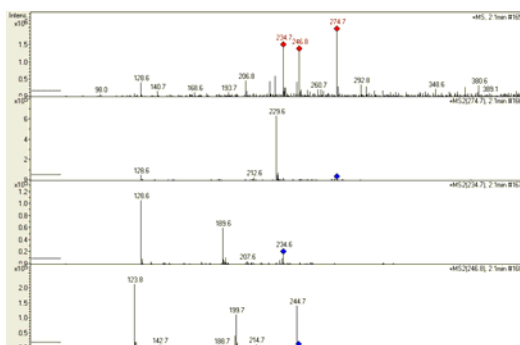
**Figure C.9** Chromatogram of isoproturon solution during photodegradation process using commercial zinc oxide as catalyst at pH 10 of solution (0-360 min during reaction process) are shown in (a). MS/MS spectrums at various retention times are display in (b)-(k).



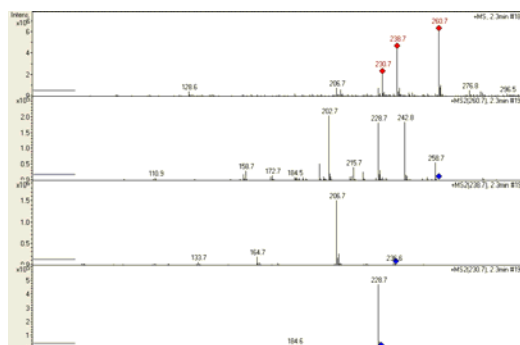
(b) Retention time 0.9 min



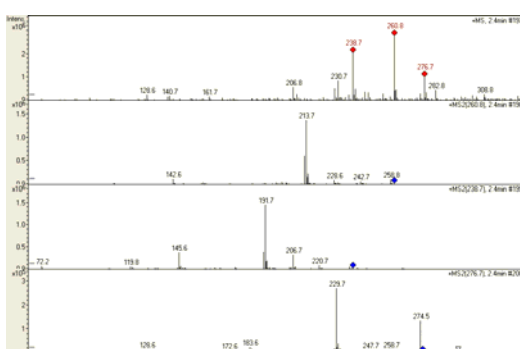
(c) Retention time 1.9 min



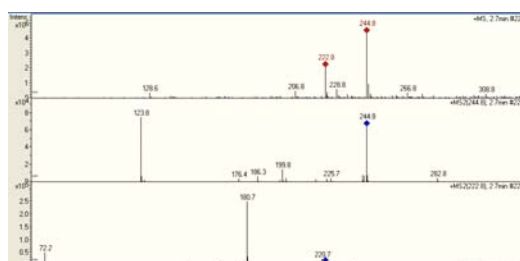
(d) Retention time 2.1 min



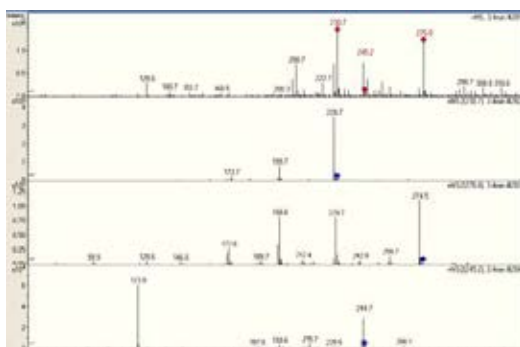
(e) Retention time 2.3 min



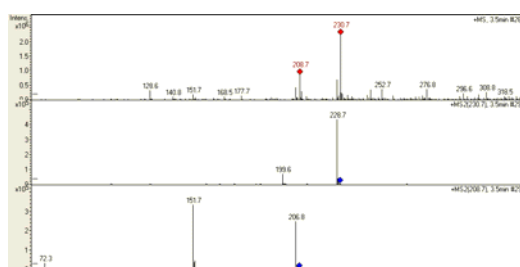
(f) Retention time 2.4 min



(g) Retention time 2.7 min



(h) Retention time 3.4 min



(i) Retention time 3.5 min

Figure C.9 (continued)

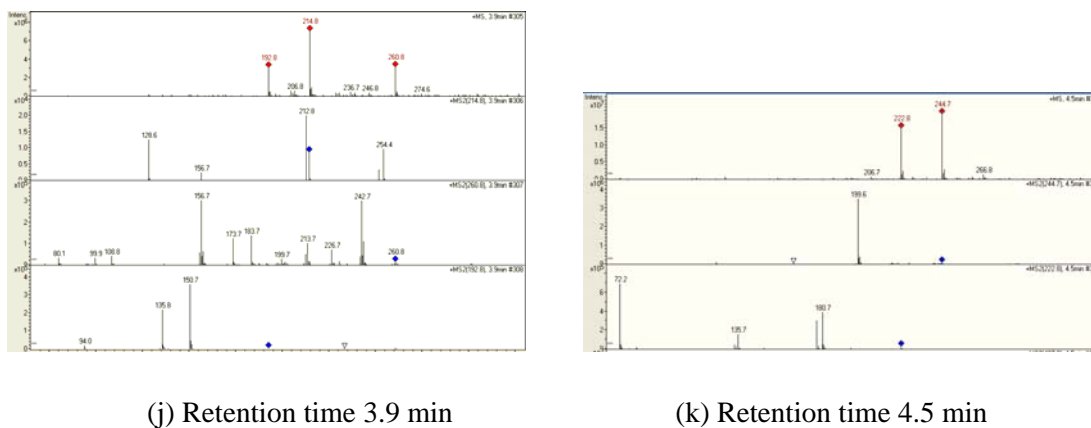


**Figure C.9** (continued)

C.4 MS/MS spectrum of isoproturon solution from photodegradation by synthesized zinc oxide

C4.1 At natural of solution

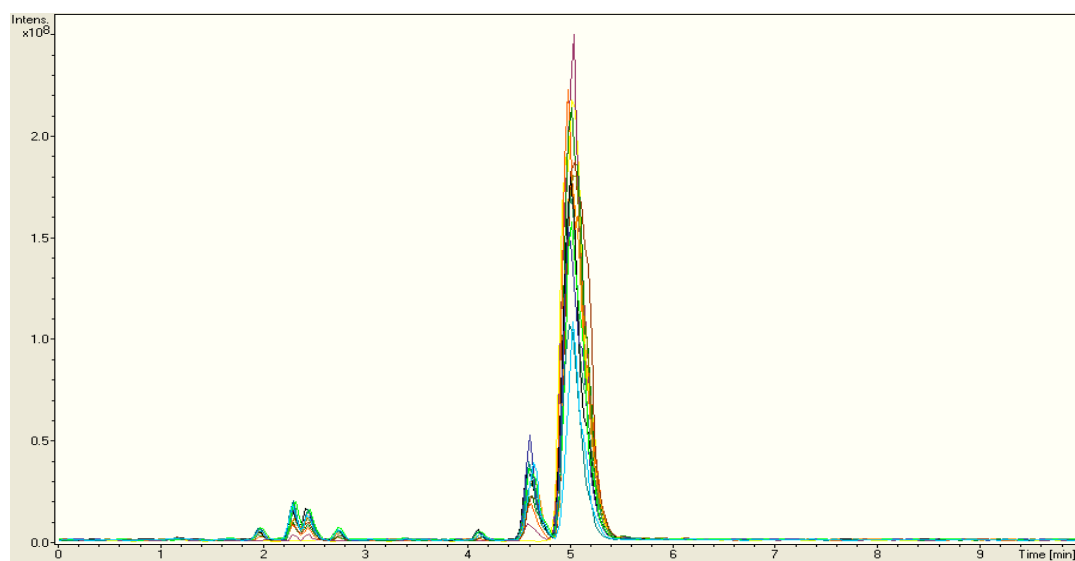
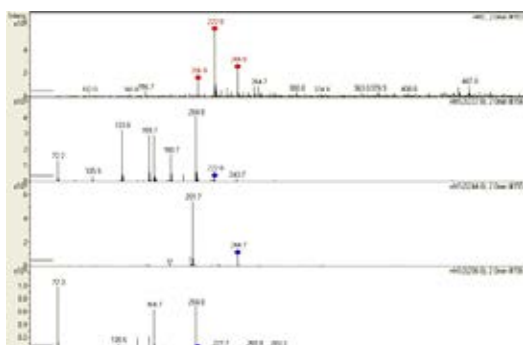
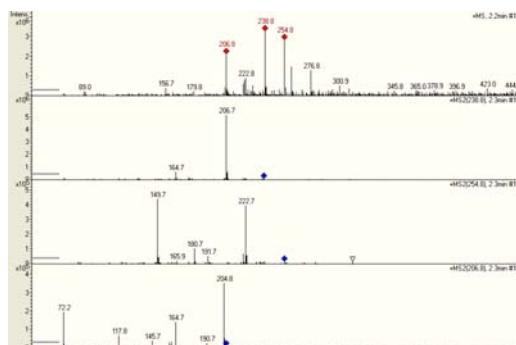


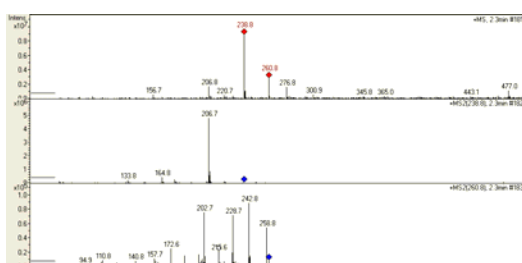
**Figure C.10** Chromatogram of isoproturon solution during photodegradation process using synthesized zinc oxide as catalyst at natural of solution (0-360 min during reaction process) are shown in (a). MS/MS spectrums at various retention times are display in (b)-(h).



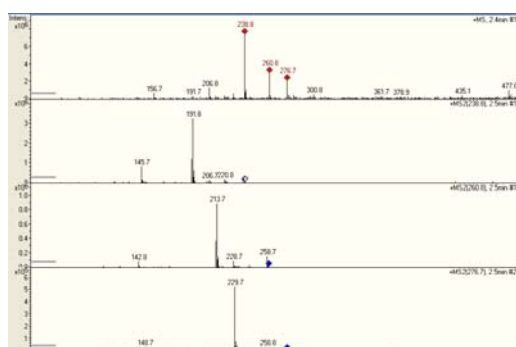
(b) Retention time 2.0 min



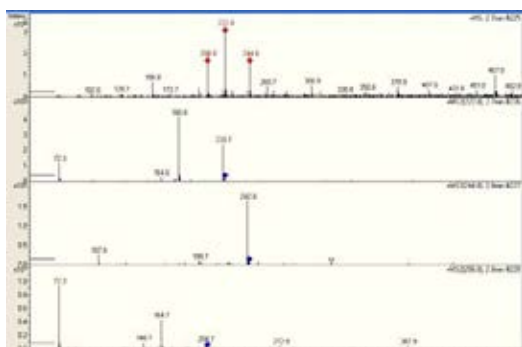
(c) Retention time 2.2 min



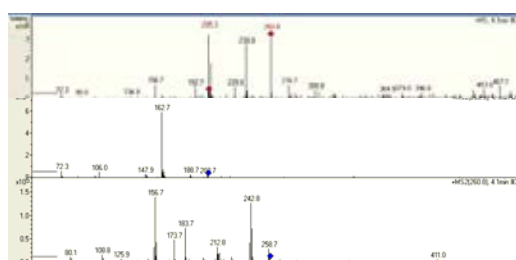
(d) Retention time 2.3 min



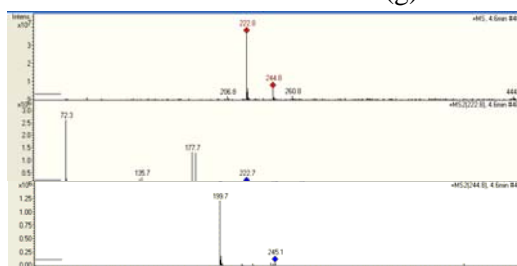
(e) Retention time 2.4 min



(f) Retention time 2.7 min



(g) Retention time 4.1 min



(h) Retention time 4.6 min

**Figure C.10** (continued)

## C4.2 At pH 3 of solution

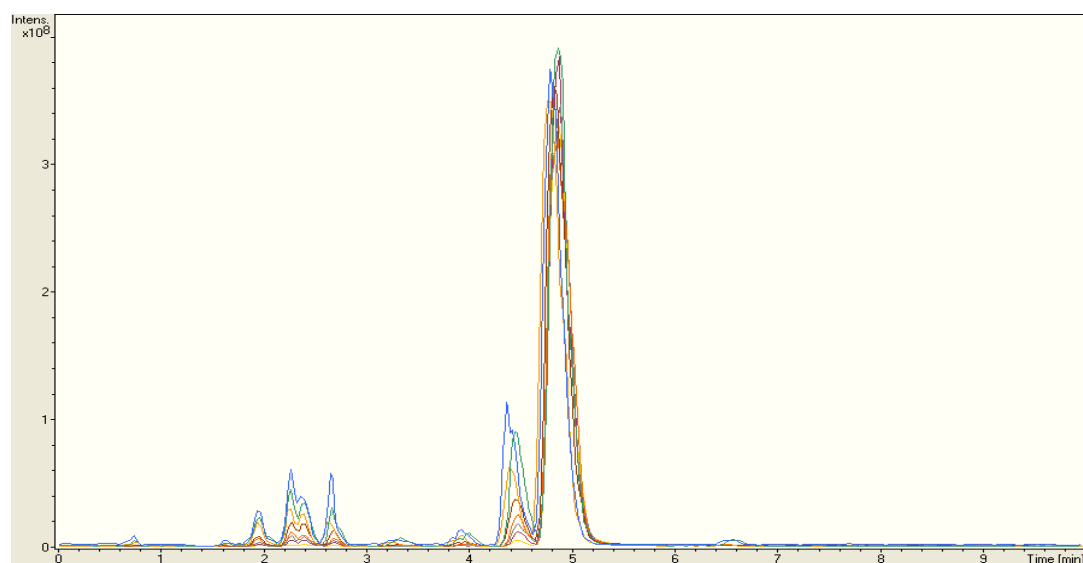
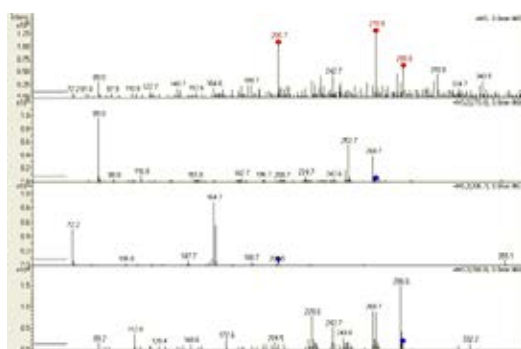
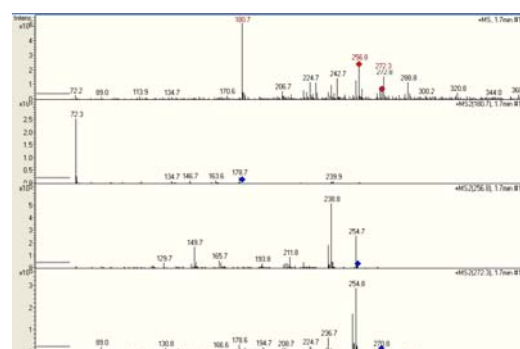


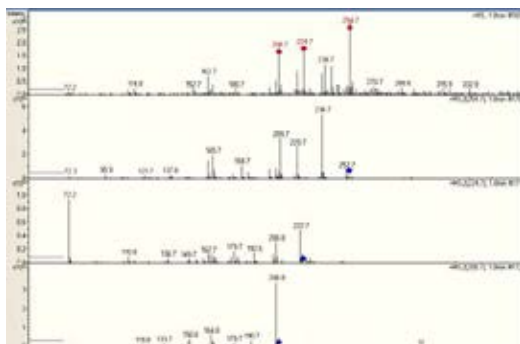
**Figure C.11** Chromatogram of isoproturon solution during photodegradation process using synthesized zinc oxide as catalyst at pH 3 of solution (0-360 min during reaction process) are shown in (a). MS/MS spectrums at various retention times are display in (b)-(n).



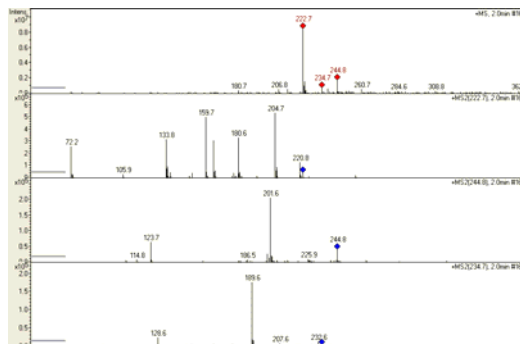
(b) Retention time 0.8 min



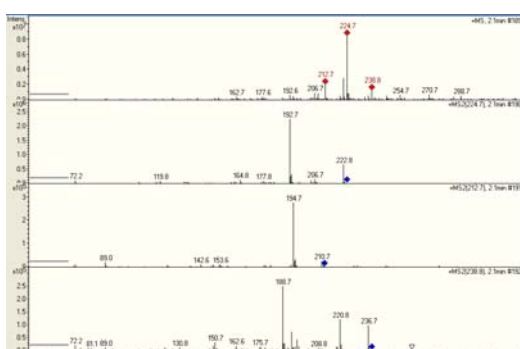
(c) Retention time 1.7 min



(d) Retention time 1.8 min



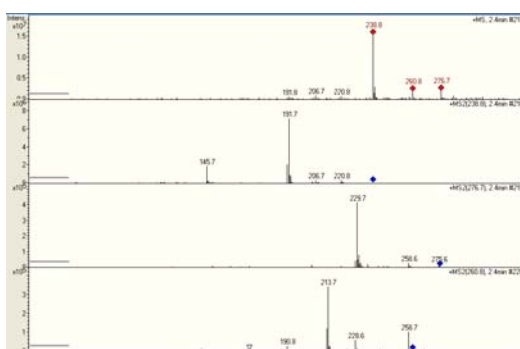
(e) Retention time 2.0 min



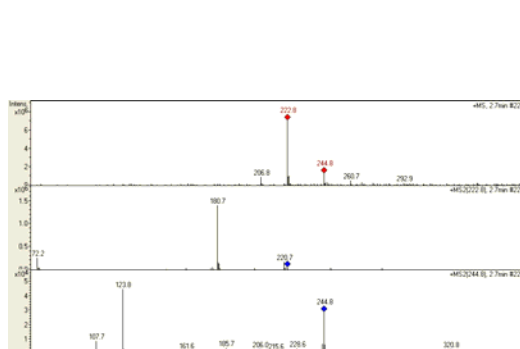
(f) Retention time 2.1 min



(g) Retention time 2.3 min



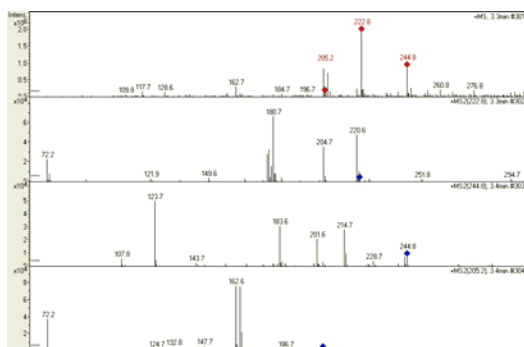
(h) Retention time 2.4 min



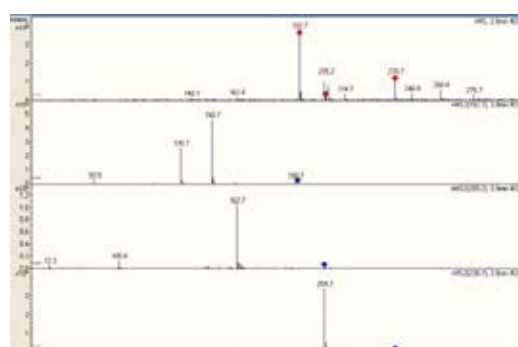
(i) Retention time 2.5 min

Figure C.11 (continued)





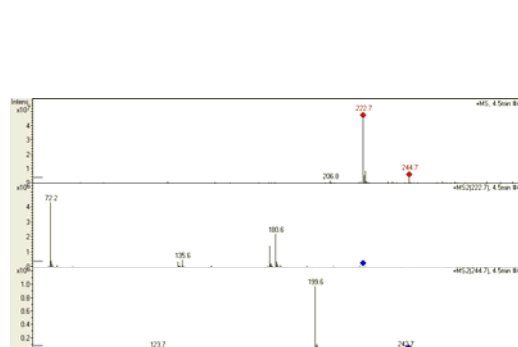
(j) Retention time 3.3 min



(k) Retention time 3.9 min



(l) Retention time 4.0 min



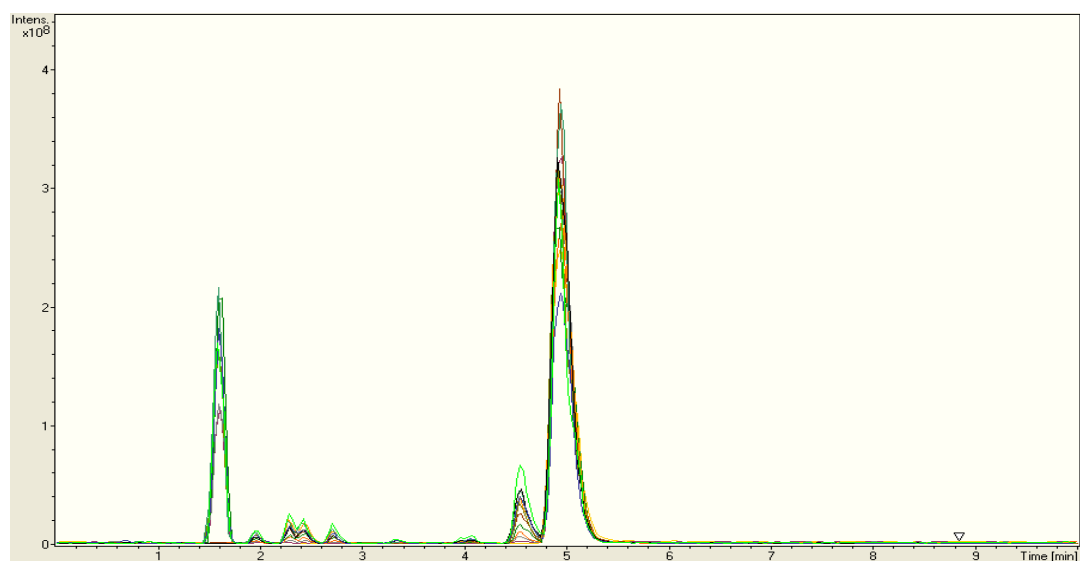
(m) Retention time 4.5 min



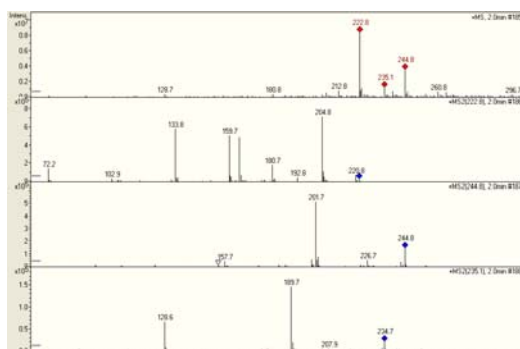
(n) Retention time 6.6 min

Figure C.11 (continued)

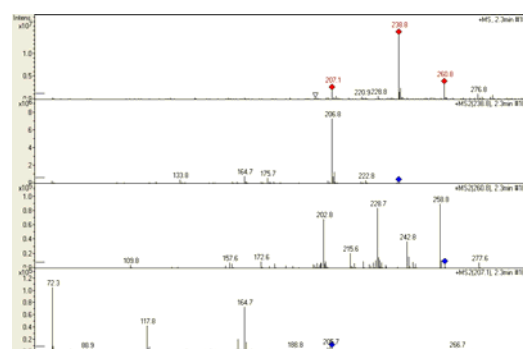
## C4.3 At pH 5 of solution



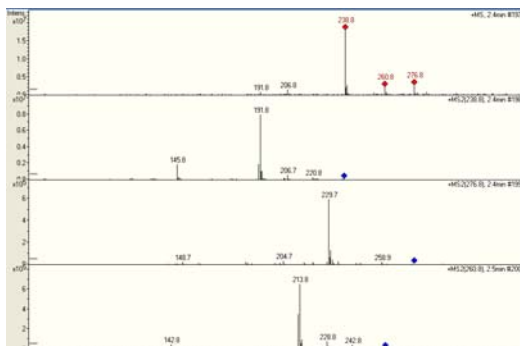
**Figure C.12** Chromatogram of isoproturon solution during photodegradation process using synthesized zinc oxide as catalyst at pH 5 of solution (0-360 min during reaction process) are shown in (a). MS/MS spectrums at various retention times are display in (b)-(i).



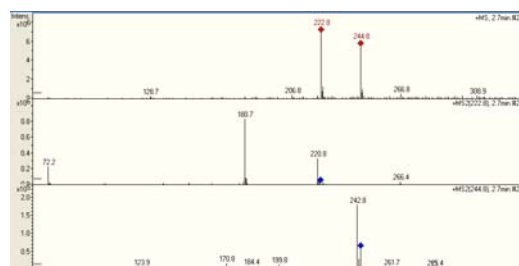
(b) Retention time 2.0 min



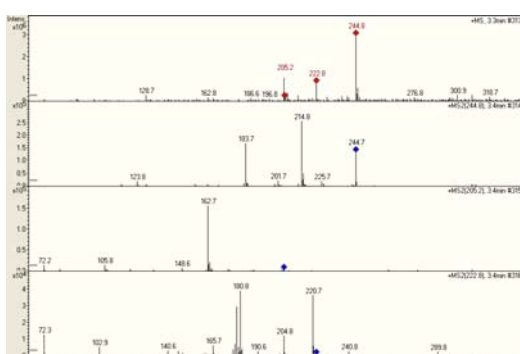
(c) Retention time 2.3 min



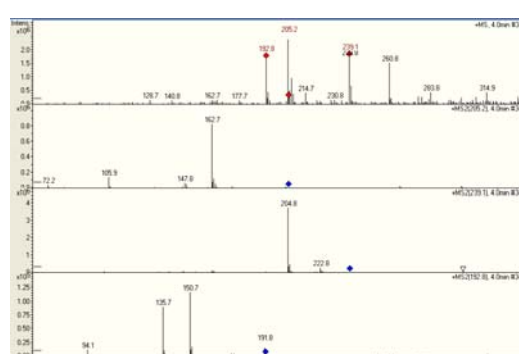
(d) Retention time 2.4 min



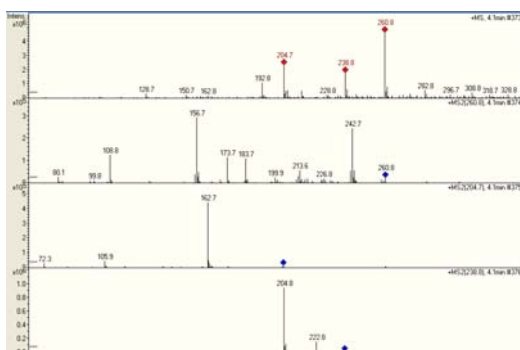
(e) Retention time 2.7 min



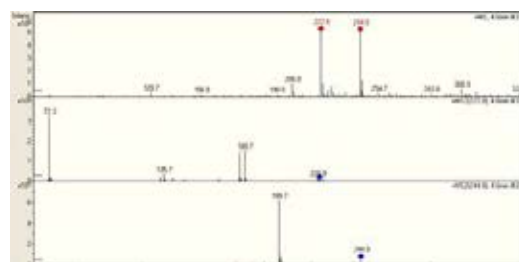
(f) Retention time 3.3 min



(g) Retention time 4.0 min



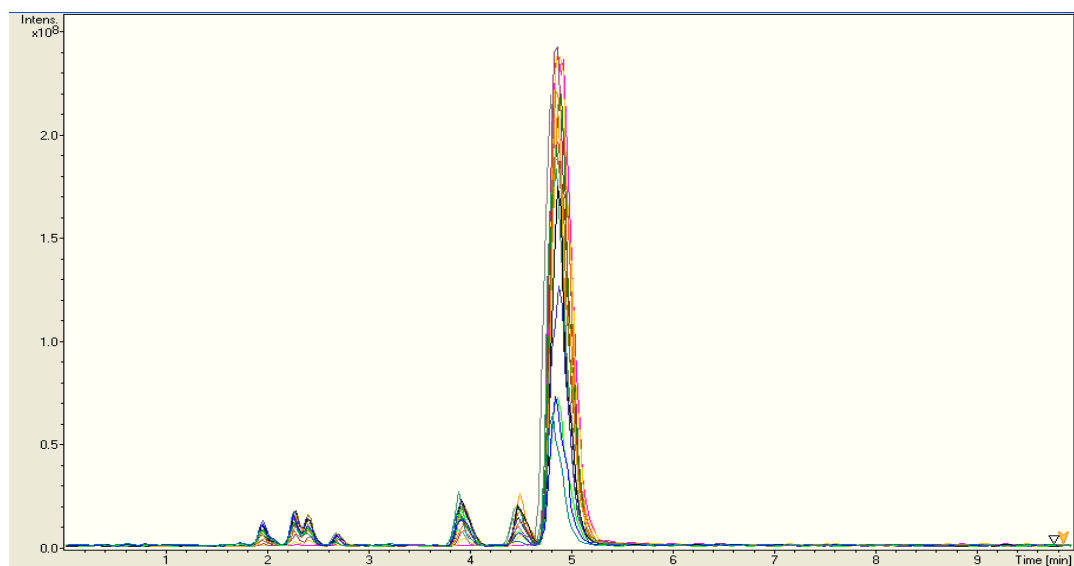
(h) Retention time 4.1 min



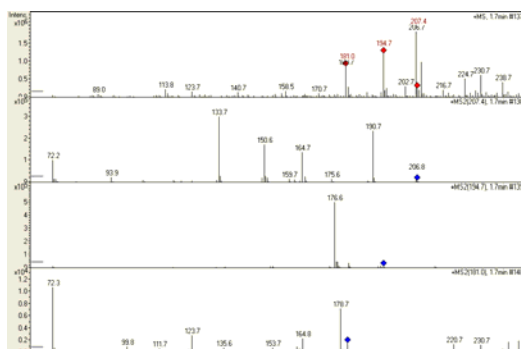
(i) Retention time 4.6 min

Figure C.12 (continued)

## C4.4 At pH 10 of solution



**Figure C.13** Chromatogram of isoproturon solution during photodegradation process using synthesized zinc oxide as catalyst at pH 10 of solution (0-360 min during reaction process) are shown in (a). MS/MS spectrums at various retention times are display in (b)-(i).

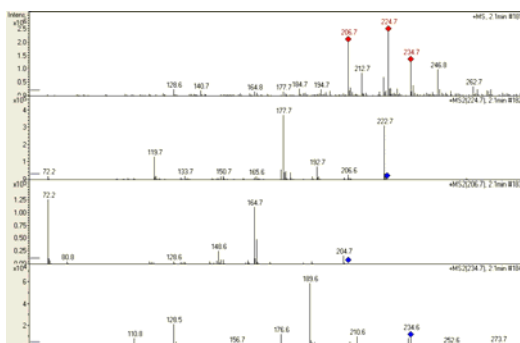


(b) Retention time 1.7 min

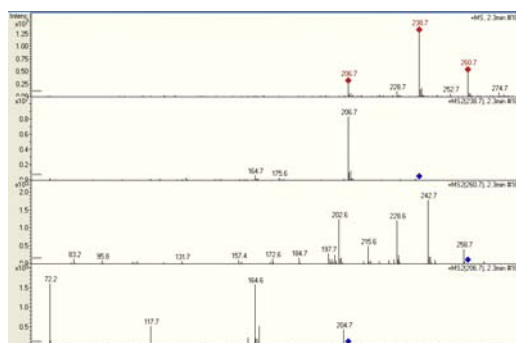


(c) Retention time 2.0 min

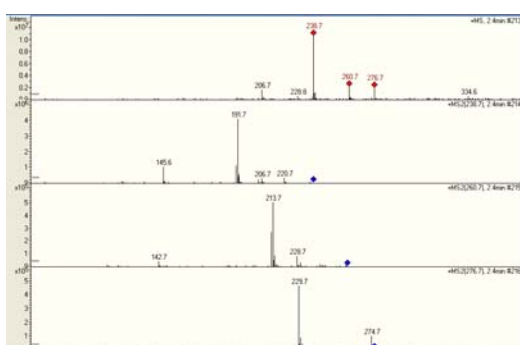
**Figure C.13** (continued)



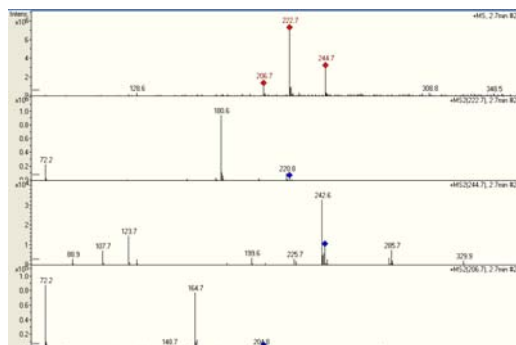
(d) Retention time 2.1 min



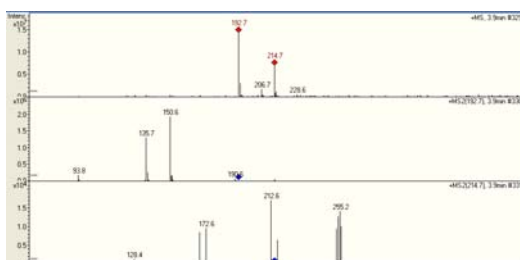
(e) Retention time 2.3 min



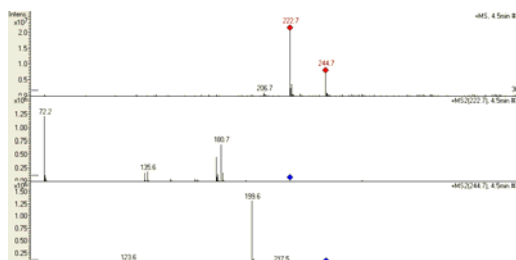
(f) Retention time 2.4 min



(g) Retention time 2.7 min



(h) Retention time 3.9 min



(i) Retention time 4.5 min

Figure C.13 (continued)

**APPENDIX D**  
**LIST OF PUBLICATION**

1. Napaporn Chanchaoenlap and Varong Pavarajarn. “Photocatalytic Degradation of Isoproturon on Zinc Oxide”. The 1<sup>st</sup> Joint Conference in Renewable Energy and Nanotechnology, Bangkok, Thailand, November 19, 2012.
  
2. Napaporn Chanchaoenlap and Varong Pavarajarn. “Comparative Study on Photocatalytic Degradation of Isoproturon on Titanium Dioxide and Zinc Oxide”. The 10<sup>th</sup> Biomass-Asia Workshop, Bangkok, Thailand, August 5-6, 2013.

## VITA

Miss Napaporn Chancharoenlap was born on September 19, 1988 in Bangkok, Thailand. She received the Bachelor Degree of Chemical Technology from Faculty of Science, Chulalongkorn University in 2011. She continued her Master's study at Chulalongkorn University in June, 2011.